Memoirs of the Faculty of Engineering, Nagoya University
Vol. 39, No. 1 (1987)

ON THE LATERAL VIBRATIONS OF A ROTATING SHAFT DRIVEN BY A UNIVERSAL JOINT

HIROSHI OTA and MASAYOSHI KATO

Department of Mechanical Engineering

(Received May 30, 1987)

Abstract

A rotating shaft driven by a universal joint suffers an angular velocity fluctuation which is decided by an angle between the driven shaft and the drive shaft rotating with a constant speed. An existing shaft surely has some moment of inertia. Therefore the driven shaft needs a moment to make the angular velocity fluctuation even if it does not take frictions or external loads against its rotation. This moment evidently concerns a torsional vibration. Simultaneously the driven shaft gains a moment perpendicular to the shaft, a secondary moment. The secondary moment causes a lateral vibration in the driven shaft. The lateral vibration consists of components which vibrate with even multiple as large as the rotating speed of the drive shaft.

When an asymmetrical shaft is used as a shaft driven by a universal joint, the asymmetrical shaft experiences vibrations influenced by the angular velocity fluctuation of shaft. The vibrations consist of unstable vibrations and forced vibrations. The unstable vibrations occur not only at the major critical speed but also at a half of it. The forced vibrations appear when the asymmetrical shaft is horizontally assembled, and they occur not only at a half but also at a quarter of the major critical speed.

CONTENTS

General Introduction 3
1. Generation of Even Multiple Vibrations by Secondary Moment 5
1. 1. Introduction 5

1. 2. Moment transmitted to the driven shaft through a universal joint 5
1. 3. Experiments 11
1. 4. Conclusions 13
2. Analyses and Experiments on Even Multiple Vibrations by Secondary Moment 13
2. 1. Introduction 13
2. 2. Rotating force and moment equivalent to secondary moment 13
2. 3. Equations of motion and their solution 16
2. 4. Experiments 18
2. 4. 1. Experimental apparatus and method 18
2. 4. 2. Experimental results and consideration 19
2. 5. Conclusions 22
3. Forced Vibrations Caused by Frictions between a Cross-Pin and Yokes 23
3. 1. Introduction 23
3. 2. Moment given to the driven shaft through a universal joint 23
3. 3. Vibration caused by viscous friction 25
3. 4. Vibration caused by Coulomb's friction 26
3. 5. Experiments 28
3. 6. Conclusions 29
Appendix 29
4. Unstable Vibration of an Asymmetrical Shaft due to Angular Velocity Fluctuation 30
4. 1. Introduction 30
4. 2. Equations of motion 31
4. 3. Analyses of vibration 32
4. 3. 1. $k=1$ ($\Omega \fallingdotseq 1$) 33
4. 3. 2. $k=2$ ($\Omega \fallingdotseq 1/2$) 34
4. 4. Numerical results and discussions 35
4. 4. 1. $\Omega \fallingdotseq 1$ 35
4. 4. 2. $\Omega \fallingdotseq 1/2$ 37
4. 5. Conclusions 40
5. Generation Mechanism of Unstable Vibrations Caused by a Shaft Asymmetry and an Angular Velocity Fluctuation 41
5. 1. Introduction 41
5. 2. Natural angular frequency and unstable regions 41
5. 3. Energy supplied to rotating shaft system 45
5. 4. Conclusions 50
6. Forced Vibrations of an Asymmetrical Shaft Caused by Gravity 50
6. 1. Introduction 50
6. 2. Equations of motion 51
6. 3. Solution for forced vibration 51
6. 3. 1. $\Omega \fallingdotseq 1/2$ 52
6. 3. 2. $\Omega \fallingdotseq 1/4$ 53
6. 4. Experiments 55
6. 4. 1. Experimental apparatus and its method 55
6. 4. 2. Experimental results and some discussions 56
6. 5. Conclusions 57
Appendix 59
References 59

General Introduction

This paper explains, when a rotating shaft is driven by a universal joint, what characteristics of vibration and what dynamical properties the driven shaft has. The universal joint is what is called Cardan joint or Hooke's joint which has spherical double-crank mechanism containing a cross-pin. J. Cardan (1501–1576, Italian) invented a universal joint, and R. Hooke (1635–1703, Englishman) found out that the universal joint transmits non-uniform rotating speed. This quantitative relation is found in the paper of R. Burkhalter and others[1]. Though a universal joint does not uniformly transmit a rotation, the universal joint has advantages that it can stand high load and can be assembled more easily than a constant speed joint such as a ball joint. Therefore the universal joint is being used also at present to transmit a power from a rotating shaft to the other one which make a certain joint angle. As such machines, there are transport machines, machine tools, and work machines.

While the critical speed of a rotating shaft has been studied by many investigators, including R. Grammel[2], A. Stodola[3], and J. P. Den Hartog[4] since W. J. Mc. Q. Rankine[5] performed the first investigation on the dynamics of a rotating shaft in 1869. From the end of the 19th century to the beginning of the 20th century, the most part of investigations concerned the critical speed of a shaft system or the determination of a natural frequency. But it invites a fall of relative rigidity and a diversification of vibration phenomena that machines grow larger. Consequently the engineering study has began to head also vibration phenomena which was not considered before. Also the subject of the investigation took up many topics, the vibration through a critical speed[6~9], the vibration of an asymmetrical shaft or rotor[10~15], the nonlinear vibration of a rotating shaft[16,17], the vibration of a rotating shaft supported by bearing with anisotropic rigidity[18~20], and the vibration of a rotating shaft being accompanied with angular velocity fluctuation[21,22]. Thus many investigations have explained the causes and the characteristics of the vibration generated in a rotating shaft system. The results of these investigations gave a principle guiding to a vibration-proof counterplan for every kind rotating machines, and made possible more quiet operation of turbines, pumps, motors and so forth.

We can often find such examples as a universal joint is used between two rotating shafts which make a certain joint angle. A vibration-proof counterplan for these rotating machines becomes more complicated because a universal joint causes vibrations based on its mechanism.

Several investigations concerned the vibration of a rotating shaft driven by a universal joint, which is also the subject of the present study. There is a well known relation about angular velocities between the drive shaft and the driven one[1,23,24]. This relation is a base for the elucidation of vibration problem. Applying this relation for analyses of the vibration, we have conveniences by expanding the angular velocity of the driven shaft into Fourier series. The Fourier series expansion will be shown in Chapter 1 of the present paper.

B. Porter[25] and V. Zeman[26] analyzed the instability of the torsional vibration, and S. H. Crandall et al.[27] analyzed the instability in the shaft system with an asymmetrical rotor. O. Föppl[28], S. Fujii[23], and R. M. Rosenberg[29] treated the vibrations of the shaft whirling with odd multiple as large as the drive speed.

This odd multiple vibrations were elucidated by the explanation that they are caused by multiplicational action of the angular velocity fluctuation and the eccentricity.

We cannot find but the investigation by S. Fujii et al.[30] which concerns the vibrations of shaft whirling with even multiple as large as the angular velocity of the drive shaft. They explained that the even multiple vibrations are caused by frictions between the cross-pin and the yokes of a universal joint. But the report deals with the frictions only between one pin of the cross-pin and one yoke, furthermore it does not exactly give the relative angular velocity between the yokes and the cross-pin. The vibration caused by these frictions will be treated in Chapter 3 of the present paper.

R. Burkhalter et al.[1], J. A. Kayser[31], and S. Kato[32] analyzed the vibration of the shaft whirling with the angular velocity equal to two times as large as the rotating speed of the drive shaft. They assumed that the drive shaft has simultaneously a constant angular velocity and a constant torque. But it is clear under the simple dynamical consideration that this assumption does not hold.

Besides the above mentioned papers, there are studies on the speed characteristics of a universal joint[33~35] and on the response of a universal joint used as gyroscope[36].

An approximate solution must be frequently treated when equations of motion can be not exactly solved because they have small parameters, that is, parametric excitation terms, nonlinear terms and the like. As for methods to analyze approximately, there are the perturbation method, the method of averaging, the method of Van der Pol, the method of harmonic balance and so forth in addition to the asymptotic method[37] which will be used in Chapters 4 and 6 of the present paper. Some one of these methods makes what is a called secular term generate in the approximate solution (the method of Poison), and the other does not show the method for higher order approximation (the method of Van der Pol).

The present paper deals with the following driven shaft systems. The driven shaft system in Chapter 1 to Chapter 3 is composed of a flexible shaft with circular section and a symmetrical rotor. The driven shaft system in Chapter 4 to Chapter 6 is composed of an asymmetrical shaft and a concentrated mass. In all the chapters, the driven shaft is supported by a universal joint at one end and by a ball bearing at the other end.

The assumptions applied to each of chapters are as follows;

(1) The drive shaft is rigid, and it rotates with a constant angular velocity ω.

(2) Each of parts of the universal joint is also rigid, and the universal joint has neither a discrepancy of center or a play.

(3) The felxible driven shaft has no distributed mass.

(4) The deflection of the driven shaft does not influence the rotating speed of the driven yoke, namely, that of the driven shaft.

Chapter 1 gives a consideration on the the transmission mechanism of moment by a universal joint. The universal joint generates a secondary moment perpendicular to the driven shaft when the shaft suffers a load against its rotation. The generation of this secondary moment is dynamically explained. Force and moment equivalent to the secondary moment are considered. They are regarded to act at the position of a rotor installation to the shaft.

Chapter 2 discusses the characteristics of the forced vibration caused by the secondary moment. Analytical and experimental examinations are performed on how the secondary moment changes when the joint angle or the drive speed ω is

changed.

Chapter 3 deals with the forced vibration generated on account of frictions between the cross-pin and the yokes. The frictions are considered to be viscous and of Coulomb.

Chapter 4 analyzes the unstable vibration which occurs when an asymmetrical shaft is driven by a universal joint. It is mentioned how the angular velocity fluctuation influences on the vibration excited in the asymmetrical shaft.

Chapter 5 gives a physical interpretation on the unstable vibration of the asymmetrical shaft in Chapter 4, and discusses on the generation mechanism. When the unstable vibration occurs, it is considered how the whirling mode relates with the increase in rate of dynamical energy of the shaft system.

Chapter 6 deals with the forced vibration caused by the shaft asymmetry, angular velocity fluctuation, and gravity when an asymmetrical shaft is driven by a universal joint and also is horizontally assembled. In this chapter, analyses and experiments are performed on the asymmetrical shaft which whirls with the angular velocity of even multiple as large as the drive speed ω.

1. Generation of Even Multiple Vibrations by Secondary Moment[38,39]

1. 1. Introduction

As is well known, a shaft driven by a universal joint makes a resonance at an angular velocity ω which is equal to one of the integer submultiples of natural angular frequency p ($p=\pm N\omega$, $N=2, 3, 4, \ldots$), and has a violently whirling lateral vibration. Each of these vibrations has a frequency of integer multiples of the shaft angular velocity. Vibrations with only the frequencies which are equal to odd integer multiples of the angular velocity ($N=2k+1$, $k=1, 2, 3, \ldots$) have been treated analytically[21,23,29]. Fujii et al.[30] assumed the vibrations of even multiples of the angular velocity ($N=2k$) caused by frictions between a cross-pin and yokes of a universal joint. There have been many investigations regarding 2ω vibration[1,31,32], in which analyses are performed under the assumption that a drive shaft has both a constant angular velocity and a constant drive torque. However, if the angular velocity of the drive shaft is assumed to be constant, then the drive torque can, in fact, no longer be constant, and it should be determined only by a load resisting the rotation of the driven shaft.

This chapter shows that a universal joint generates the secondary moment, by which the driven shaft makes the even multiple vibration.

1. 2. Moment transmitted to the driven shaft through a universal joint

A universal joint considered here is assumed to have no play, no friction, and no misalignment in its center. As shown in Fig. 1. 1, let the center lines of a drive shaft and a driven shaft be the z_{a1} and z axes, respectively. These two axes cross at the joint center A and make the joint angle α_a. In two stationary rectangular co-ordinate systems A-$x_{a1}y_az_{a1}$ and A-x_ay_az, the y_a axis is perpendicular to the z_{a1}Az plane. Consider the following two pins forming the cross-pin of the universal joint: one is called the Ψ pin, which always exists in the $x_{a1}y_a$ plane, and the other is the Θ pin, which always exists in the x_ay_a plane. A rotating angle of

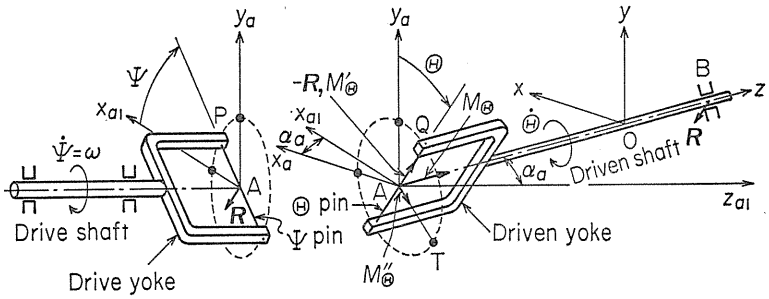

Fig. 1. 1. Moment transmitted to driven shaft through universal joint (when there is no friction between a cross-pin and yokes, i. e., $M_\theta'=0$).

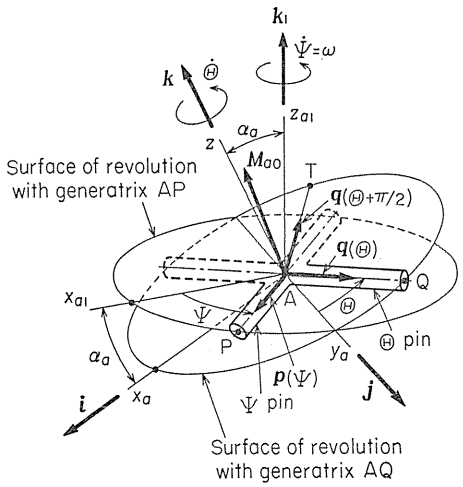

Fig. 1. 2. Relation between stationary rectangular co-ordinate systems A-$x_{a1}y_az_{a1}$ and A-x_ay_az ($\angle$PAQ=$\angle$QAT=$\pi/2$).

the drive shaft is represented by Ψ, and that of the driven shaft by Θ. These angles Ψ and Θ are zero when the Ψ pin and Θ pin coincide with the x_{a1} and y_a axes, respectively. Let one end of the Ψ pin be P, and that of the Θ pin be Q.

We introduce here the unit vectors $\boldsymbol{i}$, $\boldsymbol{j}$, $\boldsymbol{k}$, $\boldsymbol{k}_1$, $\boldsymbol{p}(\Psi)$, and $\boldsymbol{q}(\Theta)$ as shown in Fig. 1. 2. The unit vectors $\boldsymbol{i}$, $\boldsymbol{j}$, $\boldsymbol{k}$, and $\boldsymbol{k}_1$ have the same directions as the x_a, y_a, z, and z_{a1} axes; $\boldsymbol{p}(\Psi)$ and $\boldsymbol{q}(\Theta)$ have the same ones as $\overrightarrow{AP}$ and $\overrightarrow{AQ}$, respectively, and they are given by the following equation (1. 1) as can be seen from Fig. 1. 2.

$$\left.\begin{aligned}\boldsymbol{p}(\Psi)&=\cos\alpha_a\cos\Psi\,\boldsymbol{i}+\sin\Psi\,\boldsymbol{j}+\sin\alpha_a\cos\Psi\,\boldsymbol{k}\\ \boldsymbol{q}(\Theta)&=-\sin\Theta\,\boldsymbol{i}+\cos\Theta\,\boldsymbol{j}\end{aligned}\right\}\tag{1.1}$$

Scalar product of $\boldsymbol{p}(\Psi)$ and $\boldsymbol{q}(\Theta)$ must be zero because of their orthogonal condition as follows:

$$\boldsymbol{p}(\Psi)\cdot\boldsymbol{q}(\Theta)=0\tag{1.2}$$

Substitution of Eq. (1. 1) into Eq. (1. 2) yields the following relation[24]

$$\tan\Theta=\frac{\tan\Psi}{\cos\alpha_a}\tag{1.3}$$

that is,

$$\sin\theta=\frac{\sin\Psi}{\sqrt{H(\Psi)}},\quad \cos\theta=\frac{\cos\alpha_a\cos\Psi}{\sqrt{H(\Psi)}}\quad\left(-\frac{\pi}{2}<\alpha_a<\frac{\pi}{2}\right)\tag{1.4}$$

where

$$H(\Psi)=1-\sin^2\alpha_a\cos^2\Psi\tag{1.5}$$

The Ψ pin moment transmitted from the drive yoke to the Ψ pin is equal to the Θ pin moment exerted on the driven yoke through the Θ pin. This speaks for itself by the law of action and reaction. It is assumed that there exists no friction between the cross-pin and the yokes in this chapter. Accordingly, the Ψ pin moment given by the drive shaft has no component in the direction of Ψ pin ($\overrightarrow{AP}$); and the Θ pin moment acting on the driven yoke either has no component in the direction of Θ pin ($\overrightarrow{AQ}$). Thus the universal joint can transmit only a moment perpendicular to the plane PAQ containing the cross-pin. This moment vector $\boldsymbol{M}_{a0}$ is expressed by the vector product as shown in Fig. 1. 2:

$$\boldsymbol{M}_{a0}=M_{a0}\boldsymbol{p}(\Psi)\times\boldsymbol{q}(\theta)\tag{1.6}$$

Generally, since the direction of the moment vector $\boldsymbol{M}_{a0}$ coincides neither with the center line of the drive shaft (z_{a1} axis) nor with that of the driven shaft (z axis), the vector $\boldsymbol{M}_{a0}$ has a component perpendicular both to the drive shaft and to the driven shaft.

As shown in Fig. 1. 1, the moment $\boldsymbol{M}_{a0}$ is resolved into the following three components: M_θ in the z direction, and M'_θ and M''_θ in the $\overrightarrow{AQ}$ and $\overrightarrow{AT}$ directions perpendicular to the z direction, respectively. The moment M_θ has influence on the rotation of the driven shaft, and the moment M'_θ and M''_θ have influence on the lateral vibration of the driven shaft. Reference to Fig. 1. 2, and use of Eqs. (1. 1), (1. 4), and (1. 6) yield the following equations:

$$\left.\begin{aligned}M_\theta&=\boldsymbol{M}_{a0}\cdot\boldsymbol{k}=M_{a0}\sqrt{H(\Psi)}\\M'_\theta&=\boldsymbol{M}_{a0}\cdot\boldsymbol{q}(\theta)=0\\M''_\theta&=\boldsymbol{M}_{a0}\cdot\boldsymbol{q}\left(\theta+\frac{\pi}{2}\right)=M_{a0}\sin\alpha_a\cos\Psi\end{aligned}\right\}\tag{1.7}$$

The components M_Ψ, M'_Ψ, and M''_Ψ of the moment $\boldsymbol{M}_{a0}$ in the z_{a1}, $\boldsymbol{p}(\Psi)$, and $\boldsymbol{p}(\Psi+\pi/2)$ directions are derived as follows:

$$\left.\begin{aligned}M_\Psi&=\boldsymbol{M}_{a0}\cdot\boldsymbol{k}_1=\boldsymbol{M}_{a0}\cdot(-\sin\alpha_a\,\boldsymbol{i}+\cos\alpha_a\,\boldsymbol{k})=M_{a0}\frac{\cos\alpha_a}{\sqrt{H(\Psi)}}\\M'_\Psi&=\boldsymbol{M}_{a0}\cdot\boldsymbol{p}(\Psi)=0\\M''_\Psi&=\boldsymbol{M}_{a0}\cdot\boldsymbol{p}\left(\Psi+\frac{\pi}{2}\right)=-M_{a0}\frac{\sin\alpha_a\sin\Psi}{\sqrt{H(\Psi)}}\end{aligned}\right\}\tag{1.8}$$

Differentiating Eq. (1. 2) with respect to time t, and using Eqs. (1. 1), (1. 4), (1. 7), and (1. 8), we have

$$\frac{d}{dt}\{\boldsymbol{p}(\Psi)\cdot\boldsymbol{q}(\Theta)\}=\dot{\Psi}\frac{\cos\alpha_a}{\sqrt{H(\Psi)}}-\dot{\Theta}\sqrt{H(\Psi)}=\frac{1}{M_{a0}}(\dot{\Psi}M_\Psi-\dot{\Theta}M_\Theta)\equiv 0 \qquad (1.9)$$

where the dot over the variables Ψ and Θ means differentiation with respect to t. From Eq. (1. 9) the following two equations are obtained:

$$\dot{\Theta}=\dot{\Psi}\frac{\cos\alpha_a}{H(\Psi)} \qquad (1.10)$$

$$M_\Psi\dot{\Psi}=M_\Theta\dot{\Theta} \qquad (1.11)$$

Equation (1. 10) is a familiar relation[24] between the angular velocity of the drive shaft and that of the driven shaft. Equation (1. 11) shows clearly that the time rate of work done by the drive shaft (the left-hand side of Eq. (1. 11)) and that by the driven yoke (the right-hand side of it) are equal to each other; this shows the truism that there is no energy loss in a frictionless universal joint.

Figure 1. 1 shows all the moments and forces acting on the shaft driven by a universal joint which has no friction between the cross-pin and the yokes. In this figure the force vectors $\boldsymbol{R}$ and $-\boldsymbol{R}$ are the reactions given by the bearing B and the drive shaft, respectively; they are proportional to the moment M''_θ in magnitude, and coincide with Θ pin ($\overrightarrow{AQ}$) in direction.

In the following, the drive shaft is assumed to rotate with a constant angular velocity ω, and Ψ pin is assumed to exist in a plane containing both the z_{a1} and z axes when $t=0$, namely,

$$\Psi=\omega t \qquad (1.12)$$

Here, a revolutional angle Θ is given as a known function of time; if a dynamical property is given to the driven shaft system, then M_Θ is obtained from Eq. (1. 7), and a secondary moment M''_θ is determined by

$$M''_\theta=M_\Theta\sin\alpha_a\frac{\cos\Psi}{\sqrt{H(\Psi)}} \qquad (1.13)$$

Consider a driven shaft system such as shown in Fig. 1. 3. A flexible shaft S_h has a uniform circular cross section of length l, and has a balanced symmetrical rotor D. Point A supported by a rigid drive shaft is a center of the universal joint. One end of the flexible shaft S_h is simply supported at the point A. The rotor D is mounted at a position S which is at distances of a and b from the shaft ends A and B, respectively. The secondary moment and also the angular velocity of the driven shaft are assumed not to be influenced by deflection in the driven shaft.

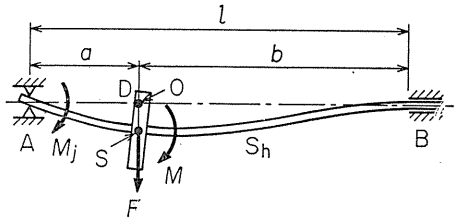

Fig. 1. 3. Force F and moments M, M_j in driven shaft.

For convenience, an equivalent force F and an equivalent moment M at the point S are considered instead of a moment M_j which acts at the point A in the direction perpendicular to the driven shaft. Simultaneous action of F and M causes the same deflection and the same angle of

deflection in the driven shaft as caused only by the moment M_j. Use of the theory of elasticity gives

$$F=\frac{3M_j}{2a},\quad M=-\frac{M_j}{2} \tag{1.14}$$

whether the support condition at the shaft end B is simple or fixed. The positive directions of the vectors F, M, and M_j are shown in Fig. 1. 3.

Let a torsional angle at the point S with respect to the point A be $\Theta_s-\Theta$, the positive direction of which is the same as the shaft rotation. The torsional angle $\Theta_s-\Theta$ and the rotating angle Θ_s are given by the following equations:

$$M_\Theta=-\delta_t(\theta_s-\theta) \tag{1.15}$$

$$I_p\ddot{\Theta}_s=-\delta_t(\theta_s-\theta)-M_b \tag{1.16}$$

where, I_p denotes a polar moment of inertia of the rotor D, δ_t a spring constant for a twist of shaft between A and S, and M_b a constant resisting moment acting on the driven shaft end B.

Equation (1. 10) can be transformed into the following form*1:

$$\dot{\theta}=\omega\left(1+2\sum_{N=2,4,\cdots}\varepsilon^{N/2}\cos N\omega t\right) \tag{1.17}$$

Here the coefficient ε is given by the following equation:

$$\varepsilon=\cos\alpha_a\sum_{k=1}^{\infty}{}_{2k}C_{k-1}\left(\frac{\sin\alpha_a}{2}\right)^{2k} \tag{1.18}$$

which is a function only of the joint angle α_a as shown in Fig. 1. 4. Equation (1. 17) shows clearly that the component fluctuating with the angular velocity $N\omega$ is $2\omega\varepsilon^{N/2}$ in magnitude. Since the coefficient ε consists of even powers with respect to the joint angle α_a, the following approximate equation

$$\varepsilon=\frac{1}{4}\alpha_a{}^2+\frac{1}{24}\alpha_a{}^4 \tag{1.18}'$$

can also be used instead of the infinite polynomial (1. 18). The broken line in Fig. 1. 4 indicates the value ε derived from Eq. (1. 18)', and it shows a fairly good approximation to Eq. (1. 18) when α_a is smaller than $\pi/6$. Substitution of Eq. (1. 17) into Eq. (1. 16) gives the following differential equation with respect to the torsional angle $\Theta_s-\Theta$:

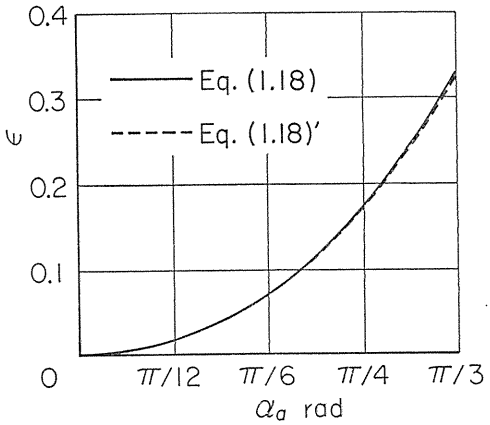

Fig. 1. 4. Variation of coefficient ε by joint angle α_a.

*1 Although the direct derivation of Eq. (1. 17) is very difficult, the equivalence of Eq. (1. 17) to Eq. (1. 10) may be proved rather easily.

$$I_p(\ddot{\Theta}_s-\ddot{\Theta})+\delta_t(\theta_s-\theta)=2I_p\omega^2\sum_{N=2,4,\cdots}\varepsilon^{N/2}N\sin N\omega t-M_b \tag{1.19}$$

Substituting the solution of Eq. (1. 19) into Eq. (1. 15), we have

$$\left.\begin{aligned} M_\theta&=M_b-\delta_t\sum_{N=2,4,\cdots}\varepsilon^{N/2}d_N\sin N\omega t\\ d_N&=\frac{2NI_p\omega^2}{\delta_t-I_p(N\omega)^2}\end{aligned}\right\} \tag{1.20}$$

As pointed out in the introduction, a drive torque M_Ψ acting on the drive yoke should not be presumed in advance, and it is determined necessarily by Eqs. (1. 7) and (1. 8), namely,

$$M_\Psi=M_\theta\frac{\cos\alpha_a}{H(\Psi)}=(M_b-\delta_t\sum_{N=2,4,\cdots}\varepsilon^{N/2}d_N\sin N\omega t)\frac{\cos\alpha_a}{H(\Psi)} \tag{1.21}$$

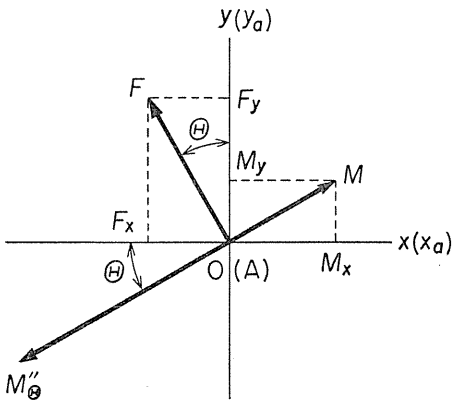

Fig. 1. 5. Force F and moment M equivalent to secondary moment M_θ''.

Here one may set up a stationary rectangular co-ordinate system O-xyz parallel to A-x_ay_az in which point S overlaps with the origin O when there is no deflection in the driven shaft. Substituting M_θ'' in Eq. (1. 13) into M_j in Eq. (1. 14), we obtain the equivalent force F and moment M expressed on the O-xy plane (Fig. 1. 5). Comparison of Eq. (1. 10) with Eq. (1. 17) yields

$$\frac{\cos\alpha_a}{H(\Psi)}=1+2\sum_{N=2,4,\cdots}\varepsilon^{N/2}\cos N\Psi \tag{1.22}$$

Use of Eqs. (1. 4), (1. 13), (1. 20), (1. 22), and Fig. 1. 5 gives the following x components F_x and M_x, and y components F_y and M_y:

$$\left.\begin{aligned} F_x&=-\frac{3M_\theta''}{2a}\sin\theta\\ &=-\frac{3}{4a}\tan\alpha_a\sin 2\omega t(1+2\sum_{N=2,4,\cdots}\varepsilon^{N/2}\cos N\omega t)(M_b-\delta_t\sum_{N=2,4,\cdots}\varepsilon^{N/2}d_N\sin N\omega t)\\ F_y&=\frac{3M_\theta''}{2a}\cos\theta\\ &=\frac{3}{4a}\sin\alpha_a(1+\cos 2\omega t)(1+2\sum_{N=2,4,\cdots}\varepsilon^{N/2}\cos N\omega t)(M_b-\delta_t\sum_{N=2,4,\cdots}\varepsilon^{N/2}d_N\sin N\omega t)\end{aligned}\right\} \tag{1.23}$$

$$M_x=\frac{aF_y}{3},\quad M_y=-\frac{aF_x}{3} \tag{1.24}$$

Apparently, the equivalent force (1. 23) and moment (1. 24) have the components of whirling velocities $\pm N\omega$ ($N=2, 4, 6, \ldots$). Consequently, when any one among $\pm N\omega$ is nearly equal to the natural angular frequency p in relation to a whirling motion of the shaft (i. e., $\omega \fallingdotseq \pm p/N$ holds well), the shaft undergoes a violent lateral vibration whirling with any one angular velocity among $\pm N\omega$. Also, when the drive shaft rotates with an angular velocity nearly equal to one of the even integer submultiples of the natural frequency regarding torsional vibration of the driven shaft, the shaft may have a violent lateral vibration accompanied by a violent torsional vibration.

1. 3. Experiments

Experiments are performed for the purpose of confirming the analytical results obtained in section 1. 2. Lateral deflections and angles of deflection at the mounting point S of a rotor D are measured for the joint angle α_a and the axial moment M_θ.

A universal joint used in the experiments is shown in Fig. 1. 6. This joint is not one available on the market but one produced especially for the present investigation, and has the following characteristics: Both single-row radial ball bearings (nominal No. 6002) and thrust ball bearings (nominal No. 51104) are used between the cross-pin and yokes. Consequently, play and frictions between the cross-pin and the yokes will be smaller than those of the conventional universal joint obtained on the market. The coefficient of the viscous friction to the relative swinging motion between the cross-pin and the yokes is about 0. 3 s·N·m/rad, and the moment caused by Coulomb's friction is 0. 81 mN·m. The magnitude of play is about 0. 01 mm. The driven shaft S_h is made of mild steel with a uniform circular section, and one end B of it is supported in fixed condition (Fig. 1. 3). The dimensions of the driven shaft are $l=625.4$ mm in length ($a=237.5$ mm, $b=387.9$ mm) and 17. 97 mm in diameter.

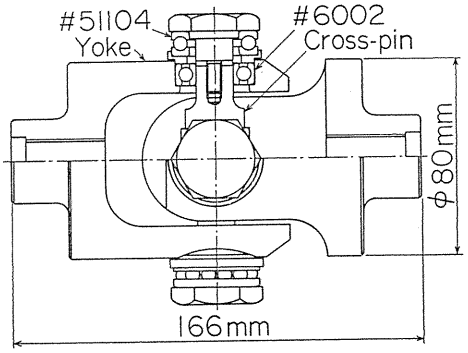

Fig. 1. 6. Universal joint used in experiments.

The experiments are performed as follows: A moment M_b is externally given at the shaft end B, and its direction is clockwise as viewed from the driven shaft. Under the action of the moment M_b, the drive shaft is fixed to rotate. Therefore $\omega=0$ and $d_N=0$ hold, and from Eq. (1. 20) the moment M_θ exerted at the point A is

$$M_\theta=M_b \tag{1.20}'$$

Thereupon static deflections and angles of deflection at the point S are measured. The following equations

$$\left.\begin{aligned}\frac{aF_x}{M_\theta}&=\frac{a}{M_\theta}(\alpha x+\gamma\theta_x)\\ \frac{aF_y}{M_\theta}&=\frac{a}{M_\theta}(\alpha y+\gamma\theta_y)\end{aligned}\right\}\qquad(1.25)$$

are used for non-dimensional quantities. They are shown as functions of Ψ in Fig. 1. 7, where α and γ in Eq. (1. 25) are the spring constants of shaft deflection. The solid line and the broken line in Fig. 1. 7 represent the calculated values from the following equations

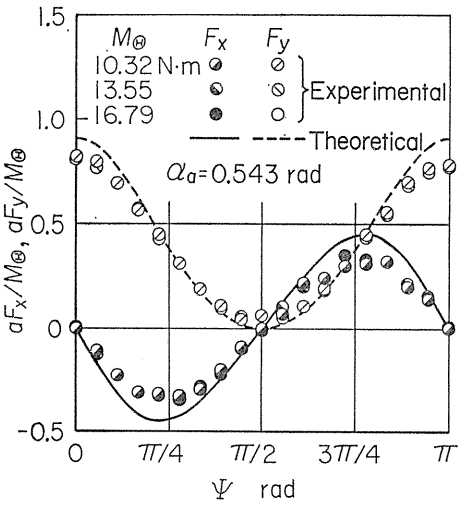

Fig. 1. 7. Variations of equivalent forces F_x, F_y by rotating angle Ψ of drive shaft.

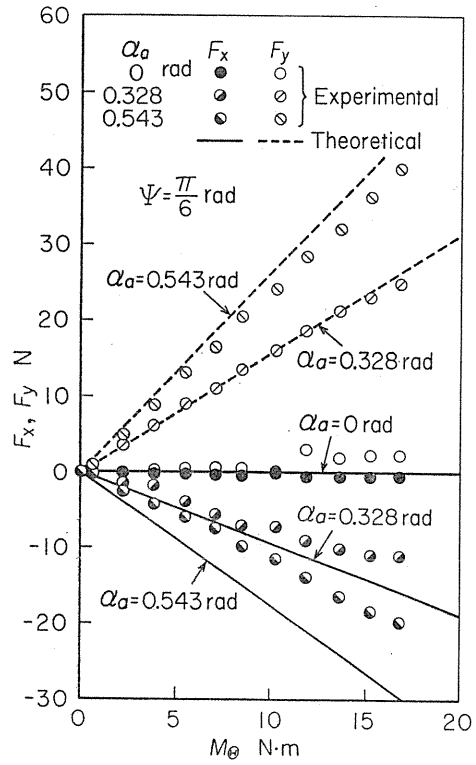

Fig. 1. 8. Variations of equivalent forces F_x, F_y by drive moment M_Θ acting on driven shaft.

$$\left.\begin{aligned}\frac{aF_x}{M_\theta}&=-\frac{3\sin\alpha_a\sin 2\Psi}{4H(\Psi)}\\ \frac{aF_y}{M_\theta}&=\frac{3\sin\alpha_a\cos\alpha_a(1+\cos 2\Psi)}{4H(\Psi)}\end{aligned}\right\}\qquad(1.26)$$

which are given by substitution of Eqs. (1. 4), (1. 13), and (1. 20)′ into Eq. (1. 23). Figure 1. 8 shows the measured results for the purpose of confirmation of the proportional relation (1. 25) between the equivalent forces F_x, F_y and the moment M_Θ when $\Psi=\pi/6$ rad for many values of M_Θ. Since these measured values coincide well with the calculated values, it is clear that the lateral deflection of the shaft is generated by the secondary moment M''_Θ, and the analytical results derived in

section 1. 2 are valid.

1. 4. Conclusions

In this chapter, consideration has been given to the mechanism of a moment transmitted by a universal joint. Also, a dynamically clear interpretation has been proposed for generation of a secondary moment which concerns a lateral vibration of the driven shaft. The results obtained may be summarized as follows:

(1) Owing to the secondary moment generated by the universal joint, the driven shaft makes a resonance and has a number of forced lateral vibrations. These vibrations increase when the drive shaft rotates with an angular velocity nearly equal to one of the even integer submultiples of natural angular frequencies in the driven shaft system. The whirling angular velocities of these vibrations are equal to even integer multiples of the angular velocity of the drive shaft.

(2) An equivalent force and moment acting on a rotor mounted on the shaft can be used instead of the secondary moment.

(3) When the drive shaft rotates with a constant angular velocity, the shaft driven by a universal joint rotates with the angular velocity represented by simple Fourier series (Eq. (1. 17)). Use of this equation can facilitate vibration analyses for the driven shaft system.

(4) The experimental results show validity of the present analyses.

2. Analyses and Experiments on Even Multiple Vibrations by Secondary Moment[40]

2. 1. Introduction

A secondary moment generated by a universal joint has components fluctuating with even multiple of an angular velocity of drive shaft. The manner in which these fluctuating components change due to a joint angle and an angular velocity is investigated. Equations of motion in consideration of the fluctuating components are introduced, and the solution is given as forced vibration. Experiments are conducted for each magnitude of the joint angle and the drive moment concerning torsional vibration, and the even multiple vibrations generated in the driven shaft are measured. The analyses and the experiments indicate that the even multiple vibrations generated in the experimental apparatus are caused mainly by the secondary moment.

2. 2. Rotating force and moment equivalent to secondary moment

A drive shaft and a driven shaft are shown schematically in Fig. 2. 1. The drive shaft carrying a flywheel F is rigid, and it rotates with a constant angular velocity ω. The driven shaft S_h with no initial bend is flexible, and it has a uniform circular cross section, l in length. One end of the shaft S_h is supported by a universal joint J and the other end by a self-aligning double-row ball bearing B. At the point S of the shaft a balanced rotor D is mounted. Notations, co-ordinate systems, and terms are the same as those in Chapter 1 except when they are especially mentioned.

The secondary moment is assumed not to be influenced by a small deflection

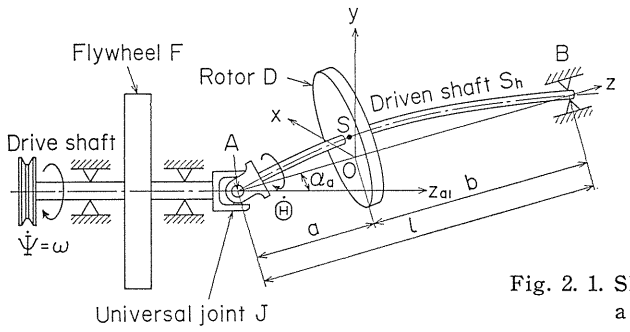

Fig. 2. 1. Shaft S_h and rotor D driven by a universal joint J.

of the driven shaft. Therefore, no reference to self-sustained vibration or parametric vibration is made[41,42].

The equivalent force and moment given by Eqs. (1. 23) and (1. 24) are expanded into Fourier series, and are written as follows:

$$\left.\begin{aligned} F_z&=F_x+iF_y=\boldsymbol{F}[0]+\sum_{N=2,4,\cdots}\{\boldsymbol{F}[+N\omega]e^{N\omega t}+\boldsymbol{F}[-N\omega]e^{-iN\omega t}\}\\ M_z&=-iaF_z/3 \quad (i=\sqrt{-1}) \end{aligned}\right\} \tag{2.1}$$

where F_z and M_z are rotating vectors represented on a complex plane which has the x axis as real axis and the y axis as imaginary axis. The components $\boldsymbol{F}[0]$ and $\boldsymbol{F}[\pm N\omega]$ of the equivalent force are classified according to loads against rotation of the shaft. One is a component due to the constant moment M_b,

$$\left.\begin{aligned} \frac{a\boldsymbol{F}[0]}{M_b}&=i\frac{3}{4}\sin\alpha_a(1+\varepsilon)\\ \frac{a\boldsymbol{F}[\pm N\omega]}{M_b}&=i\frac{3}{8}\varepsilon^{N/2-1}\{(1+\varepsilon)^2\sin\alpha_a\pm(1-\varepsilon^2)\tan\alpha_a\} \end{aligned}\right\} \tag{2.2}$$

the other is a component due to the torsional vibration of the shaft section AS,

$$\left.\begin{aligned} \frac{a\boldsymbol{F}[0]}{\delta_t}&=\frac{3}{8}(1-\varepsilon^2)\tan\alpha_a\sum_{k=2,4,\cdots}\varepsilon^{k-1}d_k\\ \frac{a\boldsymbol{F}[\pm N\omega]}{\delta_t}&=\frac{3}{16}\varepsilon^{N/2-1}\Big[(1-\varepsilon^2)\tan\alpha_a\Big\{\sum_{k=2,4,\cdots}\varepsilon^k(d_{k+N}+d_k)-D_N\Big\}\\ &\quad\mp(1+\varepsilon^2)\sin\alpha_a\Big\{\frac{2\varepsilon(1+\varepsilon)}{1+\varepsilon^2}d_N+\sum_{k=2,4,\cdots}\varepsilon^k(d_{k+N}-d_k)+D_N\Big\}\Big] \end{aligned}\right\} \tag{2.3}$$

where

$$D_2=0,\ D_K=\sum_{k=2,4,\cdots}^{K-2}d_k,\ K=4,\ 6,\ \cdots \tag{2.4}$$

The characteristics of $\boldsymbol{F}[\pm N\omega]$ are explained in Figs. 2. 2 and 2. 3(a), (b), and (c) which show the numerical results of Eqs. (2. 2) and (2. 3). In these figures notations [0], [+2ω], [−2ω], ... represent $\boldsymbol{F}[0]$, $\boldsymbol{F}[+2\omega]$, $\boldsymbol{F}[-2\omega]$, ..., respec-

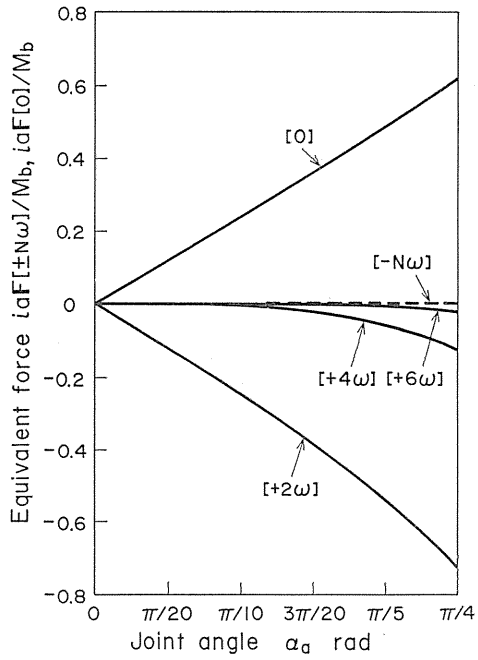

Fig. 2. 2. Equivalent forces caused by constant resisting moment M_b.

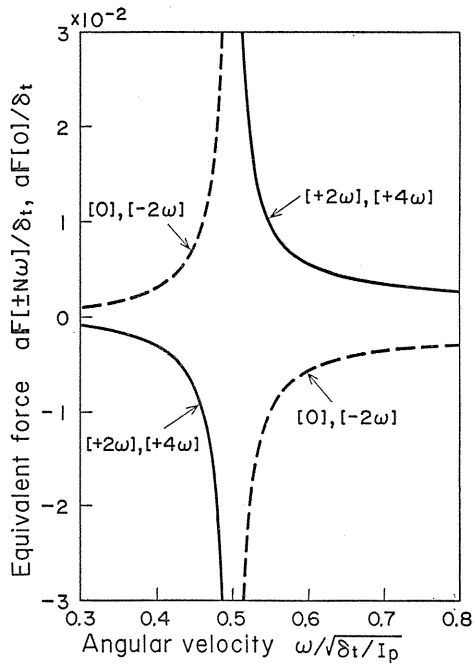

(a) $\omega/\sqrt{\delta_t/I_p} \fallingdotseq 1/2$, $\alpha_a=\pi/12$ rad.

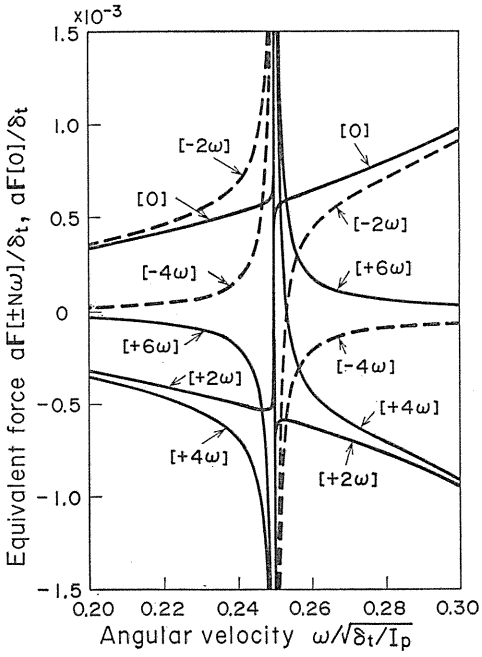

(b) $\omega/\sqrt{\delta_t/I_p} \fallingdotseq 1/4$, $\alpha_a=\pi/12$ rad.

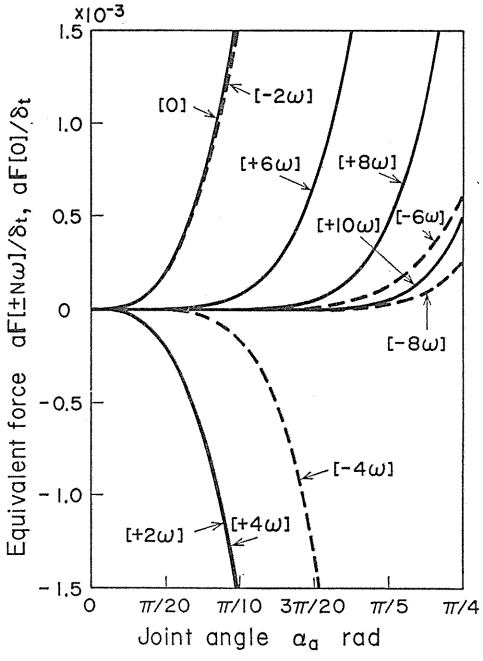

(c) $\omega/\sqrt{\delta_t/I_p}=0.3$.

Fig. 2. 3. Equivalent forces caused by torsional vibration of shaft S_h.

tively. Figure 2. 2 shows the influence of α_a on the equivalent force due to M_b. The magnitude of these forces, as is known from Eq. (2. 2), depends only on the joint angle α_a, and does not concern the angular velocity of the drive shaft ω. Equivalent forces except for $F[0]$, $F[+2\omega]$, $F[+4\omega]$, and $F[+6\omega]$ are very small when α_a is smaller than $\pi/4$. Figures 2. 3(a) and (b) show the equivalent forces in the case that the drive shaft rotates with an angular velocity nearly equal to one-second and one-fourth as large as the natural angular frequency of torsional vibration $p_t=\sqrt{\delta_t/I_p}$. These equivalent forces, except for the torsional resonance ($\omega/p_t=1/N$), vary monotonously with the angular velocity ω. As shown in Fig. 2. 3(a), $F[+2\omega]$ is nearly equal to $F[-2\omega]$ in absolute value and differs from it in sign. Accordingly, resultant force $F[+2\omega]e^{i2\omega t}+F[-2\omega]e^{-i2\omega t}$ varies only in the y direction. Figure 2. 3(c) shows the equivalent forces for the joint angle α_a, where $\omega/p_t=0.3$. These equivalent forces show a steep increase for a certain value of α_a. Thus the equivalent force F_z is generally given by composition of the vectors rotating with the angular velocities $\pm N\omega$. The component (2. 2) due to the constant moment differs in phase by $\pi/2$ from the component (2. 3) due to the torsional vibration.

The equivalent moments, apparently from Eq. (2. 1), have the same characteristics as the equivalent forces.

2. 3. Equations of motion and their solution

Equations of motion of the shaft system shown in Fig. 2. 1 are introduced on the following assumptions: The rotor D is well balanced, subjected only to the equivalent force and moment. The displacements of the rotor D, that is, z and θ_z concerning its translation and inclination, are considered

$$z=x+iy,\ \theta_z=\theta_x+i\theta_y \tag{2.5}$$

Variables x and y are x and y components in deflection, and θ_x and θ_y are angles projectional to the xz and yz planes of deflection angle of shaft at the position S where the rotor is mounted, respectively.

Equations of motion have been reported[22,43,44] for a shaft which rotates with variable speed. The equations of motion involve the second order of a small displacement. Here considering the angular velocity of the rotor D

$$\dot{\theta}_s=\omega\{1+\sum_{N=2,4,\cdots}\varepsilon^{N/2}(2+Nd_N)\cos N\omega t\} \tag{2.6}$$

we arrive at the following equations of motion:

$$\left.\begin{aligned} &m\ddot{z}+c_1\dot{z}+\alpha z+\gamma\theta_z=F_z \\ &I\ddot{\theta}_z-iI_p\omega\dot{\theta}_z+c_2\dot{\theta}_z+\delta\theta_z+\gamma z=M_z \end{aligned}\right\} \tag{2.7}$$

where m is mass of the rotor; α, γ, and δ are spring constants of the shaft; c_1 and c_2 are viscous damping coefficients for translation and inclination of the rotor, respectively.

In the following discussion, the terms $[+N\omega]$ vibration and $[-N\omega]$ vibration are used. They are vibrations of the driven shaft whirling with the angular velocity $N\omega$. The $[+N\omega]$ vibration means a vibration of the shaft whirling in the same direction as the drive shaft rotation, and the $[-N\omega]$ vibration that of the shaft

whirling in the reverse direction.

The forced vibrations for z and θ_z are given in the following form:

$$\left.\begin{aligned} z &= \boldsymbol{A}[0] + \sum_{N=2,4,\cdots} \{\boldsymbol{A}[+N\omega]e^{iN\omega t} + \boldsymbol{A}[-N\omega]e^{-iN\omega t}\} \\ \theta_z &= \boldsymbol{B}[0] + \sum_{N=2,4,\cdots} \{\boldsymbol{B}[+N\omega]e^{iN\omega t} + \boldsymbol{B}[-N\omega]e^{-iN\omega t}\} \end{aligned}\right\} \quad (2.8)$$

where, $\boldsymbol{A}[0]$ and $\boldsymbol{B}[0]$ are the static deflection and the static angle of deflection, $\boldsymbol{A}[+N\omega]$ and $\boldsymbol{B}[+N\omega]$ are the complex amplitudes of the $[+N\omega]$ vibration, $\boldsymbol{A}[-N\omega]$ and $\boldsymbol{B}[-N\omega]$ are those of the $[-N\omega]$ vibration.

Calculated amplitudes $\boldsymbol{A}[+2\omega]$ and $\boldsymbol{A}[+4\omega]$ are shown in Figs. 2. 4(a), (b), (c), and (d). In these figures, the solid line ($p_t/\sqrt{\alpha/m}=0.816$) shows the results which are calculated by using parameters of an experimental apparatus (experiment I for rigid coupling C_r in section 2. 4); the broken line ($p_t/\sqrt{\alpha/m}=1.042$) shows the results which are derived by using torsional rigidity $\delta_t/(\alpha l^2)$ somewhat larger than that of the experimental apparatus. As can be seen from Fig. 2. 4, $p_t/2$ and $p_t/4$ in this apparatus nearly coincide with the critical speeds $\omega_c[+2\omega]$ and $\omega_c[+4\omega]$ of the $[+2\omega]$ and $[+4\omega]$ vibrations for $p_t/\sqrt{\alpha/m}=0.816$, whereas they are separated for $p_t/\sqrt{\alpha/m}=1.042$.

Figure 2. 4(a) shows the amplitude $|\boldsymbol{A}[+2\omega]|$ in the case that the drive shaft rotates near the critical speed $\omega_c[+2\omega]/\sqrt{\alpha/m}=0.448$. The amplitude is considerably large in this neighborhood because $p_t/2$ is nearly equal to $\omega_c[+2\omega]$. Figure 2. 4(b) shows that the double frequency vibrations passing through the critical speed do not change in phase because the phase reverses twice. When $p_t/2$ is different from $\omega_c[+2\omega]$, the double frequency vibrations generated near $\omega_c[+2\omega]$ are smaller than those when it is nearly equal to $\omega_c[+2\omega]$ and a new peak of amplitude due to the torsional resonance appears near $\omega=p_t/2$. The $[-2\omega]$ vibration has the peak of amplitude near the critical speeds $\omega_c[-2\omega]/\sqrt{\alpha/m}=0.435$ and 1.041, and near the resonance point of the torsional vibration. The characteristic of the $[-2\omega]$ vibration near $\omega/\sqrt{\alpha/m}=0.435$ is similar to that of the $[+2\omega]$ vibration. In this experimental apparatus, $\omega_c[+2\omega]/\sqrt{\alpha/m}=0.448$ is nearly equal to $\omega_c[-2\omega]/\sqrt{\alpha/m}=0.435$; accordingly, the double frequency vibrations are seemingly reduced to a rectilinear vibration.

Figure 2. 4(c) shows the amplitude $|\boldsymbol{A}[+4\omega]|$ in the case that the drive shaft rotates near the critical speed $\omega_c[+4\omega]/\sqrt{\alpha/m}=0.223$. The left-hand peak of the two peaks shown by the solid line is due to the torsional resonance. The $[+4\omega]$ vibration reduces to zero in amplitude at an angular velocity ($\omega/\sqrt{\alpha/m}\fallingdotseq 0.207$) slightly larger than $p_t/4$. This is known from Fig. 2. 3(b) too. A phase diagram is shown in Fig. 2. 4(d). The $[-4\omega]$ vibration makes a resonance near $\omega/\sqrt{\alpha/m}=0.219$ and 0.596, and its amplitude is smaller than that of the $[+4\omega]$ vibration.

The $[\pm N\omega]$ vibrations concerning the deflection angle are similar to the deflection in characteristic.

The angular velocity $\dot{\Theta}$ of the driven yoke has components which vary with the even multiples of ω. Accordingly, the torsional vibration makes a resonance when the drive shaft rotates with one of the even submultiples of the natural angular frequency concerning torsional vibration. As a result, the secondary moment due to the torsional vibration excites an even multiple lateral vibration, and this

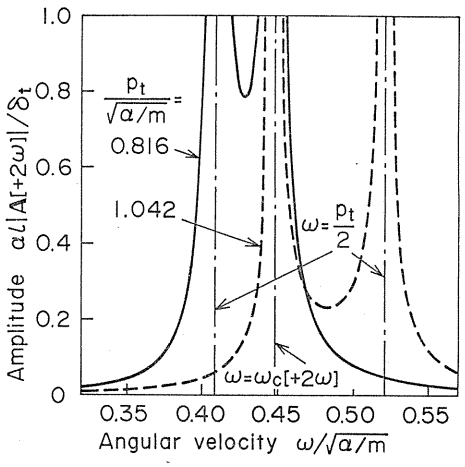

(a) Amplitude of $[+2\omega]$ vibration.

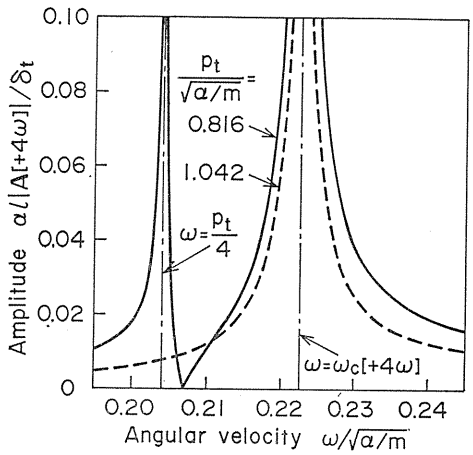

(c) Amplitude of $[+4\omega]$ vibration.

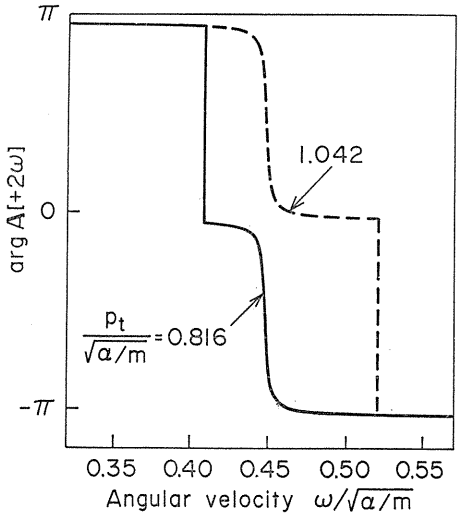

(b) Phase angle of $[+2\omega]$ vibration.

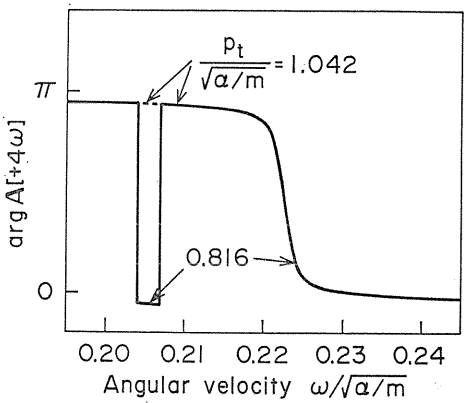

(d) Phase angle of $[+4\omega]$ vibration.

$\alpha_a=0.271$ rad, $I_p/(ml^2)=0.04609$, $I/(ml^2)=0.02315$,
$\gamma/(\alpha l)=-0.1931$, $\delta/(\alpha l^2)=0.1891$, $a/l=0.3798$,
$\delta_t/(\alpha l^2)=0.03074$, $c_1/\sqrt{m\alpha}=0.0073$,
$c_2\sqrt{\alpha/m}/(\alpha l^2)=0.00038$, $M_b=0$.

Fig. 2. 4. Amplitude and phase angle of even multiple vibrations.

resonance diagram has a peak similar to normal resonance.

2. 4. Experiments

2. 4. 1. Experimental apparatus and method

A schematic diagram of the experimental apparatus is shown in Fig. 2. 5. Drive source is 5 kW D. C. motor, which drives a shaft S_{d1} through a stepless speed converter, V-belt, and V-pulley. A flywheel F with a large polar moment of inertia

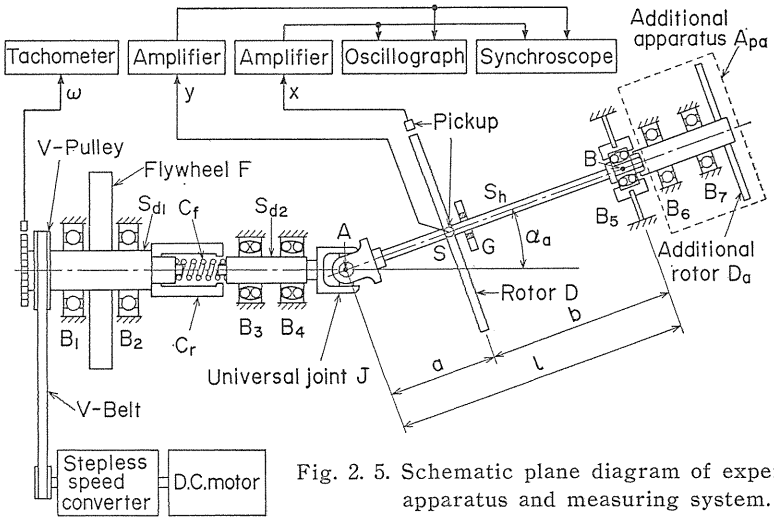

Fig. 2. 5. Schematic plane diagram of experimental apparatus and measuring system.

is mounted on the shaft S_{d1} so that it rotates with a constant speed. The shaft S_{d1} drives a shaft S_{d2} connected directly with the drive yoke of the universal joint J through either a rigid coupling C_r or a flexible one C_f. The coupling C_f is made of a coil spring with a torsional rigidity smaller than that of a driven shaft S_h. When the coupling C_f is used in place of the coupling C_r, a secondary moment will be much smaller. The driven shaft S_h is made of round-bar steel, and carries a rotor D of thin disk form. An additional apparatus A_{pa} is prepared to be attached to or detached from the shaft end B. The additional apparatus A_{pa} consists of an additional rotor D_a and a rigid shaft supported by two bearings B_6, B_7. The torsional natural frequency can be varied by removing the rotor D_a.

Polar moment of inertia of the flywheel F is 0.8028 kg·m^2. The rotor D is 377.2 mm in diameter, 7.1 mm in thickness, 6.196 kg in mass, I_p=0.117 kg·m^2 in polar moment of inertia, and I=0.0561 kg·m^2 in diametral moment of inertia. The driven shaft S_h is l=625.4 mm (a=237.5 mm, b=387.9 mm) in length, 17.97 mm in diameter, 1.912 kg in mass, 207.4 GPa in Young's modulus, and 81.54 GPa in shear modulus. Torsional rigidity of the flexible coupling C_f is 1.42 N·m/rad. Polar moment of inertia of the additional rotor D_a is I_{pa}=0.0200 kg·m^2. The viscous damping coefficient of lateral vibration is 9.8 N·s/m.

Experiments consist of the following I and II.

(1) Experiment I: The additional apparatus A_{pa} is removed. The joint angle α_a is set at 0.117, 0.218, 0.271, and 0.426 rad. Amplitudes are measured in the case that either the rigid coupling C_r or the flexible one C_f is used.

(2) Experiment II: The additional apparatus A_{pa} is attached, and the drive shaft S_{d2} is connected directly to the shaft S_{d1} by the rigid coupling C_r. The joint angle α_a is set at 0.105 rad. Amplitudes of the driven shaft are measured either with the additional rotor D_a attached or without the rotor D_a.

2. 4. 2. Experimental results and consideration

Vibratory waves obtained in experiment I are shown in Figs. 2. 6(a) and (b), and the amplitudes are shown in Figs. 2. 7(a), (b), (c), and (d). The amplitudes

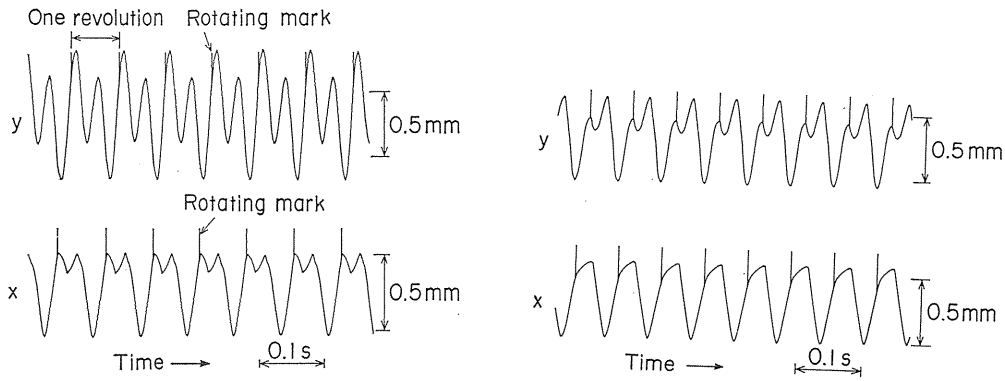

(a) $\omega<\omega_c[+2\omega]$ (ω=826 rpm). (b) $\omega>\omega_c[+2\omega]$ (ω=920 rpm).

Fig. 2. 6. Vibratory waves of $[\pm 2\omega]$ vibrations in rigid coupling C_r (α_a=0.117 rad).

obtained from experiment II are shown in Fig. 2. 8. Notations $[\pm 2\omega]$, $[\pm 3\omega]$, $[\pm 4\omega]$, ... in Figs. 2. 7 and 2. 8 represent the lateral vibrations whirling with two, three, four, ... times as large as ω; abbreviation R. C. or F. C. in Fig. 2. 7 indicates that the coupling C_r or C_f is used.

Figures 2. 6(a) and (b) show the vibratory waves x, y for the rigid coupling C_r and the joint angle α_a=0.117 rad when the drive shaft rotates near the critical speed $\omega_c[+2\omega]$. Figure 2. 6(a) shows the vibratory waves at the angular velocity lower than $\omega_c[+2\omega]$, while Fig. 2. 6(b) indicates those at higher velocity. The comparison between the phase of the vibratory wave and the rotating mark of the rotor reveals that the double frequency vibration varies largely by 4.85 rad in phase when the angular velocity ω is passed through $\omega_c[+2\omega]$ (refer to Fig. 2. 4(b)). Apparently, this characteristic appears due to a simultaneous resonance of the lateral and torsional vibrations. The double frequency vibration is certainly a forced vibration caused by a secondary moment. The amplitude of the y direction is larger than that of the x direction because the $[+2\omega]$ and $[-2\omega]$ vibrations simultaneously make a resonance.

The amplitudes for each joint angle α_a of 0.117, 0.218, 0.271, and 0.426 rad are shown in Figs. 2. 7(a), (b), (c), and (d), respectively (experiment I). The even multiple vibration for the flexible coupling C_f is much smaller than that for the rigid coupling C_r. This shows that the main cause of the even multiple vibration is the secondary moment M''_θ proportional to the drive moment M_θ which the universal joint gives to the driven shaft (refer to Eq. (1. 13)). When the rigid coupling C_r is used, the even multiple vibration increases with the joint angle α_a, and the $[\pm 2\omega]$ vibrations have a component predominantly in the y direction.

The calculated results of the rotating forces $F[\pm N\omega]$ equivalent to the secondary moment M''_θ are shown in Table 2. 1. $F[+2\omega]$ is nearly equal to $F[-2\omega]$ in absolute value, opposite to $F[-2\omega]$ in direction. Except for $F[\pm 2\omega]$, $F[+N\omega]$ is larger than $F[-N\omega]$ in absolute value. These coincide well with the results shown in Fig. 2. 7. Figure 2. 8 shows the resonance curves when the additional rotor D_a is attached or detached (experiment II). The amplitude of the $[\pm 2\omega]$ vibrations with additional rotor D_a is considerably smaller than that without D_a, while the $[\pm 4\omega]$ vibrations change little. The calculated results about the rotating forces $F[\pm N\omega]$ are given in Table 2. 2. These values match well the results shown in Fig. 2. 8.

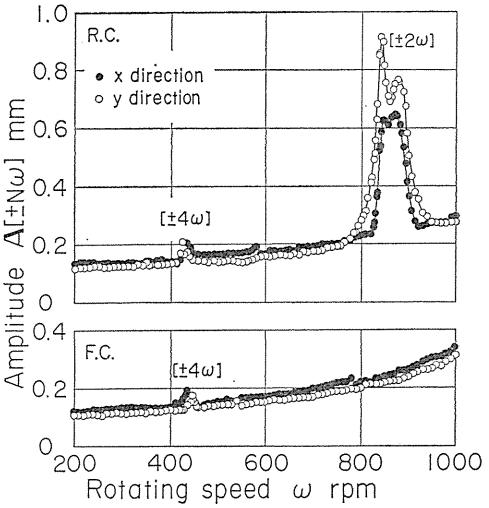

(a) α_a=0.117 rad.

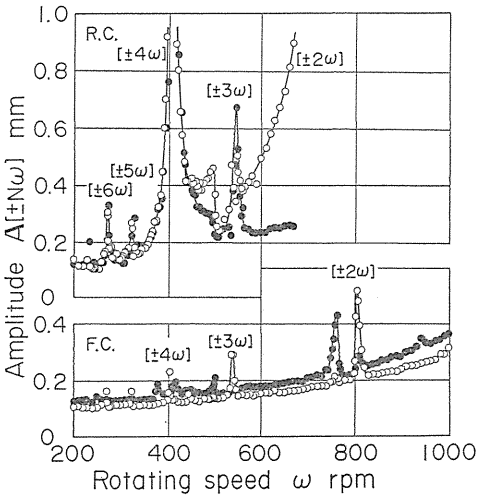

(c) α_a=0.271 rad.

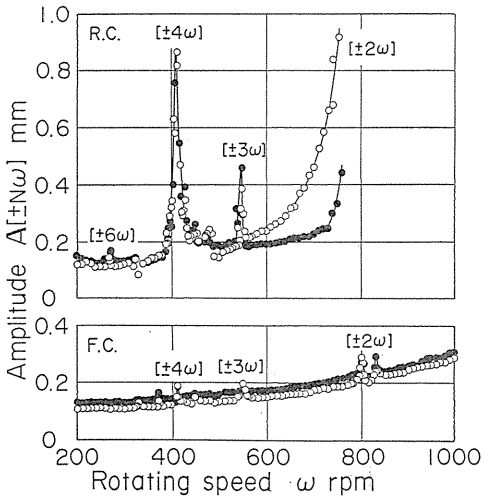

(b) α_a=0.218 rad.

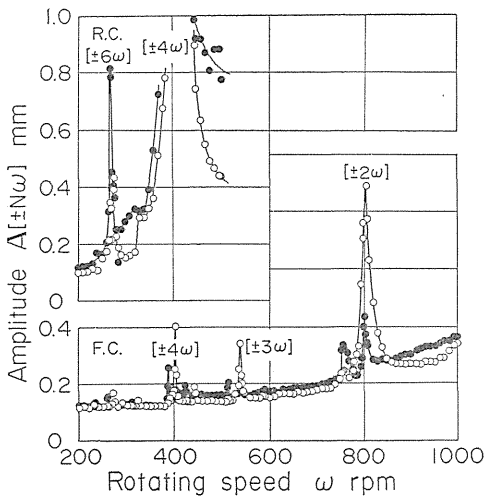

(d) α_a=0.426 rad.

Fig. 2. 7. Comparison of even multiple vibrations $[\pm N\omega]$ in rigid coupling C_r and those in flexible coupling C_f (Experiment I).

Table 2. 1. Comparison of equivalent forces for rigid coupling C_r and those for flexible coupling C_f (α_a=0.271 rad).

$\omega/\sqrt{\alpha/m}$	N	Rigid coupling C_r		Flexible coupling C_f	
		$aF[+N\omega]/\delta_t$	$aF[-N\omega]/\delta_t$	$aF[+N\omega]/\delta_t$	$aF[-N\omega]/\delta_t$
0.448	2	-2.15×10^{-3}	2.16×10^{-3}	-7.83×10^{-7}	7.61×10^{-7}
0.223	4	-3.09×10^{-4}	1.32×10^{-5}	7.16×10^{-7}	2.14×10^{-8}
0.148	6	-7.83×10^{-6}	1.49×10^{-7}	-2.15×10^{-8}	-5.00×10^{-10}

Table 2. 2. Comparison of equivalent forces without additional rotor D_a and those with D_a ($\alpha_a=0.105$ rad).

$\omega/\sqrt{\alpha/m}$	N	$I_{pa}/I_p=0$		$I_{pa}/I_p=0.1791$	
		$aF[+N\omega]/\delta_t$	$aF[-N\omega]/\delta_t$	$aF[+N\omega]/\delta_t$	$aF[-N\omega]/\delta_t$
0.496	2	1.69×10^{-4}	-1.69×10^{-4}	1.12×10^{-4}	-1.12×10^{-4}
0.248	4	-3.16×10^{-5}	-2.04×10^{-7}	-4.30×10^{-5}	-1.96×10^{-7}
0.165	6	-1.00×10^{-7}	-4.20×10^{-10}	-1.85×10^{-7}	-6.07×10^{-10}

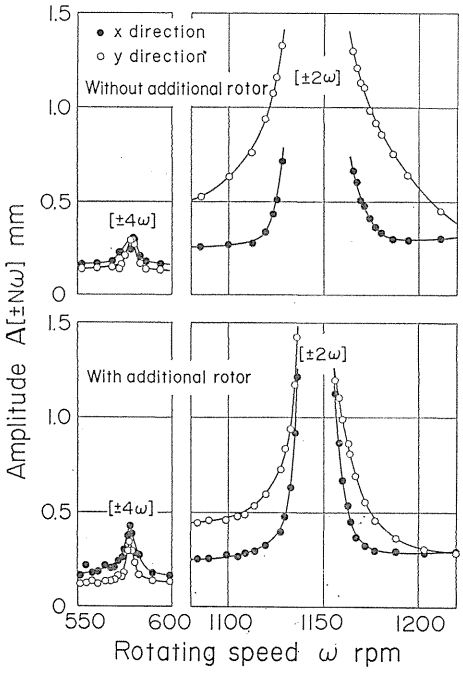

$I_{pa}/I_p=0.1791$, $\alpha_a=0.105$ rad.

Fig. 2. 8. Comparison of even multiple vibrations $[\pm N\omega]$ without additional rotor D_a and those with D_a (Experiment II).

Since the above-mentioned experimental results coincide well with the analytical results in section 2. 3, the even multiple vibrations are clearly caused by the secondary moment M''_θ.

2. 5. *Conclusions*

Forced vibrations due to the secondary moment of a universal joint are studied, and the results obtained may be summarized as follows:

(1) When the drive shaft rotates with an angular velocity ω nearly equal to even integer submultiple of the torsional or lateral natural frequencies, the driven shaft makes a resonance and undergoes an even multiple vibration.

(2) A constant moment M_b resisting the rotation of the driven shaft causes the $[+N\omega]$ vibrations ($N=2, 4, 6, \ldots$), in which the driven shaft whirls forward with even integer multiples of angular velocity $N\omega$. When the joint angle α_a is small, only the $[+2\omega]$ vibration is caused and its amplitude increases proportionally to α_a.

(3) The secondary moment by the torsional vibration is the main cause of the even multiple vibration, especially for $[\pm2\omega]$ and $[+4\omega]$ vibrations. The amplitudes increase steeply with a joint angle α_a larger than a certain value.

(4) The even multiple vibration caused by the constant resisting moment M_b differs by $\pi/2$ in phase from that by the torsional vibration.

(5) An appropriate dimension of the driven shaft system causes large $[-2\omega]$ and $[+4\omega]$ vibrations near the major critical speed too.

3. Forced Vibrations Caused by Frictions between a Cross-Pin and Yokes[45]

3. 1. Introduction

A rotating shaft driven by a universal joint can make vibrations because of frictions between a cross-pin and yokes of the universal joint. This chapter investigates the force exciting the driven shaft system by viscous and Coulomb's frictions for the relative angular motion between the cross-pin and the yokes. And it is explained what lateral vibrations the driven shaft performs. Analyses and experiments showed the following results. Viscous friction between the cross-pin and the yokes can hardly cause a vibration. When the vibration occurs, the amplitude increases with the larger joint angle. Coulomb's friction causes the vibration independent of the joint angle.

3. 2. Moment given to the driven shaft through a universal joint

Moment due to viscous and Coulomb's frictions are assumed to act on the relative angular motion between the cross-pin and the yokes. When frictions does not act on the relative motion between the cross-pin and the yokes, the transmitted moment of universal joint $\mathbb{M}_{a0}$ is expressed by the vector product (1. 6). When the frictions act, the transmitted moment $\mathbb{M}_a$ has both components of $\boldsymbol{p}(\Psi)$ and $\boldsymbol{q}(\Theta)$ directions. Let these components be M'_Ψ and M'_Θ, respectively. Then $\mathbb{M}_a$ is given by the following equation.

$$\mathbb{M}_a=\mathbb{M}_{a0}+M'_\Psi\boldsymbol{p}(\Psi)+M'_\Theta\boldsymbol{q}(\theta) \tag{3.1}$$

The moments M'_Ψ and M'_Θ caused by the frictions are obtained as follows.

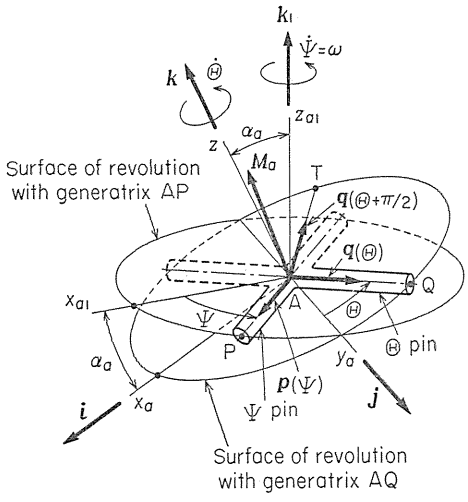

Fig. 3. 1. Relation between a cross-pin A-PQ and two stationary rectangular co-ordinate systems A-$x_{a1}y_az_{a1}$, A-x_ay_az ($\angle$PAQ=$\angle$QAT=$\pi/2$).

Let $\dot\Psi'$ be an angular velocity of Θ pin about Ψ pin, and $\dot\Theta'$ be an angular velocity of Ψ pin about Θ pin. That is, $\dot\Psi'$ is the component of $\dot\Theta\boldsymbol{k}$ to the direction $\boldsymbol{p}(\Psi)$, and $\dot\Theta'$ is that of $\dot\Psi\boldsymbol{k}_1$ to the direction $\boldsymbol{q}(\Theta)$. Then $\dot\Psi'$ and $\dot\Theta'$ are given by the following equations (refer to Fig. 3. 1 and appendix).

$$\left.\begin{aligned}\dot\Psi'&=\dot\theta\boldsymbol{k}\cdot\boldsymbol{p}(\Psi)=\dot\theta\sin\alpha_a\cos\Psi\\ \dot\theta'&=\dot\Psi\boldsymbol{k}_1\cdot\boldsymbol{q}(\theta)=\dot\Psi\sin\alpha_a\sin\theta\end{aligned}\right\} \tag{3.2}$$

where dot notation means differentiation with respect to time t. The drive shaft gives Ψ pin the moment

$$M'_\Psi=-c_\Psi\dot\Psi'-M_{\Psi0}\,\mathrm{sgn}(\dot\Psi') \tag{3.3}$$

which points to $\boldsymbol{p}(\Psi)$ direction, and Θ pin gives the driven shaft the moment

$$M'_\Theta = c_\Theta \dot{\theta}' + M_{\Theta 0} \operatorname{sgn}(\dot{\theta}') \tag{3.4}$$

which points to $\boldsymbol{q}(\Theta)$ direction. Where c_Ψ and $M_{\Psi 0}$ are a coefficient of viscous friction and a moment caused by Coulomb's friction for the relative angular motion between the drive yoke and Ψ pin, and c_Θ and $M_{\Theta 0}$ are those for the relative angular motion between the driven yoke and Θ pin, respectively.

Considering Eqs. (1. 3) and (1. 4), we obtain each components M_Θ, M'_Θ, and M''_Θ of the transmitted moment $\mathbb{M}_a$ to $\boldsymbol{k}$, $\boldsymbol{q}(\Theta)$, and $\boldsymbol{q}(\Theta+\pi/2)$ directions as follows.

$$\begin{aligned} M_\Theta &= \mathbb{M}_a \cdot \boldsymbol{k} \\ &= M_{a0}\sqrt{H(\Psi)} - c_\Psi \dot{\theta} \sin^2 \alpha_a \cos^2 \Psi - M_{\Psi 0} |\sin \alpha_a \cos \Psi| \end{aligned} \tag{3.5}$$

$$\begin{aligned} M'_\Theta &= \mathbb{M}_a \cdot \mathbb{q}(\Theta) \\ &= c_\Theta \dot{\Psi} \sin \alpha_a \sin \Theta + M_{\Theta 0} \operatorname{sgn}(\sin \alpha_a \sin \Theta) \end{aligned} \tag{3.6}$$

$$\begin{aligned} M''_\Theta &= \mathbb{M}_a \cdot \boldsymbol{q}(\Theta+\pi/2) \\ &= M_{a0} \sin \alpha_a \cos \Psi + \{c_\Psi \dot{\theta} \sin \alpha_a \cos \Psi + M_{\Psi 0} \operatorname{sgn}(\sin \alpha_a \cos \Psi)\} \sqrt{H(\Psi)} \end{aligned} \tag{3.7}$$

in which M_Θ influences the torsional vibration of shaft, M'_Θ and M''_Θ the lateral vibration.

Furthermore, the component of $\mathbb{M}_a$ to $\boldsymbol{k}_1$ direction, namely, the drive torque M_Ψ is given by the following equation.

$$\begin{aligned} M_\Psi &= \mathbb{M}_a \cdot \boldsymbol{k}_1 \\ &= M_{a0} \cos \alpha_a / \sqrt{H(\Psi)} + c_\Theta \dot{\Psi} \sin^2 \alpha_a \sin^2 \Theta + M_{\Theta 0} |\sin \alpha_a \sin \Theta| \end{aligned} \tag{3.8}$$

Energy loss E_l per unit time is found by differentiating orthogonal condition of the cross-pin (1. 2) with respect to time t and by using Eqs. (3. 5) and (3. 8).

$$\begin{aligned} E_l &= \dot{\Psi} M_\Psi - \dot{\theta} M_\Theta \\ &= (c_\Theta \omega^2 \sin^2 \Theta + c_\Psi \dot{\theta}^2 \cos^2 \Psi) \sin^2 \alpha_a \\ &\quad + \omega M_{\Theta 0} |\sin \alpha_a \sin \Theta| + \dot{\theta} M_{\Psi 0} |\sin \alpha_a \cos \Psi| \end{aligned} \tag{3.9}$$

Equation (3. 9) shows that $E_l > 0$ holds and the drive shaft needs a surplus torque E_l/ω owing to the frictions.

The quantity M'_Θ is a known function of time t, and M''_Θ of Eq. (3. 7) is rewritten by using Eq. (3. 5) and eliminating M_{a0} as follows:

$$M''_\Theta = \{M_\Theta \sin \alpha_a \cos \Psi + c_\Psi \dot{\theta} \sin \alpha_a \cos \Psi + M_{\Psi 0} \operatorname{sgn}(\sin \alpha_a \cos \Psi)\} / \sqrt{H(\Psi)} \tag{3.10}$$

The quantity M_Θ is decided by a dynamical character of the driven shaft system. The secondary moment concerning M_Θ (the first term in the right-hand side of Eq. (3. 10)) coincides with Eq. (1. 13) in Chapter 1.

3. 3. Vibration caused by viscous friction

A driven shaft of Fig. 3. 3 is considered. The sections AS and SB of the shaft have uniform circular sections, which may differ from one another in diameter.

This section explains characteristics of the forced vibration caused by the viscous friction between the cross-pin and the yokes. That is, M'_θ and M''_θ are assumed to be given by the following equations.

$$\left.\begin{aligned} M'_\theta &= c_\theta \omega \sin \alpha_a \sin \theta \\ M''_\theta &= c_\theta \dot{\theta} \sin \alpha_a \cos \Psi / \sqrt{H(\Psi)} \end{aligned}\right\} \tag{3.11}$$

The method similar to Chapter 1 gives a force F' and a moment M' equivalent to M'_θ and those F'' and M'' equivalent to M''_θ, which act on the rotor D. Figure 3. 2 shows the equivalent forces F' and F'' and the moments M' and M'' shown in the xy plane. The following equations hold regardless of the supporting condition at the shaft end B, that is, whether the shaft end B is simply supported or fixed.

$$\left.\begin{aligned} F' &= 3M'_\theta/(2a),\ M' = -M'_\theta/2 \\ F'' &= 3M''_\theta/(2a),\ M'' = -M''_\theta/2 \end{aligned}\right\} \tag{3.12}$$

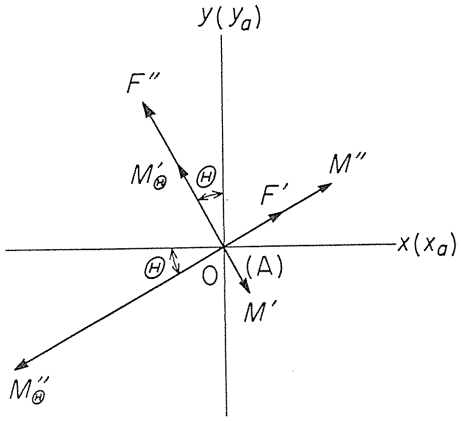

Fig. 3. 2. Equivalent forces F' and F'' and moments M' and M'' acting on a rotor D.

Using Eqs. (1. 17) and (1. 18) yields Fourier series for F_x, F_y, M_x, and M_y which are the sums of each components of F', F'', M', and M'' to the directions x and y as the following equations.

$$\left.\begin{aligned} F_x &= \sum_{N=2,4,\cdots} F_{xN} \sin N\Psi \\ F_y &= F_{y0} + \sum_{N=2,4,\cdots} F_{yN} \cos N\Psi \end{aligned}\right\} \tag{3.13}$$

$$M_x = aF_y/3,\ M_y = -aF_x/3 \tag{3.14}$$

where

$$\left.\begin{aligned} aF_{xN}/\omega &= (3/32)\,\varepsilon^{N/2-2}(1-\varepsilon^2)\tan\alpha_a \\ &\quad \times[4N\varepsilon(c_\theta - c_\Psi) - c_\theta\{N-2+2N\varepsilon+(N+2)\varepsilon^2\}\sin^2\alpha_a] \\ aF_{y0}/\omega &= (3/4)\tan\alpha_a\left\{c_\theta(1-\varepsilon)+c_\Psi\cos\alpha_a\left(1+2\sum_{k=1}^{\infty}\varepsilon^k\right)\right\} \\ aF_{yN}/\omega &= (3/4)\,\varepsilon^{N/2-1}\tan\alpha_a \\ &\quad \times\left[-c_\theta(1-\varepsilon)^2+c_\Psi\cos\alpha_a\left\{N(1+\varepsilon)^2/2-2\varepsilon+4\sum_{k=1}^{\infty}\varepsilon^k\right\}\right] \end{aligned}\right\} \tag{3.15}$$

Because the exciting moments M_x and M_y are proportional to the exciting forces F_y and $-F_x$, F_x and F_y are considered hereafter. Equations (3. 13) and (3. 15) show that F_x and F_y generally consist of components of even multiple as large as the drive speed ω. Therefore the driven shaft can make even multiple vibrations with the frequencies $N\omega$ ($N=2, 4, \ldots$).

A small parameter

$$\varepsilon_\alpha = \sin \alpha_a \tag{3.16}$$

is considered in order to expand Eq. (3. 15) into power series of ε_α. If small quantities of ε_α to the fifth or more powers are neglected, the following equations are obtained by using Eq. (1. 18).

$$\left.\begin{aligned}
aF_{x2}/\omega &= 3\varepsilon_\alpha(c_\Theta - c_\Psi)/4 - 3\varepsilon_\alpha^3 c_\Psi/8 \\
aF_{x4}/\omega &= 3\varepsilon_\alpha^3(c_\Theta - 2c_\Psi)/16 \\
aF_{y0}/\omega &= 3\varepsilon_\alpha(c_\Theta + c_\Psi)/4 + 3\varepsilon_\alpha^3(c_\Theta + 2c_\Psi)/16 \\
aF_{y2}/\omega &= -3\varepsilon_\alpha(c_\Theta - c_\Psi)/4 + 3\varepsilon_\alpha^3 c_\Psi/4 \\
aF_{y4}/\omega &= -3\varepsilon_\alpha^3(c_\Theta - 2c_\Psi)/16
\end{aligned}\right\} \tag{3.17}$$

Generally, F_{xN} and F_{yN} ($N=2, 4, \ldots$) are small quantities of the order of $\varepsilon_\alpha{}^{N-1}$. In a universal joint on the market, the friction between Ψ pin and the drive yoke is nearly equal to that between Θ pin and the driven yoke. Accordingly,

$$c_\Theta = c_\Psi \tag{3.18}$$

is assumed to hold in Eq. (3. 17). Then the relation (3. 18) cancels the exciting forces of the order of ε_α which are caused by the viscous friction between Θ pin or Ψ pin and the yoke. Consequently, if small quantities of ε_α to the third or more power are neglected, the exciting forces F_x and F_y are reduced to the following equations.

$$\left.\begin{aligned}
F_x &= 0 \\
F_y &= 3\varepsilon_\alpha c_\Theta \omega/(2a)
\end{aligned}\right\} \tag{3.19}$$

That is, the driven shaft only has a static deflection caused by a constant force to the y direction perpendicular to the plane containing both the drive shaft and the driven one. Exciting forces are not recognized until small quantities of the order of $\varepsilon_\alpha{}^3$ are taken into account under the condition (3. 18), and then the vibration components of 2ω and 4ω appear. But the forced vibrations with frequencies 2ω and 4ω are very small, and the vibration due to viscous friction can be considered hardly to occur. Thus, in order to suppress a vibration caused by the viscous friction, the coefficients of the viscous friction c_Ψ and c_Θ should be made equal to each other and, obviously, the joint angle α_a must be small.

3. 4. Vibration caused by Coulomb's friction

When Coulomb's friction between the cross-pin and the yokes is considered, the moments M'_Θ and M''_Θ can be given by the following equations

$$\left.\begin{aligned} M'_\theta &= M_{\theta 0}\,\mathrm{sgn}(\sin\theta) \\ M''_\theta &= M_{\Psi 0}\,\mathrm{sgn}(\cos\Psi)/\sqrt{H(\Psi)} \end{aligned}\right\} \tag{3.20}$$

Here the case of $\sin\alpha_a>0$, namely, $0<\alpha_a<\pi/2$ is treated.

Equivalent forces F_x and F_y, the sums of each components of F' and F'' to the directions x and y are expressed by the same form as Eq. (3. 13).

$$\left.\begin{aligned} aF_{xN} &= (3/8)M_{\theta 0}\cos\alpha_a \sum_{k=1}^{\infty}(P_k+P_{k+1})(G_{|k-N/2|}-G_{k+N/2}) \\ &\quad +(3/4)M_{\Psi 0}\sec\alpha_a \sum_{k=1}^{\infty}(-1)^k(P_k+P_{k+1})(\varepsilon^{|k-N/2|}-\varepsilon^{k+N/2}) \\ aF_{y0} &= (3/8)M_{\theta 0}(Q_0G_0+2\sum_{k=1}^{\infty}Q_kG_k)+(3/4)M_{\Psi 0}\left\{Q_0+2\sum_{k=1}^{\infty}(-\varepsilon)^kQ_k\right\} \\ aF_{yN} &= (3/4)M_{\theta 0}\left\{Q_0G_N+\sum_{k=1}^{\infty}Q_k(G_{|k-N/2|}+G_{k+N/2})\right\} \\ &\quad +(3/2)M_{\Psi 0}\left\{\varepsilon^{N/2}Q_0+\sum_{k=1}^{\infty}(-1)^kQ_k(\varepsilon^{|k-N/2|}+\varepsilon^{k+N/2})\right\} \end{aligned}\right\} \tag{3.21}$$

, where

$$\left.\begin{aligned} G_k &= \sum_{n=k}^{\infty}\frac{({}_{2n}C_n)({}_{2n}C_{n-k})}{2^{4n-1}}\sin^{2n}\alpha_a \\ P_k &= 4/\{(2k-1)\pi\} \\ Q_k &= -4/\{(4k^2-1)\pi\} \end{aligned}\right\} \tag{3.22}$$

The exciting moments M_x and M_y are given by Eq. (3. 14). The exciting forces F_x and F_y caused by the Coulomb friction consist of the frequency components of even multiple as large as the drive speed ω, and they excite the rotating shaft to the even multiple vibration. The magnitudes of these frequency components are independent of ω (the force caused by the viscous friction is proportional to ω). The terms of the order of $\varepsilon_\alpha{}^0$ are generally contained in power series for $\varepsilon_\alpha=\sin\alpha_a$ of Eq. (3. 21), picking up only these terms produces the following equations

$$\left.\begin{aligned} aF_{xN} &= (3/4)(P_{N/2}+P_{N/2+1})\{M_{\theta 0}+(-1)^{N/2}M_{\Psi 0}\} \\ aF_{y0} &= 3(M_{\theta 0}+M_{\Psi 0})/\pi \\ aF_{yN} &= (3/2)Q_{N/2}\{M_{\theta 0}+(-1)^{N/2}M_{\Psi 0}\} \end{aligned}\right\} \tag{3.23}$$

Here the case of $M_{\Psi 0}=M_{\theta 0}$ is considered. Then the exciting terms for odd integer of $N/2$ disappear, the exciting forces F_x and F_y are approximately expressed by the following equations.

$$\left.\begin{aligned} F_x &= \frac{12M_{\theta 0}}{\pi a}\sum_{N=4,8,\cdots}\frac{N}{N^2-1}\sin N\Psi \\ F_y &= \frac{12M_{\theta 0}}{\pi a}\left(\frac{1}{2}-\sum_{N=4,8,\cdots}\frac{1}{N^2-1}\cos N\Psi\right) \end{aligned}\right\} \tag{3.24}$$

That is, the forced vibrations with the frequencies of 4ω, 8ω, ... can occur in the driven shaft, they have the amplitudes of the order of $\varepsilon_\alpha{}^0$. Such the other vibrations as 2ω, 6ω, ... have the amplitudes of the order of $\varepsilon_\alpha{}^2$. Thus, for the vibration caused by the Coulomb friction, the effect of vibration proof cannot be expected even if the joint angle α_a is made small. But, by putting as $M_{\Psi 0}=M_{\Theta 0}$, the vibrations with frequencies 2ω, 6ω, ... can be fairly suppressed.

3. 5. Experiments

The following experiments are performed to confirm the analytical results of section 3. 4. Figure 3. 3 shows a schematic diagram of experimental apparatus. The drive shaft drives a steel shaft S_h through a universal joint J, and has a flywheel F. The driven shaft S_h carries a rotor D of thin disk form. Bearings B_1 and B_2 are plummer blocks (nominal No. S513), B_3 is a self-aligning double-row ball bearing (nominal No. 1203). The universal joint used in the experiments is shown in Fig. 3. 4. This joint is an article on the market, a joint of Kyowa C-35 type. Each tip of the yokes, as shown in Fig. 3. 4, has a small internal thread. Four bolts B_{t1}, B_{t2}, B_{t3}, and B_{t4} are properly tightened, and the frictions between the cross-pin and the yokes are changed. The majority of frictions is considered to be Coulomb's friction. The moments $M_{\Psi 0}$ and $M_{\Theta 0}$ caused by the friction are measured from the wave form of the damped free vibration in non-rotation ($\omega=0$). For an example, we consider the case that a free vibration is made in a plane perpendicular to Ψ pin. If the frequency is p, and the change in amplitude per one period is $\Delta A(<0)$, then $M_{\Psi 0}$ is given by the following equation[38,46].

$$M_{\Psi 0}=-\Delta A m a p^2/6 \tag{3.25}$$

$M_{\Psi 0}=M_{\Theta 0}$ is adopted and only $M_{\Psi 0}$ is used as parameter because many measurements nearly give $M_{\Psi 0}=M_{\Theta 0}$.

Main dimensions of the experimental apparatus are as follows: Polar moment of inertia of the flywheel F is 0. 341 kg·m^2. The rotor D is 350 mm in diameter, 6. 3 mm in thickness, 4. 690 kg in mass, 0. 0718 kg·m^2 in polar moment of inertia, and 0. 0359 kg·m^2 in diametral moment of inertia. The driven shaft S_h is 207. 4 GPa

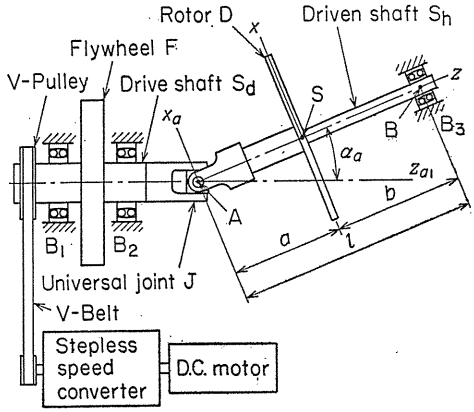

Fig. 3. 3. Schematic plane diagram of experimental apparatus.

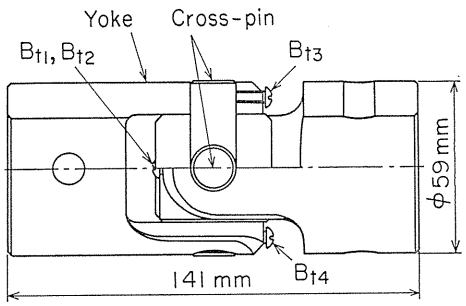

Fig. 3. 4. Universal joint with friction between a cross-pin and yokes.

in Young's modulus, 81.54 GPa in shear modulus, 3.49 kg in mass, $a=300$ mm in length and 40 mm in diameter of the section AS, $b=360$ mm in length and 20 mm in diameter of the section SB.

Figure 3. 5 shows the amplitudes of the even multiple vibrations for the joint angle $\alpha_a=0.183$ rad. The vibrations of frequencies 3ω and 5ω occur too, they are considered to be caused by that the eccentricity coexists with the angular velocity fluctuation. The vibrations of frequencies 2ω, 4ω, and 6ω are considered to contain the vibrations caused by the secondary moment. We can recognize that the vibration with frequency 4ω increases in amplitude with larger $M_{\Psi 0}$. This coincides well with the analytical results for the forced vibration caused by the Coulomb friction in section 3. 4.

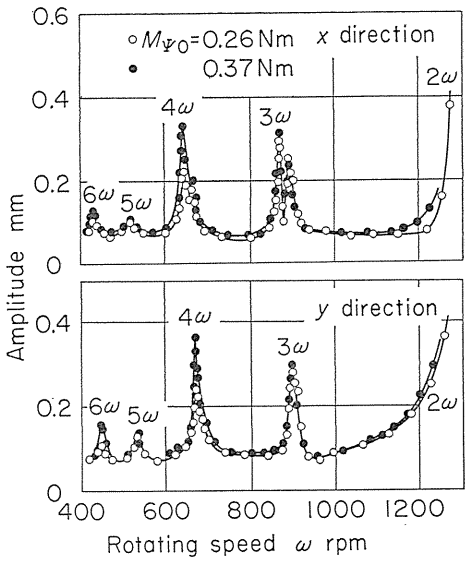

Fig. 3. 5. Change of even multiple vibrations due to friction moment $M_{\Psi 0}$ in a universal joint ($\alpha_a=0.183$ rad).

3. 6. Conclusions

This chapter has dealt with the vibrations generated by the frictions between the cross-pin and the yokes of a universal joint. The results obtained may be summarized as follows:

(1) The viscous friction generally causes the vibrations with the frequencies of even multiple as large as the angular velocity of the drive shaft. These vibrations increase with larger joint angle. When the friction between the cross-pin and the drive yoke is equal to that between the cross-pin and the driven yoke, such even multiple vibration hardly occur. Accordingly for vibration proof the coefficient of the viscous friction in the drive side should be made equal to that in the driven side.

(2) Also the Coulomb friction generally causes the vibrations with the frequencies of even multiple as large as the drive speed ω. The magnitudes of these vibrations are independent of the joint angle. When Coulomb's friction between the cross-pin and the drive yoke is equal to that between the cross-pin and the driven yoke, the vibrations with frequencies 2ω, 6ω, ... are very small in amplitude, and the vibrations with frequencies 4ω, 8ω, ... show the conspicuous magnitudes. Thus the vibrations caused by the Coulomb friction do not become small even if the joint angle becomes smaller. The vibrations with frequencies 2ω, 6ω, ... can be fairly suppressed when the friction between the cross-pin and the drive yoke is equal to that between the cross-pin and the driven yoke.

Appendix

Fujii et al.[30] discuss that the relative angular velocity about one side pivot of the cross-pin in a universal joint is

$$-\alpha_a \omega \sin \omega t \tag{3.26}$$

, which gives a projection angle of conical motion with a vertical angle $2\alpha_a$. But this relative angular velocity (3. 26) coincides neither with $\dot{\Psi}'$ nor with $\dot{\Theta}'$ of Eq. (3. 2).

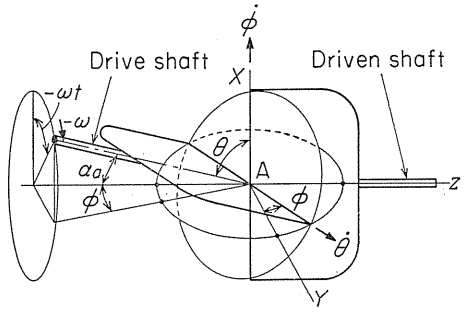

Fig. 3. 6. Eulerian angles θ and ϕ to show angular positions of a cross-pin.

Let's confirm the relation (3. 2) according to Fujii and others. When the drive shaft is viewed from the co-ordinate system A-XYz fixed in the driven shaft, the drive shaft rotates about the center axis Az of the driven shaft. The motion of this rotation can be expressed by Eulerian angles θ, ϕ, and $\psi(\equiv 0)$. Quantities $\dot{\theta}$ and $\dot{\phi}$ give the relative angular velocities about the pivots of the universal joint. From Fig. 3. 6 the following equations

$$\left.\begin{aligned} \cos\theta &= \sin\alpha_a \cos\omega t \\ \tan\phi &= -\tan\alpha_a \sin\omega t \end{aligned}\right\} \tag{3.27}$$

are obtained, and differentiation of Eq. (3. 27) with respect to time t yields

$$\left.\begin{aligned} \dot{\theta} &= \omega \sin\alpha_a \sin\omega t / \sqrt{1-\sin^2\alpha_a \cos^2\omega t} \\ \dot{\phi} &= -\omega \tan\alpha_a \cos\omega t / (1+\tan^2\alpha_a \sin^2\omega t) \end{aligned}\right\} \tag{3.28}$$

Putting $\Psi=\omega t$ in Eq. (3. 28) and using Eqs. (1. 3), (1. 4), and (1. 5) arrive at an expression similar to Eq. (3. 2). Here, $\dot{\theta}=\dot{\Theta}'$ and $\dot{\phi}=-\dot{\Psi}'$ hold. Furthermore, if the first equation in Eq. (3. 28) is expanded into power of α_a and the terms of α_a to the third or more powers are neglected, then it becomes the same form as Eq. (3. 26).

4. Unstable Vibration of an Asymmetrical Shaft due to Angular Velocity Fluctuation[47,48]

4. 1. Introduction

In an asymmetrical shaft rotating with a constant speed, an unstable vibration occurs near the major critical speed[49~51]. Then the shaft whirls forward with the same angular velocity as that of shaft rotation.

This chapter deals with lateral vibrations of an asymmetrical shaft driven by a universal joint. The driven shaft with asymmetrical stiffness is vertically assembled, and is connected by the universal joint to a rigid drive shaft which rotates with a constant angular velocity. The shaft system is assumed to have a concentrated mass at the middle point of the shaft with no distributed mass. Equations of motion of the shaft are given by simultaneous equations with parametric excitation, and the solution is obtained in asymptotic expansion form. The

analytical results explain some characteristics concerning the unstable vibrations which are generated on account of the angular velocity fluctuation.

4. 2. Equations of motion

A rotating shaft system driven by a universal joint is assumed as shown in Fig. 4. 1. Bearing B is a self-aligning double-row ball bearing. The flexible driven shaft AB is supported simply by points A and B, and it has an asymmetrical stiffness. The concentrated mass m is attached at the middle point S of the shaft.

As shown in Fig. 4. 2, k_1 and k_2 represent maximum and minimum values of spring constant for deflection at the point S. The direction of maximum rigidity coincides with S1 direction which turns by angle β from the Θ pin (AQ) in the same direction as the shaft rotation. Of course, the direction of maximum rigidity (S1 direction) is at right angles to that of minimum rigidity (S2 direction).

When the vibration is not steady due to small perturbations, that is, the asymmetry and the angular velocity fluctuation of shaft, the drive source delivers an energy to the driven shaft. In this case, the universal joint gives a moment to the driven shaft. Since this moment is a small quantity of the second order of the shaft deflection[52], the influence of such moment can be ignored. The secondary moment mentioned in Chapters 1 and 2 does not occur, provided that no resisting moment acts on the shaft rotation. When z axis is taken vertically, the equations of motion for the deflections x, y at the point S are given by the following:

$$\left.\begin{aligned} m\ddot{x}+c\dot{x}+\frac{k_1+k_2}{2}x-\frac{k_1-k_2}{2}\{x\cos 2(\theta+\beta)+y\sin 2(\theta+\beta)\}=0 \\ m\ddot{y}+c\dot{y}+\frac{k_1+k_2}{2}y-\frac{k_1-k_2}{2}\{x\sin 2(\theta+\beta)-y\cos 2(\theta+\beta)\}=0 \end{aligned}\right\} \quad (4.1)$$

, where c is a viscous damping coefficient for lateral vibration of the point S.

We introduce a parameter

$$p=\sqrt{(k_1+k_2)/(2m)} \quad (4.2)$$

which is the rms value of natural angular frequencies of the asymmetrical shaft.

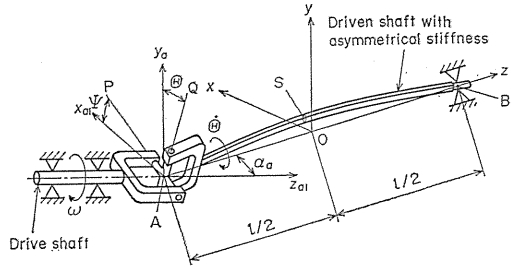

Fig. 4. 1. Asymmetrical shaft driven by a universal joint.

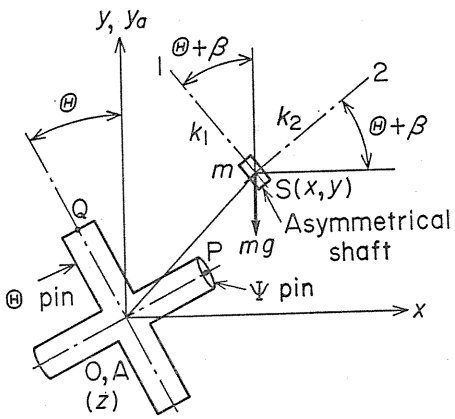

Fig. 4. 2. Co-ordinate systems viewed from z direction ($k_1>k_2$).

The asymmetry of the shaft

$$\Delta=(k_1-k_2)/(k_1+k_2) \tag{4.3}$$

and the damping ratio

$$\zeta=c/(2mp) \tag{4.4}$$

are assumed to be small quantities of the same order as ε given by Eq. (1. 18). The rotating angle Θ of the driven shaft is obtained by integrating Eq. (1. 17) with respect to time as follows:

$$\theta=\omega t+2\sum_{N=2,4,\cdots}\frac{\varepsilon^{N/2}}{N}\sin N\omega t \tag{4.5}$$

By using the notations $\delta_{st}=g/p^2$ (g is acceleration by gravity), $i=\sqrt{-1}$, and the following non-dimensional quantities

$$\left.\begin{aligned} &Z=X+iY=e^{-i\beta}(x+iy)/\delta_{st}\\ &\tau=pt,\ \ \Omega=\omega/p \end{aligned}\right\} \tag{4.6}$$

Eq. (4. 1) is rewritten as the following equation

$$\ddot{Z}+Z=\varepsilon f(\Omega\tau,\ \overline{Z},\ \dot{Z}) \tag{4.7}$$

, where

$$\varepsilon f(\Omega\tau,\ \overline{Z},\ \dot{Z})=-2\zeta\dot{Z}+\Delta\overline{Z}\left[e^{i2\Omega\tau}+\sum_{N=2,4,\cdots}\varepsilon^{N/2}\{e^{i(N+2)\Omega\tau}-e^{i(N-2)\Omega\tau}\}\right] \tag{4.8}$$

$\overline{Z}$ is a conjugate complex number of Z. Dot notation means differentiation with respect to non-dimensional time τ after Eq. (4. 7).

As Eqs. (4. 7) and (4. 8) do not contain β, stability of the driven shaft is independent of the angle β between the principal axis S1 of shaft cross section and the Θ pin.

4. 3. Analyses of vibration

The solution of Eq. (4. 7) for $\varepsilon=0$ is given by

$$Z=Ae^{i(\tau+\phi)}+A^*e^{i(-\tau+\phi^*)} \tag{4.9}$$

Consider the case that the frequency obtained by substitution of Eq. (4. 9) into Eq. (4. 7) is nearly equal to the natural angular frequency. Then

$$1-(k\Omega)^2=d=\varepsilon h\ \ (k=1,\ 2,\cdots) \tag{4.10}$$

holds, and Eq. (4. 7) is rewritten as the following equation

$$\ddot{Z}+(k\Omega)^2Z=\varepsilon\{f(\Omega\tau,\ \overline{Z},\ \dot{Z})-hZ\} \tag{4.11}$$

Here, asymptotic solutions of Eq. (4. 11) are given by applying the method of Bogoliubov and Mitropolsky[37]. As it is not expected until the second approximation that the effect of the angular velocity fluctuation is recognized, the second approximate solutions are studied. In the following, the solutions for $k=1$ and

$k=2$ are shown, and the unstable condition and the characteristic of unstable vibration are examined.

4. 3. 1. $k=1$ ($\Omega \fallingdotseq 1$)

$$Z=Ae^{i(\Omega\tau+\Phi)}+A^*e^{i(-\Omega\tau+\Phi^*)}-\frac{\Delta A^*}{8\Omega^2}e^{i(3\Omega\tau-\Phi^*)} \tag{4.12}$$

$$\left.\begin{aligned}
\dot{A}&=-\zeta A-\frac{\Delta A}{2\Omega}\sin 2\Phi+\frac{\varepsilon\Delta A^*}{2\Omega}\sin(\Phi+\Phi^*)\\
\dot{\Phi}&=d_1-\frac{\Delta}{2\Omega}\cos 2\Phi+\frac{\varepsilon\Delta A^*}{2\Omega A}\cos(\Phi+\Phi^*)\\
\dot{A}^*&=-\zeta A^*-\frac{\varepsilon\Delta A}{2\Omega}\sin(\Phi+\Phi^*)\\
\dot{\Phi}^*&=-d_1^*-\frac{\varepsilon\Delta A}{2\Omega A^*}\cos(\Phi+\Phi^*)
\end{aligned}\right\} \tag{4.13}$$

where

$$\left.\begin{aligned}
d_1&=\frac{1}{2\Omega}\left(d-\zeta^2-\frac{d^2-\Delta^2}{4\Omega^2}\right)\\
d_1^*&=\frac{1}{2\Omega}\left(d-\zeta^2-\frac{d^2-\Delta^2/2}{4\Omega^2}\right)
\end{aligned}\right\} \tag{4.14}$$

Equation (4. 13) is transformed into linear differential equations for U, V, U^*, and V^* defined by the following expressions:

$$\left.\begin{aligned}
&U=A\cos\Phi,\ V=A\sin\Phi\\
&U^*=A^*\cos\Phi^*,\ V^*=A^*\sin\Phi^*
\end{aligned}\right\} \tag{4.15}$$

A characteristic equation is derived from the linear differential equations. The unstable conditions of the shaft system are obtained by the Routh-Hurwitz stability criteria. Concerning the motion of representative points on the (U, V) and (U^*, V^*) planes, the statically unstable condition is either of (a) or (b),

$$\left.\begin{aligned}
&\text{(a)}\quad F_1<0\\
&\text{(b)}\quad F_1>0,\ G_1-4\zeta^2<0,\ G_1^2-4(F_1+4\zeta^4)>0
\end{aligned}\right\} \tag{4.16}$$

and the dynamically unstable condition is

$$G_1^2-4(F_1+4\zeta^4)<0 \tag{4.17}$$

where

$$\left.\begin{aligned}
F_1&=\left(d_1^2+\zeta^2-\frac{\Delta^2}{4\Omega^2}\right)(d_1^{*2}+\zeta^2)-\frac{\varepsilon^2\Delta^2}{4\Omega^2}\left(2d_1d_1^*-2\zeta^2-\frac{\varepsilon^2\Delta^2}{4\Omega^2}\right)\\
G_1&=d_1^2+d_1^{*2}+6\zeta^2-\frac{\Delta^2}{4\Omega^2}(1-2\varepsilon^2)
\end{aligned}\right\} \tag{4.18}$$

In the following the terms S-type unstable vibration and D-type unstable vibration are used. The former is a vibration in which representative points expressed on the (U, V) and (U^*, V^*) planes show a statically unstable behavior, the latter in which representative points show a dynamically unstable behavior. Thus, the S-type unstable vibration has a constant angular velocity of whirling and its amplitude increases monotonously with an exponential function of time. On the contrary, the D-type unstable vibration is accompanied by periodic fluctuation both of its amplitude and angular frequency.

When the rotating shaft system satisfies inequality (4. 16) or (4. 17), a small disturbance gives the shaft system such behavior as follows: Either (a) or (b) of the condition (4. 16) generates the S-type unstable vibrations whirling with angular velocities $\pm\Omega$ and 3Ω. The magnitude of the unstable vibration whirling with 3Ω is about $\Delta/8$ times as large as that whirling with $-\Omega$. Because the frequency does not fluctuate,

$$\dot{\Phi}=0,\ \dot{\Phi}^*=0,\ \dot{\kappa}=0 \tag{4.19}$$

holds (refer to Eq. (4. 13)), where $\kappa=A^*/A$ is used. Equations (4. 13) and (4. 19) decide the amplitude ratio κ and the phase angles Φ, Φ^* of the unstable vibrations whirling with Ω and $-\Omega$. The shaft system for $\varepsilon=0$ has also the damped vibrations whirling with $-\Omega+\dot{\Phi}^*$ and $3\Omega-\dot{\Phi}^*(\dot{\Phi}^*\neq 0)$, and at the same time it undergoes the S-type unstable vibration whirling with Ω. In this case $\cos 2\Phi=2\Omega d_1/\Delta$ is decided by $\dot{\Phi}=0$, and the unstable condition $2\Omega\dot{A}/A=-2\zeta\Omega-\Delta\sin 2\Phi>0$ coincides with the unstable condition which is attained when an asymmetrical shaft rotates with a constant angular velocity[51].

Under the condition (4. 17), the shaft undergoes the D-type unstable vibrations whirling with angular velocities $\Omega+\dot{\Phi}$, $-\Omega+\dot{\Phi}^*$, and $3\Omega-\dot{\Phi}^*$.

4. 3. 2. $k=2$ ($\Omega\fallingdotseq 1/2$)

$$Z=Ae^{i(2\Omega\tau+\Phi)}+A^*e^{i(-2\Omega\tau+\Phi^*)}+\frac{\Delta A}{4\Omega^2}e^{-i\Phi}-\frac{\Delta A^*}{12\Omega^2}e^{i(4\Omega\tau-\Phi^*)} \tag{4.20}$$

$$\left.\begin{aligned}
\dot{A}&=-\zeta A-\frac{\varepsilon\Delta}{4\Omega}\{A\sin 2\Phi-A^*\sin(\Phi+\Phi^*)\}\\
\dot{\Phi}&=d_2-\frac{\varepsilon\Delta}{4\Omega A}\{A\cos 2\Phi-A^*\cos(\Phi+\Phi^*)\}\\
\dot{A}^*&=-\zeta A^*-\frac{\varepsilon\Delta A}{4\Omega}\sin(\Phi+\Phi^*)\\
\dot{\Phi}^*&=-d_2^*-\frac{\varepsilon\Delta A}{4\Omega A^*}\cos(\Phi+\Phi^*)
\end{aligned}\right\} \tag{4.21}$$

where

$$\left.\begin{aligned}
d_2&=\frac{1}{4\Omega}\left(d-\zeta^2-\frac{d^2+4\Delta^2}{16\Omega^2}\right)\\
d_2^*&=\frac{1}{4\Omega}\left(d-\zeta^2-\frac{d^2-4\Delta^2/3}{16\Omega^2}\right)
\end{aligned}\right\} \tag{4.22}$$

Consider the motion of representative points on the (U, V) and (U^*, V^*) planes by using transformation (4. 15) for Eq. (4. 21). The statically unstable condition is

$$F_2<0 \tag{4.23}$$

and the dynamically unstable one is

$$G_2^2-4(F_2+4\zeta^4)<0 \tag{4.24}$$

where

$$\left.\begin{aligned} F_2&=\left(d_2^2+\zeta^2-\frac{\varepsilon^2\Delta^2}{16\Omega^2}\right)(d_2^{*2}+\zeta^2)-\frac{\varepsilon^2\Delta^2}{16\Omega^2}\left(2d_2d_2^*-2\zeta^2-\frac{\varepsilon^2\Delta^2}{16\Omega^2}\right)\\ G_2&=d_2^2+d_2^{*2}+6\zeta^2+\frac{\varepsilon^2\Delta^2}{16\Omega^2}\end{aligned}\right\} \tag{4.25}$$

When the condition (4. 23) is satisfied, the rotating shaft undergoes the S-type unstable vibrations whirling with angular velocities $\pm 2\Omega$ and 4Ω. The magnitude of the unstable vibration whirling with 4Ω is about $\Delta/3$ times as large as that whirling with -2Ω. As Eq. (4. 19) holds in this case, the amplitude ratio $\kappa=A^*/A$ and the phase angles Φ and Φ^* are determined. The center of vibration deviates from the equilibrium point O, and this deviation is about Δ times as large as that of the 2Ω vibration.

When the condition (4. 24) is satisfied, the rotating shaft undergoes the D-type unstable vibrations whirling with $2\Omega+\dot{\Phi}$, $-2\Omega+\dot{\Phi}^*$, and $4\Omega-\dot{\Phi}^*$. The center of vibration deviates, and the magnitude and direction of this deviation fluctuate with time.

When $\varepsilon=0$, any vibration caused by an external disturbance damps with time. This is directly understood by Eq. (4. 21) without examining the conditions (4. 23) and (4. 24).

As for $k=3, 4, \ldots$, that is, $\Omega\fallingdotseq 1/3, 1/4, \ldots$, one needs to use higher order approximate solutions (the third, fourth, ..., order).

4. 4. Numerical results and discussion

Here numerical calculation is performed by using the analytical results in section 4. 3.

4. 4. 1. $\Omega\fallingdotseq 1$

Figure 4. 3 shows the unstable regions obtained from the conditions (4. 16) and (4. 17). In this neighborhood there is no region which satisfies the dynamically unstable condition (4. 17) but only a statically unstable one (4. 16). Accordingly, it is expected that each of the representative points on (U, V) and (U^*, V^*) planes goes away on a straight line from the origin. Figures 4. 4(a) and (b) show the results obtained by integrating directly Eq. (4. 13) for the purpose to confirm this. Each initial value of U, V, U^*, and V^* is put as 0. 001, which is used to obtain the following numerical integration too. The interval of two circle marks adjoining each other on these solution curves corresponds to the time when the drive shaft makes five rotations. Each of the representative points goes away on a straight line from the origin, and it is seen that the S-type unstable vibration occurs. At

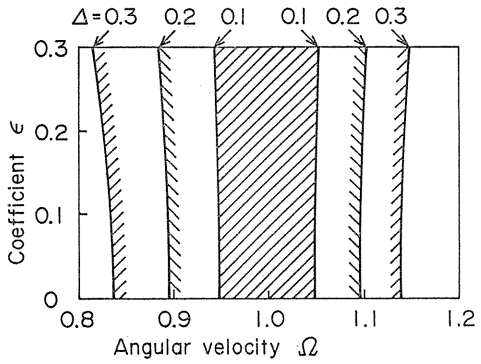

Fig. 4. 3. Influence of angular velocity fluctuation on unstable region ($\zeta=0.001$).

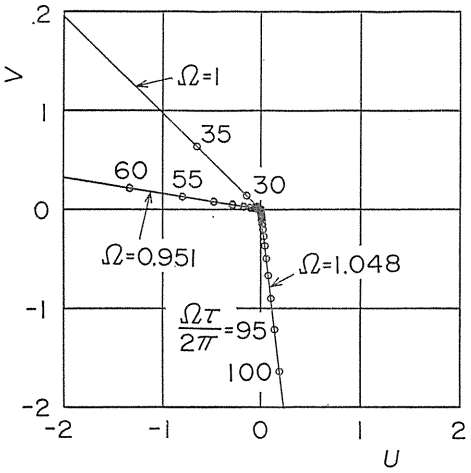

(a) Solution curves for $Ae^{i(\Omega\tau+\phi)}$ expressed on (U, V) plane.

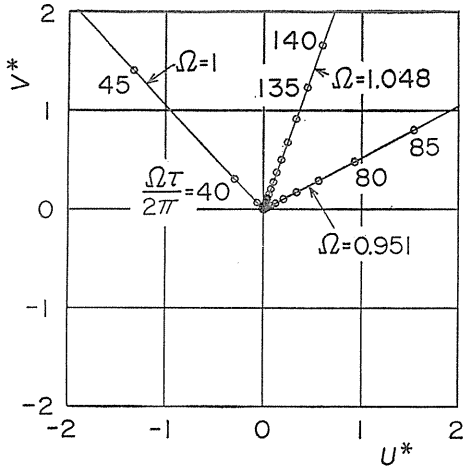

(b) Solution curves for $A^*e^{i(-\Omega\tau+\phi^*)}$ expressed on (U^*, V^*) plane.

Fig. 4. 4. $\Delta=0.1$, $\varepsilon=0.1$, $\zeta=0.001$.

the same time the other vibration $A^*e^{i(-\Omega\tau+\phi^*)}$ occurs too. This vibration cannot occur when the shaft rotates with a constant angular velocity. The values of $\Omega\tau/(2\pi)$ show that the vibration whirling forward develops more quickly than that whirling backward. Furthermore, Fig. 4. 3 shows that the fluctuation of shaft angular velocity enlarges unstable region.

Figure 4. 5 shows the locus of a whirling shaft given by Eqs. (4. 12) and (4. 13). The interval of two circle marks adjoining each other on the locus corresponds to the time when the drive shaft rotates by one-eighth. The locus is drawn while the drive shaft rotates twice after the growth of the vibration to a certain extent. The arrow shows the direction of whirl. The shaft locus makes a spiral with an elliptical form, and the shaft moves counterclockwise due to the amplitude ratio $\kappa=A^*/A<1$. Consideration of Eq. (4. 13) under the condition (4. 19) shows that the amplitude ratio κ is a small quantity of the same order as ε.

Here, consider a parameter μ representing the real part of a solution to the characteristic equation derived from Eq. (4. 13). When μ is positive, it is called the negative damping coefficient[15], which represents the growing rate of vibration

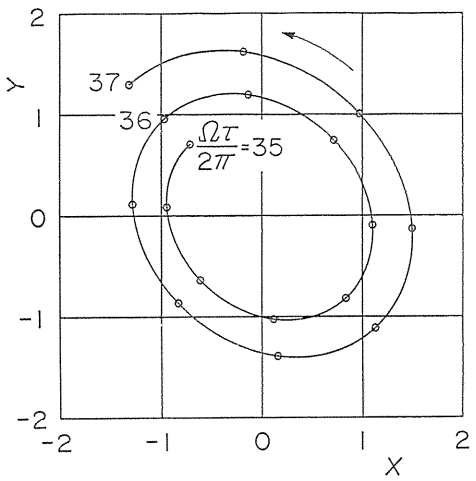

$\Omega=1$, $\Delta=0.1$, $\zeta=0.001$.
Fig. 4. 5. Locus of whirling shaft.

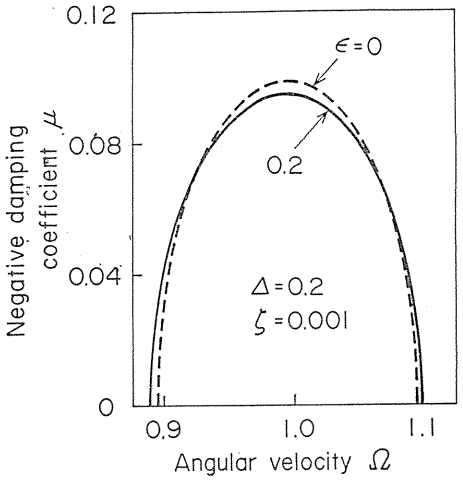

Fig. 4. 6. Negative damping coefficient.

in the unstable region. The calculated results of μ are shown in Fig. 4. 6. It takes a maximum value near the middle of the unstable region. Figure 4. 6 shows that the vibration grows more near the boundaries of unstable region while it is suppressed near the center, due to the fluctuation of the shaft angular velocity.

4. 4. 2. $\Omega \fallingdotseq 1/2$

Three unstable regions appear in this case. Figure 4. 7 shows the unstable regions obtained by numerical calculation of inequalities (4. 23) and (4. 24). It is not until both asymmetry of shaft stiffness Δ and angular velocity fluctuation ε combine that these unstable regions come to occur. For no damping $\zeta=0$ (the boundaries are indicated by broken lines), the statically unstable regions extend to two points A and C on the line $\varepsilon=0$, while the dynamically unstable region extends to a point B. For a certain value of ε, the widest unstable region extends to the point A, the second narrowest and the narrowest unstable regions extend to the points B and C, respectively. Accordingly, a small viscous damping ζ is apt to extinguish the unstable region extending to the points C, B, and A in order. The width of unstable region has the order of Δ when $\Omega \fallingdotseq 1$, and it has an order lower than $\varepsilon\Delta$ when $\Omega \fallingdotseq 1/2$.

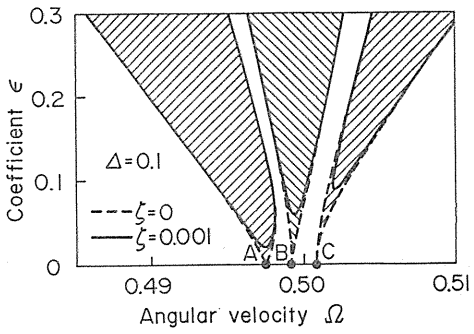

Fig. 4. 7. Influence of angular velocity fluctuation on unstable region.

The numerical integration of Eq. (4. 21) gives the solution curves of Figs. 4. 8 (a) and (b) and Figs. 4. 9 (a) and (b), which are the results in statically and dynamically unstable regions, respectively. These curves on the planes (U, V) and (U^*, V^*) represent the forward whirling $Ae^{i(2\Omega\tau+\Phi)}$ and the backward one $A^*e^{i(-2\Omega\tau+\Phi^*)}$. The interval of two circle marks adjoining each other on the solution curves cor-

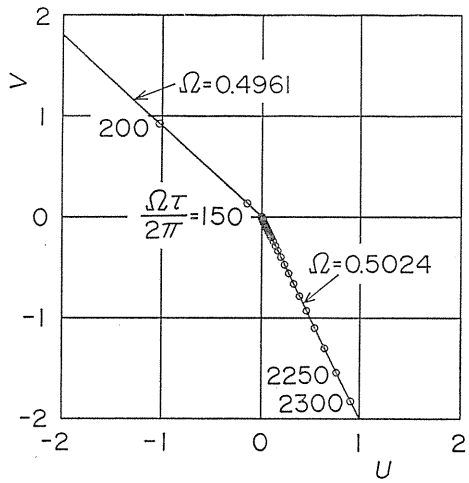

(a) Solution curves for $Ae^{i(2\Omega\tau+\phi)}$ expressed on (U, V) plane.

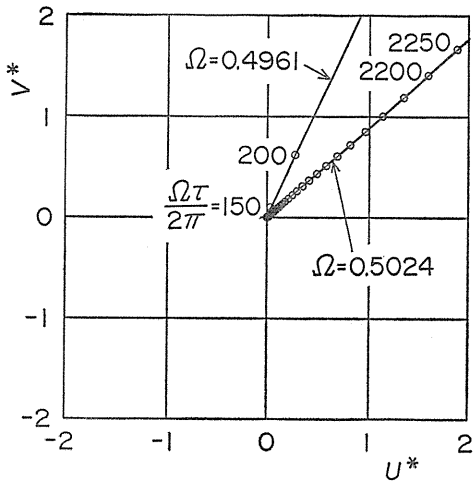

(b) Solution curves for $A^*e^{i(-2\Omega\tau+\phi^*)}$ expressed on (U^*, V^*) plane.

Fig. 4. 8. $\Delta=0.1$, $\varepsilon=0.1$, $\zeta=0.001$.

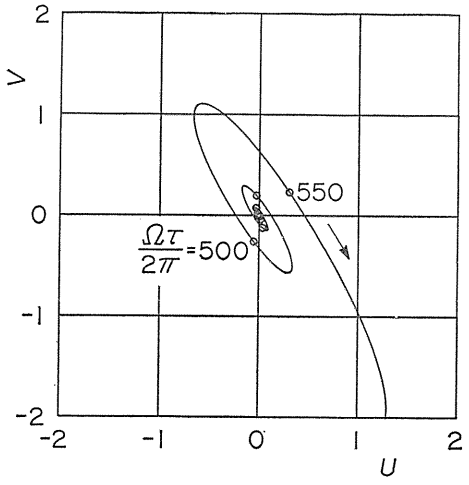

(a) Solution curve for $Ae^{i(2\Omega\tau+\phi)}$ expressed on (U, V) plane.

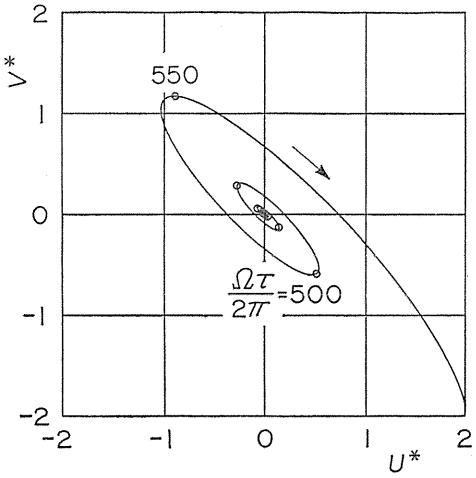

(b) Solution curve for $A^*e^{i(-2\Omega\tau+\phi^*)}$ expressed on (U^*, V^*) plane.

Fig. 4. 9. $\Omega=0.4994$, $\Delta=0.1$, $\varepsilon=0.1$, $\zeta=0.001$.

responds to the time when the drive shaft makes 50 rotations.

The solution curves of Figs. 4. 8 (a) and (b) are similar to those of Figs. 4. 4 (a) and (b), showing the S-type unstable vibration. But as mentioned in the following, this S-type unstable vibration differs in its characteristic from the vibration when $\Omega \fallingdotseq 1$. The locus of the shaft derived by Eqs. (4. 20) and (4. 21) is shown in Figs. 4. 10(a) and (b). The locus creates a spiral with an elliptical form. The center of vibration deviates slightly from the origin. In the unstable region extending to the point C ($\Omega=0.5024$), the backward whirling vibration is grater than the forward whirling one. The vibration increases so slowly that it seems to be steady.

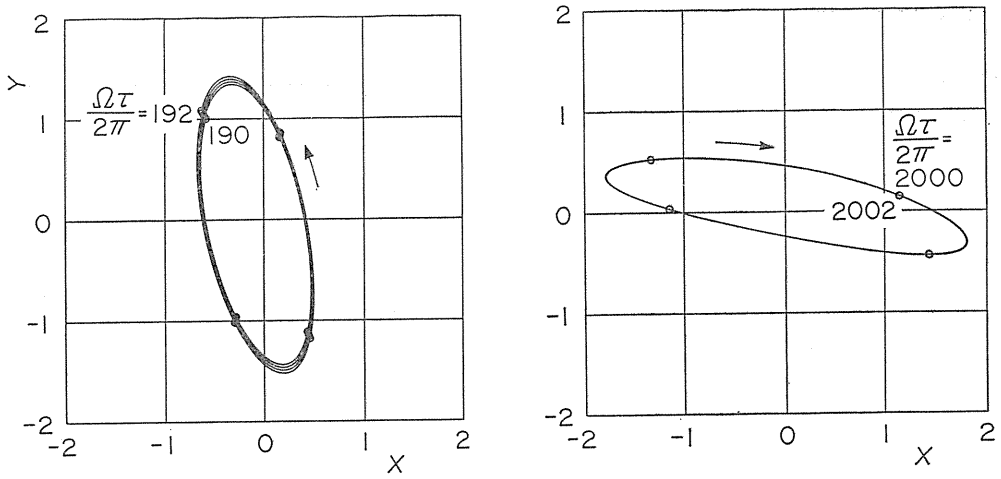

(a) $\Omega=0.4961$. (b) $\Omega=0.5024$.

Fig. 4. 10. Locus of whirling shaft ($\Delta=0.1$, $\varepsilon=0.1$, $\zeta=0.001$).

As shown in Figs. 4. 9 (a) and (b), the solution curve makes a spiral with an elliptical form in the dynamically unstable region. Accordingly, the D-type unstable vibration occurs and is accompanied by a complex fluctuation in amplitude and angular frequency. The shaft locus is shown in Figs. 4. 11 (a), (b), and (c). With time, the locus changes in its form. Each locus of (a), (b), and (c) is shown while the drive shaft rotates twice. In the passage time between (a) and (b), or (b) and (c), the drive shaft makes 23 rotations and the whirling of shaft reverses in direction. When the shaft whirls once, the locus seems to be an ellipse. Figures 4. 11 (a), (b), and (c) show that the amplitude as a whole increases changing the direction of the principal axis of the ellipse and the whirling direction with time.

Figure 4. 12 shows the calculated results of the negative damping coefficient

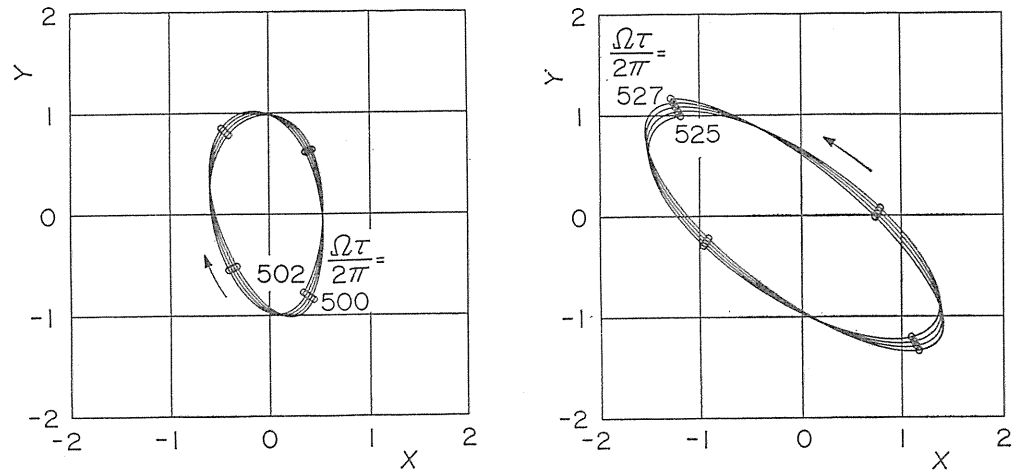

(a) $\Omega\tau/(2\pi)=500-502$. (b) $\Omega\tau/(2\pi)=525-527$.

Fig. 4. 11-1. Locus of whirling shaft ($\Omega=0.4994$, $\Delta=0.1$, $\varepsilon=0.1$, $\zeta=0.001$).

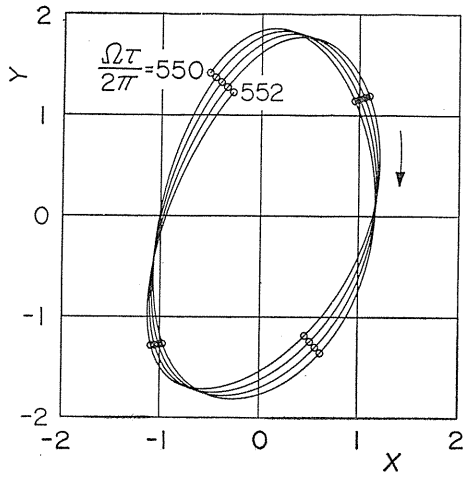

(c) $\Omega\tau/(2\pi)=550-552$.

Fig. 4. 11-2. Locus of whirling shaft ($\Omega=0.4994$, $\Delta=0.1$, $\varepsilon=0.1$, $\zeta=0.001$).

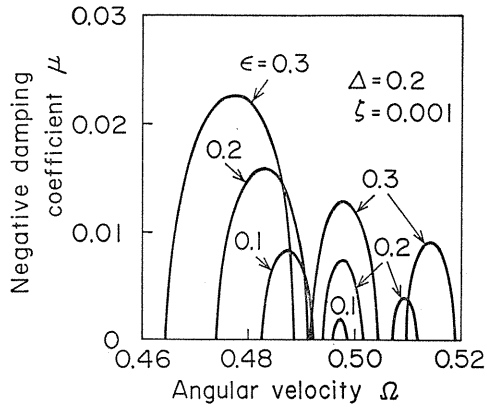

Fig. 4. 12. Negative damping coefficient.

μ. The coefficient μ takes a maximum value near the middle of the unstable region. This is similar to the case $\Omega\fallingdotseq 1$. The maximum value of μ becomes larger and larger as the coefficient of angular velocity fluctuation ε increases. As for the same value of ε, the lower or higher rotating speed region has the largest or smallest maximum value of μ. For $\varepsilon=0.2$, the comparison between Fig. 4. 6 and Fig. 4. 12 shows that the maximum value of μ in the lower speed region near $\Omega=1/2$ is about one-tenth as large as the maximum value near $\Omega=1$.

4. 5. Conclusions

The unstable vibrations of an asymmetrical shaft driven by a universal joint are analyzed, and the results may be summarized as follows:

(1) When the drive shaft rotates near its major critical speed, the driven shaft with asymmetry makes unstable vibrations whirling both forward and backward. The absolute value of the whirling angular velocity coincides with the rotating speed of the drive shaft. The amplitude of vibration whirling forward is larger than that whirling backward. As a result, the shaft locus becomes a spiral with an elliptical form.

(2) The unstable region at the major critical speed increases slightly in its width due to the angular velocity fluctuation based on the mechanism of the universal joint. This angular velocity fluctuation promotes the vibration near the boundary of the unstable region, whereas it suppresses the vibration near the middle.

(3) Near the rotating speed at half of the major critical speed, three unstable regions appear. It is not until the asymmetry of shaft stiffness and the angular velocity fluctuation combine that these unstable regions begin to grow.

(4) Of these three unstable regions, the higher rotating speed region generates a forward whirling vibration larger than a backward whirling one. The lower rotating speed region generates a backward whirling vibration larger than a forward

whirling one. When the unstable vibrations occur in these two regions, the driven shaft whirls with an angular velocity equal to twice the angular velocity of the drive shaft.

In the mid region, the driven shaft generates the unstable vibration with a complex fluctuation in amplitude and angular frequency.

(5) Near the rotating speed at half of the major critical speed, the width of the unstable region and the growth rate of vibration are considerably smaller than those near the major critical speed.

(6) The stability of the shaft system is not influenced by the angle between the principal axis of the shaft cross section and the direction of the cross-pin.

5. Generation Mechanism of Unstable Vibrations Caused by a Shaft Asymmetry and an Angular Velocity Fluctuation[53]

5. 1. Introduction

A driven shaft system treated in this chapter is the same as Chapter 4. This chapter presents physical explanations for the unstable vibrations of the asymmetrical shaft driven by a universal joint and also for their generation mechanism. For this purpose, some studies are made of the relationship between the natural angular frequency and the unstable region. Then, an increase in the rate of mechanical energy is determined.

5. 2. Natural angular frequency and unstable regions

Considering the small quantity up to the second order both of an asymmetry Δ and of a coefficient of the angular velocity fluctuation ε, we obtain the following equation of motion concerning the mass point S:

$$\ddot{Z}+Z=\Delta\overline{Z}(e^{i2\Omega\tau}+\varepsilon e^{i4\Omega\tau}-\varepsilon) \tag{5.1}$$

For $\varepsilon=0$, an exact solution of Eq. (5. 1) exists, and this solution is given in the form

$$Z=ae^{i(p_0\tau+\varphi)}+a^*e^{i\{(2\Omega-p_0)\tau-\varphi\}} \tag{5.2}$$

In Eq. (5. 2), $p_0=p_{0j}$ ($j=1$, 2, 3, and 4) are given by the following equations[49].

$$\left.\begin{aligned} p_{01}&=\Omega+\Omega_1,\quad p_{02}=\Omega-\Omega_1\\ p_{03}&=\Omega+\Omega_2,\quad p_{04}=\Omega-\Omega_2 \end{aligned}\right\} \tag{5.3}$$

where,

$$\left.\begin{aligned} \Omega_1&=\sqrt{\Omega^2+1+\sqrt{4\Omega^2+\Delta^2}}\\ \Omega_2&=\sqrt{\Omega^2+1-\sqrt{4\Omega^2+\Delta^2}} \end{aligned}\right\} \tag{5.4}$$

The frequencies p_{01} and p_{02} are always real numbers, while p_{03} and p_{04} become complex numbers when the following inequality holds.

$$\Omega^2+1<\sqrt{4\Omega^2+\Delta^2} \tag{5.5}$$

Then the shaft system generates an unstable vibration whirling with angular velocity Ω in addition to the steady state vibrations with the natural angular frequencies p_{01}, p_{02}.

The second approximation by the asymptotic method gives the following results about the unstable conditions of the shaft system.

When $\Omega \fallingdotseq 1$,

$$\text{(a)} \quad F_1 < 0 \tag{5.6}$$

$$\text{(b)} \quad F_1 > 0,\ G_1 < 0,\ G_1^2 - 4F_1 < 0 \tag{5.7}$$

When $\Omega \fallingdotseq 1/2$,

$$\text{(a)} \quad F_2 < 0 \tag{5.8}$$

$$\text{(b)} \quad G_2^2 - 4F_2 < 0 \tag{5.9}$$

where,

$$\left.\begin{aligned}
F_1 &= \left(d_1 d_1^* - \frac{\varepsilon^2 \Delta^2}{4\Omega^2}\right)^2 - \frac{\Delta^2 d_1^{*2}}{4\Omega^2} \\
G_1 &= d_1^2 + d_1^{*2} - \frac{\Delta^2}{4\Omega^2}(1 - 2\varepsilon^2) \\
d_1 &= \frac{1}{2\Omega}\left\{1 - \Omega^2 - \frac{(1-\Omega^2)^2 - \Delta^2}{4\Omega^2}\right\} \\
d_1^* &= \frac{1}{2\Omega}\left\{1 - \Omega^2 - \frac{(1-\Omega^2)^2 - \Delta^2/2}{4\Omega^2}\right\} \\
F_2 &= \left(d_2 d_2^* - \frac{\varepsilon^2 \Delta^2}{16\Omega^2}\right)^2 - \frac{\varepsilon^2 \Delta^2 d_2^{*2}}{16\Omega^2} \\
G_2 &= d_2^2 + d_2^{*2} + \frac{\varepsilon^2 \Delta^2}{16\Omega^2} \\
d_2 &= \frac{1}{4\Omega}\left\{1 - 4\Omega^2 - \frac{(1-4\Omega^2)^2 + 4\Delta^2}{16\Omega^2}\right\} \\
d_2^* &= \frac{1}{4\Omega}\left\{1 - 4\Omega^2 - \frac{(1-4\Omega^2)^2 - 4\Delta^2/3}{16\Omega^2}\right\}
\end{aligned}\right\} \tag{5.10}$$

When $\varepsilon = 0$, it is easily verified that inequality (5. 7) does not hold. Now relation (5. 5) is assumed to give an exact result about the unstable region for $\varepsilon = 0$, and we consider the unstable condition (5. 6). Putting $\varepsilon = 0$ in relation (5. 6) yields

$$\frac{4\Omega^2 F_1}{d_1^{*2}} = \left\{1 - \Omega^2 - \frac{(1-\Omega^2)^2 - \Delta^2}{4\Omega^2}\right\}^2 - \Delta^2 < 0 \tag{5.11}$$

The first approximation gives the relation $(1-\Omega^2)^2 - \Delta^2 < 0$, which coincides with

inequality (5. 5). On the other hand, inequality (5. 11) which is supposed to have had its degree of accuracy increased by the second approximation does not apparently coincide with inequality (5. 5). But simple transformation of the equation derives inequality (5. 5) from inequality (5. 11). Accordingly, inequality (5. 6) degenerates to inequality (5. 5) when $\varepsilon \to 0$. Thus, inequality (5. 6) gives the condition for generation of the unstable vibration when $\Omega \fallingdotseq 1$ and $\varepsilon \neq 0$.

When $\Omega \fallingdotseq 1/2$, the unstable regions appear near the rotating speeds which satisfy $F_2=0$ and $G_2{}^2-4F_2=0$ derived by putting $\varepsilon=0$ in relations (5. 8) and (5. 9).

$$\left.\begin{aligned} \Omega_A^2 &= (1-\Delta^2)/4 \\ \Omega_B^2 &= (1-\Delta^2/3)/4 \\ \Omega_C^2 &= (1+\Delta^2/3)/4 \end{aligned}\right\} \tag{5. 12}$$

These values Ω_A, Ω_B, and Ω_C coincide with the abscisas of three points A, B, and C lying on the base line $\varepsilon=0$ in Fig. 5. 1.

Substituting $Z=X+iY$ into equation of motion (5. 1), and separating real and imaginary parts, we obtain the following equations.

$$\left.\begin{aligned} &\ddot{X}+(1+\varepsilon\Delta)X \\ &\quad =\Delta(X\cos 2\Omega\tau+Y\sin 2\Omega\tau)+\varepsilon\Delta(X\cos 4\Omega\tau+Y\sin 4\Omega\tau) \\ &\ddot{Y}+(1-\varepsilon\Delta)Y \\ &\quad =\Delta(X\sin 2\Omega\tau-Y\cos 2\Omega\tau)+\varepsilon\Delta(X\sin 4\Omega\tau-Y\cos 4\Omega\tau) \end{aligned}\right\} \tag{5. 13}$$

Equation (5. 13) shows that the asymmetrical shaft system driven by a universal joint is equivalent to a dynamic superposition of the following three systems:

A mass system supported by the springs with such unequal rigidities as $1+\varepsilon\Delta$ in X direction and $1-\varepsilon\Delta$ in Y direction, and two asymmetries Δ and $\varepsilon\Delta$ rotating with constant angular velocities Ω and 2Ω, respectively.

This equivalent model system is shown in Fig. 5. 2. The rotating shaft system is considered to have vibrational characteristics similar to the asymmetrical shaft

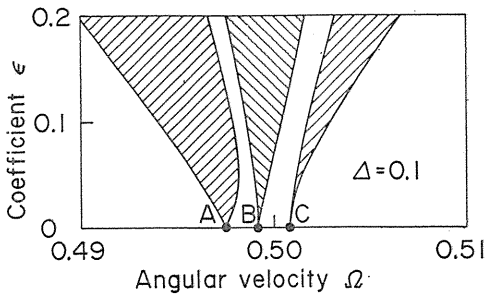

Fig. 5. 1. Unstable region.

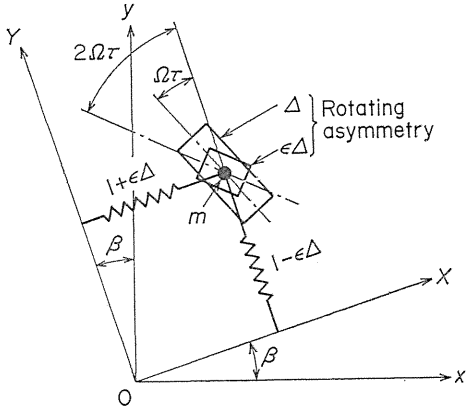

Fig. 5. 2. Equivalent model system.

supported by the pedestals with directionally unequal rigidities. Consequently, the whirling locus of the shaft becomes generally elliptic. The shaft system has the natural angular frequencies $\pm p_{0j}$ ($j=1$, 2, 3, and 4), and it produces vibrations with frequencies $4\Omega\pm p_{0j}$ which are caused by the second term of the right-hand side of Eq. (5. 13), that is, by both shaft asymmetry and angular velocity fluctuation. The angular velocity $\Omega=\Omega_A$ is a resonant point where frequencies $4\Omega-p_{03}$ and p_{03} meet, and $\Omega=\Omega_C$ is a resonant point of $4\Omega+p_{02}$ and $-p_{02}$. The angular velocity $\Omega=\Omega_B$ is a resonant point of $4\Omega+p_{02}$ and p_{03}, and also of $4\Omega-p_{03}$ and $-p_{02}$. Hence, Ω_A, Ω_B, and Ω_C are the solutions of $2\Omega-p_{03}=0$, $4\Omega+p_{02}-p_{03}=0$, and $2\Omega+p_{02}=0$, respectively.

The second approximate solution by the asymptotic method yields the simultaneous differential equations concerned with amplitudes A, A^* and phases Φ, Φ^* of the vibrations whirling forward and backward. These equations are transformed into linear differential equations concerning U, V, U^*, and V^* of Eq. (4. 15). If $\mu\pm i\lambda$ are solutions of the characteristic equation derived from the linear differential equations, then the general form of $Ae^{i\Phi}=U+iV$ is given by

$$Ae^{i\Phi}=e^{\mu\tau}\{A_1e^{i(\lambda\tau+\Phi_1)}+A_2e^{i(-\lambda\tau+\Phi_2)}\} \tag{5.14}$$

Also, $A^*e^{i\Phi^*}$ is expressed similarly. Then λ represents the natural angular frequency in the rotating co-ordinate system.

According to the asymptotic method, the vibration recognized in the first approximation is regarded as the natural vibration of the system. The natural angular frequencies p_s viewed from the stationary co-ordinate system are determined as follows. When $\Omega\fallingdotseq 1$,

$$p_s=\Omega\pm\lambda,\quad -\Omega\pm\lambda \tag{5.15}$$

because the natural vibration is $Z=Ae^{i(\Omega\tau+\Phi)}+A^*e^{i(-\Omega\tau+\Phi^*)}$. When $\Omega\fallingdotseq 1/2$,

$$p_s=2\Omega\pm\lambda,\quad -2\Omega\pm\lambda \tag{5.16}$$

because the natural vibration is $Z=Ae^{i(2\Omega\tau+\Phi)}+A^*e^{i(-2\Omega\tau+\Phi^*)}$.

Especially for $\varepsilon=0$, the following result is obtained. When $\Omega\fallingdotseq 1$,

$$\left.\begin{aligned}\dot{A}&=-\{\Delta A/(2\Omega)\}\sin 2\Phi\\ \dot{\Phi}&=d_1-\{\Delta/(2\Omega)\}\cos 2\Phi\\ \dot{A}^*&=0,\ \dot{\Phi}^*=-d_1^*\end{aligned}\right\} \tag{5.17}$$

For the unstable condition $D_1=d_1{}^2-\{\Delta/(2\Omega)\}^2<0$, $\lambda=0$ holds, and we have

$$p_s=\Omega,\ p_s=-\Omega-d_1^* \tag{5.18}$$

For the stable condition $D_1>0$, $\lambda=\sqrt{D_1}$ holds,

$$p_s=\Omega\pm\sqrt{D_1},\ p_s=-\Omega-d_1^* \tag{5.19}$$

The frequency $-\Omega-d_1{}^*$ corresponds to p_{02} in Eq. (5. 3), and $\Omega+\sqrt{D_1}$ corresponds to p_{03}. Consequently, natural vibrations with frequencies p_{02}, p_{03}, and $2\Omega-p_{03}=p_{04}$ exist. The vibration of p_{01} is not contained here because it is considered a small

one of $-\{\Delta A^*/(8\Omega^2)\}e^{i(3\Omega\tau-\Phi^*)}$, which is recognized in the second approximation and is excited by a natural vibration of p_{02}.

When $\Omega \fallingdotseq 1/2$ and $\varepsilon=0$, we obtain

$$\dot{A}=0,\ \dot{\Phi}=d_2,\ \dot{A}^*=0,\ \dot{\Phi}^*=-d_2^* \tag{5.20}$$

and

$$p_s=2\Omega+d_2,\ -2\Omega-d_2^* \tag{5.21}$$

The values p_s of Eq. (5. 21) correspond to p_{03} and p_{02} of Eq. (5. 3). Accordingly, the natural vibrations of p_{02} and p_{03} exist near this rotating speed. The vibrations of p_{01} and p_{04} are not included here, because they are both small vibrations as well as $-\{\Delta A^*/(8\Omega^2)\}e^{i(3\Omega\tau-\Phi^*)}$ when $\Omega \fallingdotseq 1$.

Furthermore, when μ is a positive value, this represents "the negative damping coefficient." We mentioned this in chapter 4.

Figures 5. 3 (a) and 5. 3 (b) show the numerical results about the natural angular frequencies λ. These figures present the curves of d_1, $\sqrt{D_1}$, d_2, and d_2^*, which are the values of λ when $\varepsilon \to 0$. The abscissas of the points A, B, and C in Fig. 5. 1 coincide with those of the intersecting points A, B, and C at which $d_2=0$, $d_2^*=-d_2$, and $d_2^*=0$ hold in Fig. 5. 3 (b), respectively. The values of p_{0j} in Eq. (5. 3) coincide well with p_s in Eqs. (5. 18), (5. 19), and (5. 21).

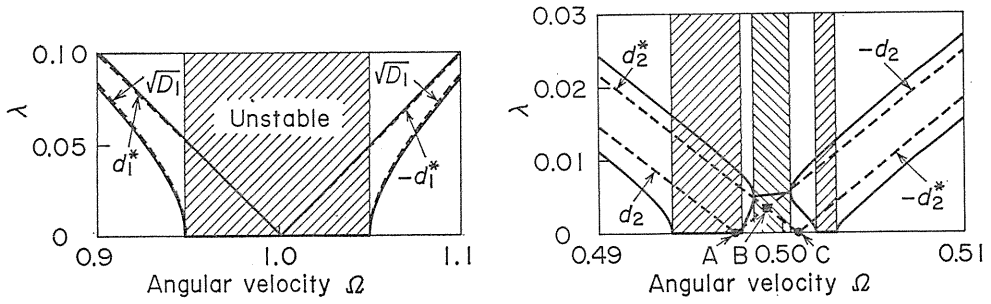

(a) $\Omega \fallingdotseq 1$. (b) $\Omega \fallingdotseq 1/2$.

Fig. 5. 3. Natural angular frequencies ($\Delta=0.1$, $\varepsilon=0.1$).

5. 3. Energy supplied to rotating shaft system

This section presents an explanation for the energy supplied to a rotating shaft system which generates an unstable vibration.

The following non-dimensional quantities are used in Eqs. (5. 25) to (5. 30).

$$\left.\begin{aligned} &F'_2=F_2/(mg),\ M'_\Theta=M_\Theta/(mg\delta_{st}) \\ &W'=W/(mg\delta_{st}p) \\ &T'=T/(mg\delta_{st}),\ V'=V/(mg\delta_{st}) \end{aligned}\right\} \tag{5.22}$$

Primes which show non-dimensional quantities are omitted hereafter.

As shown in Fig. 5. 4, let ξ be an angle of deflection OS measured counter-clockwise from the direction S2 (x') with shaft minimum rigidity. Then, the

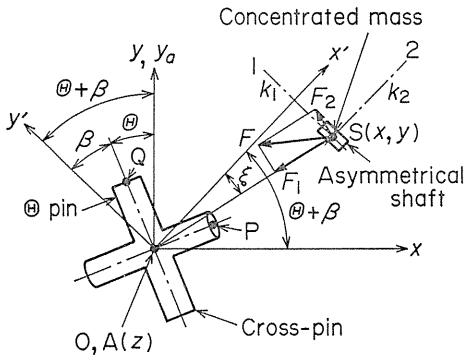

Fig. 5. 4. Cross-pin, stationary rectangular co-ordinate system O-xyz, rotatory rectangular co-ordinate system O-$x'y'z$, and restoring force F ($k_1 > k_2$, this figure is viewed from z direction, and now ξ is negative.).

following equations hold.

$$\left.\begin{aligned} \sin\xi &= (-X\sin\theta + Y\cos\theta)/|Z| \\ \cos\xi &= (X\cos\theta + Y\sin\theta)/|Z| \end{aligned}\right\} \tag{5.23}$$

Using the following relation

$$\theta + \xi = \tan^{-1}(Y/X) \tag{5.24}$$

, we obtain the whirling component F_2 of the restoring force F of the asymmetrical shaft (F_1 represents the centripetal component)*2.

$$F_2 = -\Delta|Z|\sin 2\xi \tag{5.25}$$

The whirling force F_2 is generated by the drive torque M_θ transmitted to the driven shaft by the universal joint. Therefore the following equation holds.

$$M_\theta = -\Delta|Z|^2\sin 2\xi \tag{5.26}$$

Using Eqs. (5. 23), (5. 26), and the following relations

$$e^{i2\theta} = e^{i2\Omega\tau} + \varepsilon e^{i4\Omega\tau} - \varepsilon + \cdots$$

$$\dot{\theta} = \Omega + 2\varepsilon\Omega\cos 2\Omega\tau + \cdots$$

, we obtain the supplied energy per unit time W,

$$\begin{aligned} W &= M_\theta\dot{\theta} \\ &= -\Delta\Omega\,\mathrm{Im}[Z^2(e^{-i2\Omega\tau} + 2\varepsilon e^{-i4\Omega\tau})] \end{aligned} \tag{5.27}$$

or

$$\frac{W}{\Delta\Omega|Z|^2} = -(1 + 2\varepsilon\cos 2\Omega\tau)\sin 2\xi \tag{5.28}$$

where, the symbol Im [ ] shows an imaginary part of [a complex number]. The

*2 Refer to Fig. 2 in reference (52).

value of Eq. (5. 28) for $\Omega \fallingdotseq 1$ should differ considerably from that for $\Omega \fallingdotseq 1/2$, because ξ depends on the rotating angular velocity of the shaft and the whirling mode.

On the other hand, kinetic and potential energies T and V of the shaft system are given by the following equations:

$$\left.\begin{aligned} T &= (\dot{X}^2+\dot{Y}^2)/2 \\ V &= (1-\Delta)(X^2+Y^2)/2+\Delta(X\sin\theta-Y\cos\theta)^2 \end{aligned}\right\} \tag{5. 29}$$

Calculating the increase in the rate of mechanical energy of the shaft system $\dot{T}+\dot{V}$ from Eq. (5. 29), we obtain

$$\begin{aligned} \dot{T}+\dot{V} &= \dot{X}\{\ddot{X}+X-\Delta(X\cos 2\theta+Y\sin 2\theta)\} \\ &\quad +\dot{Y}\{\ddot{Y}+Y-\Delta(X\sin 2\theta-Y\cos 2\theta)\} \\ &\quad +\Delta\dot{\theta}\{(X^2-Y^2)\sin 2\theta-2XY\cos 2\theta\} \end{aligned} \tag{5. 30}$$

The first and second terms in the right-hand side of Eq. (5. 30) are equated to zero from Lagrange's equations of motion[47]. Thus it is confirmed that the increase in the rate of mechanical energy of the shaft system $\dot{T}+\dot{V}$ coincides with W of Eq. (5. 27).

Figures 5. 5 to 5. 7 show numerical results of calculation on the increase in the rate of the energy $W/(\Delta\Omega|Z|^2)$ and on the angle $\xi=\angle x'$ OS when an unstable vibration occurs. In these figures initial values are always taken as $U=V=U^*=V^*=0.005$.

When $\Omega \fallingdotseq 1$, the results are shown in Fig. 5. 5, with solid or broken lines for $\varepsilon=0.1$ or 0 (with or without fluctuation in angular velocity). Here W is divided by $|Z|^2$ to examine the increase in the rate of energy for the same shaft deflection. The rotating speeds $\Omega=0.949$ and 1.048 are near the boundaries in the unstable region. When the shaft rotates once at $\Omega=0.949$ or 1.048, the average value of $W/(\Delta\Omega|Z|^2)$ for $\varepsilon=0.1$ is larger than that for $\varepsilon=0$. When $\Omega=1$, the average value for $\varepsilon=0$ is larger. This fact corresponds to the analytical results concerning the negative damping coefficient μ mentioned in Chapter 4.

When $\xi=-\pi/4$, energy is supplied at the maximum rate. When $\Omega=1$, the angle ξ takes somewhat different values from $-\pi/4$, because the shaft whirls along an elliptical curve and the angular velocity of whirling fluctuates. Consequently, it is more difficult for the shaft system to obtain energy than when $\varepsilon=0$. When $\Omega=0.949$ and 1.048, energy enters the shaft system more easily than when $\varepsilon=0$, because the angle ξ takes some values nearer to $-\pi/4$ than when $\varepsilon=0$.

Figures 5. 6 and 5. 7 show the increase in the rate of energy during a half rotation of the shaft when $\Omega \fallingdotseq 1/2$. Figure 5. 6 shows the results for the S-type unstable vibration which occurs in the unstable region extending from the point A in Fig. 5. 1. Here $A>A^*$ always holds. Figure 5. 7 shows the results for the D-type unstable vibration which occurs in the unstable region extending from the point B in Fig. 5. 1, and for $A<A^*$. Unlike the case of $\Omega \fallingdotseq 1$, the energy can go not only into the shaft system but also out of it.

The change of ξ in Fig. 5. 6 differs from that in Fig. 5. 7. This is due to a difference of modes in which the shaft whirls. The value $W/(\Delta\Omega|Z|^2)$ corresponding

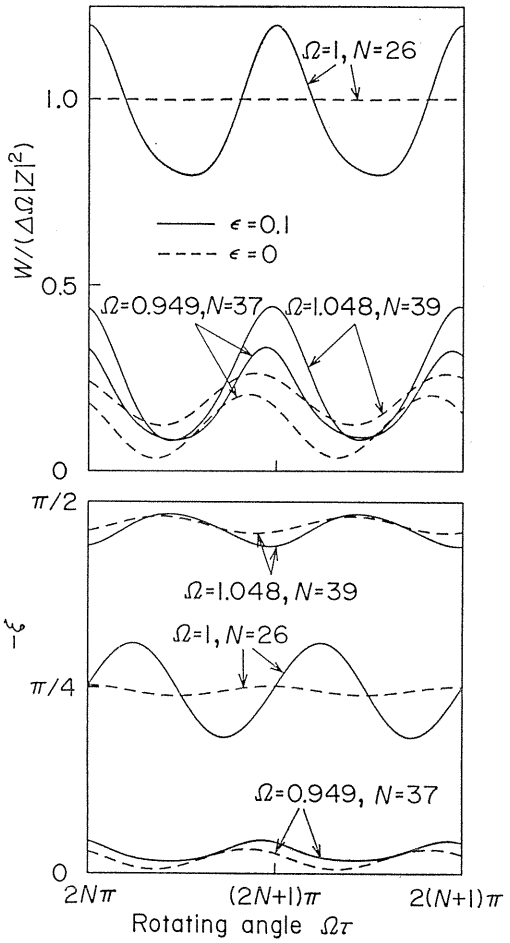

Fig. 5. 5. Increase in rate of energy during growth of unstable vibration ($\Omega \fallingdotseq 1$, $\Delta = 0.1$).

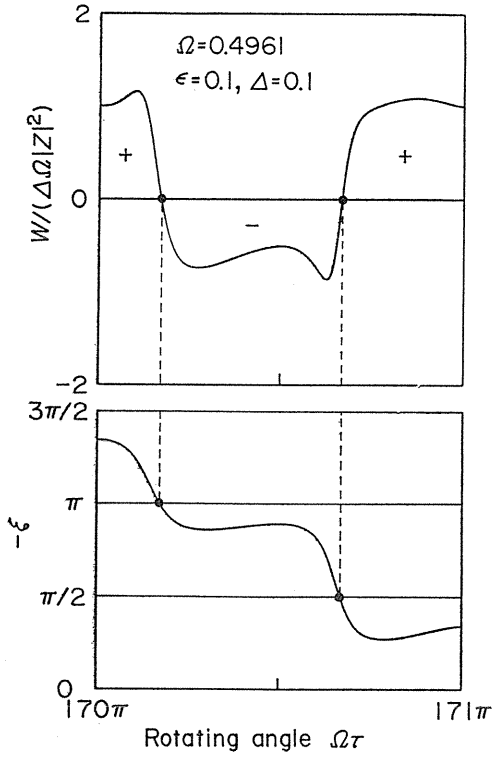

Fig. 5. 6. Increase in rate of energy during growth of S-type unstable vibration ($A > A^*$).

to angle ξ shows that it is determined only by the sign of $\sin 2\xi$ whether the energy goes into or out of the shaft system.

In the unstable region extending from the point C in Fig. 5. 1, $A < A^*$ holds, and a result similar to Fig. 5. 7 is obtained. The analytical results by the second approximation in Chapter 4 give the following equations.

When $\Omega \fallingdotseq 1$,

$$\left.\begin{aligned} \frac{d}{d\tau}(A^2 + A^{*2}) &= -\frac{\Delta A^2}{\Omega} \sin 2\Phi \\ \cos 2\Phi &= \frac{2\Omega}{\Delta}\left(d_1 - \frac{A^{*2}}{A^2} d_1^*\right) \end{aligned}\right\} \tag{5.31}$$

When $\Omega \fallingdotseq 1/2$,

$$\left.\begin{aligned}\frac{d}{d\tau}(A^2+A^{*2}) &= -\frac{\varepsilon\Delta A^2}{2\Omega^2}\sin 2\Phi \\ \dot{\Phi} &= d_2-\frac{\varepsilon\Delta}{4\Omega}\cos 2\Phi-\frac{A^{*2}}{A^2}(d_2^*+\dot{\Phi}^*)\end{aligned}\right\} \qquad (5.32)$$

Whichever the case is, it is seen that $d(A^2+A^{*2})/d\tau>0$, namely, the increase in energy of the shaft system occurs under $\sin 2\Phi<0$. Consequently, when the shaft makes the S-type unstable vibration, the locus of the representative point on the plane (U, V) ought to exist in the second or fourth quadrant. When the shaft makes the D-type unstable vibration at $\Omega\fallingdotseq 1/2$, the representative point on the plane (U, V) may exist in the first or third quadrant too, and the energy of the shaft system may decrease its average during one rotation of the shaft.

We calculate the average value of W during one rotation of the drive shaft from $\tau_1=N\pi/\Omega$ to $\tau_2=(N+2)\pi/\Omega$ (N is an arbitrary positive integer):

$$W_m=\frac{\Omega}{2\pi}\int_{\tau_1}^{\tau_2} W\,d\tau$$

The following equations are obtained with an accuracy of the second order of small quantities ε, Δ.

$$\left.\begin{aligned}W_m &= \Delta[\eta_1]_{\text{mean}} \quad (\Omega\fallingdotseq 1) \\ W_m &= \Delta[\eta_2]_{\text{mean}} \quad (\Omega\fallingdotseq 1/2)\end{aligned}\right\} \qquad (5.33)$$

where,

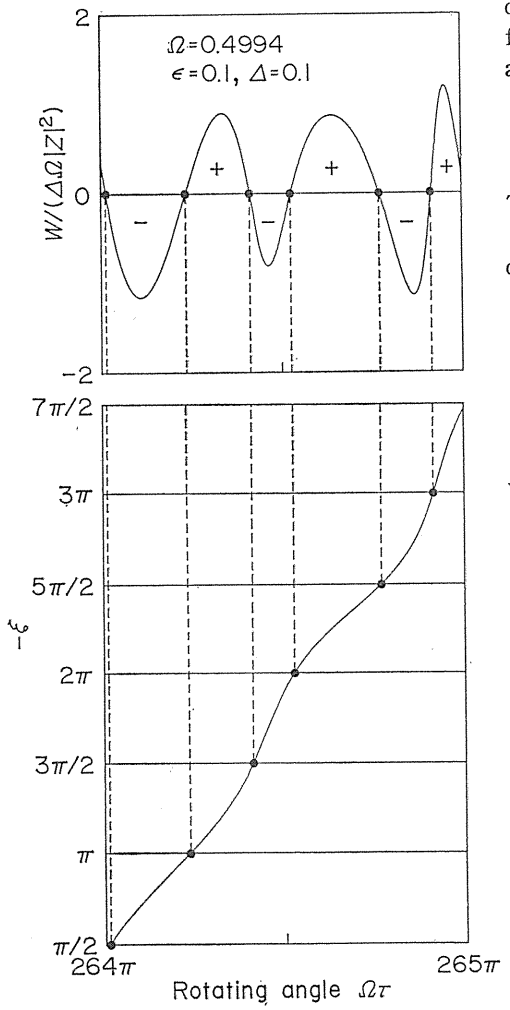

Fig. 5. 7. Increase in rate of energy during growth of D-type unstable vibration ($A<A^*$).

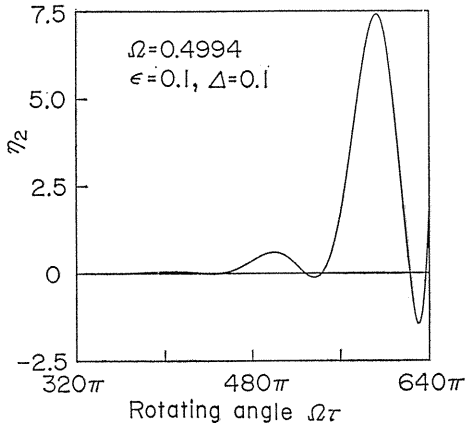

Fig. 5. 8. Increase in rate of energy during growth of D-type unstable vibration.

$$\left.\begin{aligned}\eta_1 &= -\Omega A^2 \sin 2\Phi - \Delta A A^* \sin(\Phi - \Phi^*) + \frac{1-\Omega^2}{4\Omega} A^{*2} \sin 2\Phi^* \\ \eta_2 &= \left(\frac{1-4\Omega^2}{4\Omega} - 2\varepsilon\Omega\right) A^2 \sin 2\Phi + \frac{1-4\Omega^2}{12\Omega} A^{*2} \sin 2\Phi^*\end{aligned}\right\} \quad (5.34)$$

When the rotating shaft generates the S-type unstable vibration, η_1 and η_2 take values proportional to A^2 or A^{*2}. Accordingly, the average energy supplied to the shaft changes in accordance with $e^{2\mu\tau}$ (μ is the negative damping coefficient).

When the shaft generates the D-type unstable vibration ($\Omega \fallingdotseq 1/2$), it is expected that η_2 will change in a complex manner. Figure 5. 8 shows the numerical result of η_2 in this case. The initial values are taken as $U=V=U^*=V^*=0.005$. According to Fig. 5. 8, the average value of the increase in the rate of energy sometimes becomes negative during about 7 rotations of the drive shaft.

5. 4. Conclusions

In this chapter, physical considerations were made of an asymmetrical shaft driven by a uriversal joint, and the generation mechanism of unstable vibration was explained. The results obtained may be summarized as follows:

(1) When the shaft rotates near the major critical speed, the angular velocity fluctuation decreases the growth of unstable vibration near the middle of the unstable region. This phenomenon relates to the fact that angle ξ becomes more remote from $-\pi/4$ due to angular velocity fluctuation. Near the boundaries of the unstable region, the angular velocity fluctuation increases the growth of unstable vibration because angle ξ comes closer to $-\pi/4$.

(2) When the shaft rotates near half the major critical speed, the unstable regions appear separately at three rotating speeds of Eq. (5. 12), as determined only by the asymmetry Δ.

(3) The energy supplied to the asymmetrical shaft has components which fluctuate periodically. The average energy supplied during one shaft rotation increases monotonously in proportion to the second power of amplitude when the S-type unstable vibration occurs. But it fluctuates periodically, and sometimes takes a negative value during several shaft rotations when the D-type unstable vibration occurs.

6. Forced Vibrations of an Asymmetrical Shaft Caused by Gravity[54]

6. 1. Introduction

There are many reports[55~59] on the lateral vibrations of an asymmetrical shaft. The characteristics of the vibrations are summarized as follows:

(1) When an asymmetrial shaft rotates near the major critical speed, the shaft generates unstable vibration whirling forward with an angular velocity of shaft.

(2) In a horizontal shaft, a forced vibration is excited by gravity. This forced vibration whirls forward twice during one shaft rotation, and makes a resonance near half the major critical speed.

Such vibration phenomena occur in an asymmetrical shaft which rotates with a constant angular velocity. There have been no investigations reported on the shaft system driven by a universal joint and accompanied with an angular velocity fluctuation. We analyzed, in Chapters 4 and 5, the unstable vibrations in such a rotating shaft system, and explained the behavior of shaft.

This chapter deals with a horizontal asymmetrical shaft driven by a universal joint, and explains the forced vibrations generated under the triple effect of gravity, shaft asymmetry, and angular velocity fluctuation. The universal joint combines a rigid drive shaft rotating with a constant angular velocity and a horizontal driven shaft with asymmetry in rigidity. The asymmetrical shaft system is the same as that of Chapter 4 except that the shaft is horizontally assembled. The equations of motion are simultaneous equations with parametric excitation and sinusoidal external force. Accordingly, these equations are solved by the same method as Chapter 4, and the steady state solutions are obtained from the approximate solution. Experiments are performed to confirm the propriety of the analytical results too.

6. 2. Equations of motion

Consider an asymmetrical shaft system as shown in Fig. 4. 1. Where the y axis points upward vertically. Figure 6. 1 shows the relation between a cross-pin and a stationary rectangular co-ordinate system. Gravity mg acts on mass point S in negative direction of y.

We introduce here a non-dimensional complex number which is given by the shaft deflection x, y:

$$Z=(x+iy)/\delta_{st}+iU_g \qquad (6.1)$$

where a special notation $U_g(\equiv 1)$ is used to indicate the gravity term.

An equation of motion is obtained by adding a gravitational force $-mg$ to the right-hand side of the second equation in Eq. (4. 1), as follows:

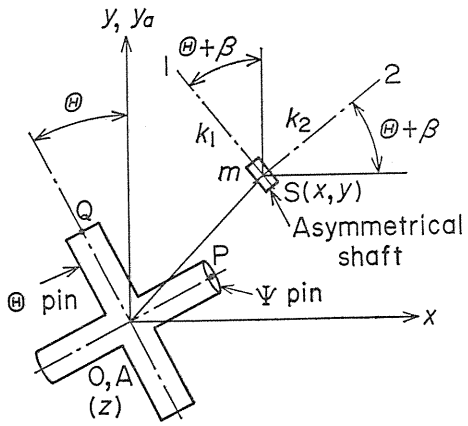

Fig. 6. 1. Cross-pin and stationary co-ordinate system viewed from z direction ($k_1>k_2$).

$$\ddot{Z}+Z=\varepsilon f(\Omega\tau,\ \overline{Z},\ \dot{Z}) \qquad (6.2)$$

where,

$$\varepsilon f(\Omega\tau,\ \overline{Z},\ \dot{Z})=-2\zeta\dot{Z}+\Delta e^{i2\beta}(\overline{Z}+iU_g)\Big[e^{i2\Omega\tau}+\sum_{N=2,4,\cdots}\varepsilon^{N/2}\times\{e^{i(N+2)\Omega\tau}-e^{i(N-2)\Omega\tau}\}\Big] \qquad (6.3)$$

6. 3. Solution for forced vibration

The same method as used in Chapter 4 is applied in analyses, the second approximate solution of the equation of motion (6. 2) is shown in asymptotic expansion form for the case of resonance. In addition, the characteristics of vibration due to gravity are described.

6. 3. 1. $\Omega \fallingdotseq 1/2$

$$Z = Ae^{i(2\Omega\tau+\Phi)} + A^*e^{i(-2\Omega\tau+\Phi^*)} + \frac{\Delta A}{4\Omega^2}e^{i(2\beta-\Phi)} - \frac{\Delta A^*}{12\Omega^2}e^{i(4\Omega\tau-\Phi^*+2\beta)} \tag{6.4}$$

$$\left.\begin{aligned}
\dot{A} &= -\zeta A - \frac{\varepsilon\Delta}{4\Omega}\{A\sin 2(\Phi-\beta) - A^*\sin(\Phi+\Phi^*-2\beta)\} \\
&\quad + \frac{\Delta U_g}{4\Omega}\left\{\left(1-\frac{d}{16\Omega^2}\right)\cos(\Phi-2\beta) + \frac{\zeta}{4\Omega}\sin(\Phi-2\beta)\right\} \\
\dot{\Phi} &= d_2 - \frac{\varepsilon\Delta}{4\Omega A}\{A\cos 2(\Phi-\beta) - A^*\cos(\Phi+\Phi^*-2\beta)\} \\
&\quad - \frac{\Delta U_g}{4\Omega}\left\{\left(1-\frac{d}{16\Omega^2}\right)\sin(\Phi-2\beta) - \frac{\zeta}{4\Omega}\cos(\Phi-2\beta)\right\} \\
\dot{A}^* &= -\zeta A^* - \frac{\varepsilon\Delta}{4\Omega}A\sin(\Phi+\Phi^*-2\beta) \\
\dot{\Phi}^* &= -d_2^* - \frac{\varepsilon\Delta A}{4\Omega A^*}\cos(\Phi+\Phi^*-2\beta)
\end{aligned}\right\} \tag{6.5}$$

where,

$$d = 1 - 4\Omega^2 \tag{6.6}$$

, and d_2 and d_2^* are given by Eq. (4. 22).

Steady state solution for A, Φ, A^*, and Φ^* are obtained when the following conditions are given in Eq. (6. 5).

$$\dot{A}=0,\ \dot{\Phi}=0,\ \dot{A}^*=0,\ \dot{\Phi}^*=0 \tag{6.7}$$

These numerical results are shown in Fig. 6. 2. The parameters used are those obtained from the experimental apparatus indicated in section 6. 4. Oblique lines in Fig. 6. 2 show the unstable regions which are explained in Chapter 4. $[-2\omega]$ vibration occurs for $\varepsilon \neq 0$ $(\alpha_a \neq 0)$, though it does not occur for $\varepsilon = 0$. Accordingly, it is seen from Eq. (6. 4) that the shaft generates $[+4\omega]$ vibration with amplitude $\Delta A^*/3$. The static deflection of shaft is

$$x + iy = \delta_{st}\{-i + \Delta A e^{i(2\beta-\Phi)}\}$$

, which is obtained from Eqs. (6. 1) and (6. 4). An equilibrium point of vibration (x, y) depends on A and Φ, and it does not come just under the origin O.

Here, a critical speed $\Omega_{1/2}$ is considered. The critical speed $\Omega_{1/2}$ makes an infinite amplitude for no damping $(\zeta = 0)$, and it satisfies the following equation

$$4\Omega d_2^*(4\Omega d_2 \pm \varepsilon\Delta) - \varepsilon^2\Delta^2 = 0 \tag{6.8}$$

Especially for $\varepsilon = 0$, $\Omega_{1/2}$ is given by the solution of

$$d_2 = 0 \tag{6.9}$$

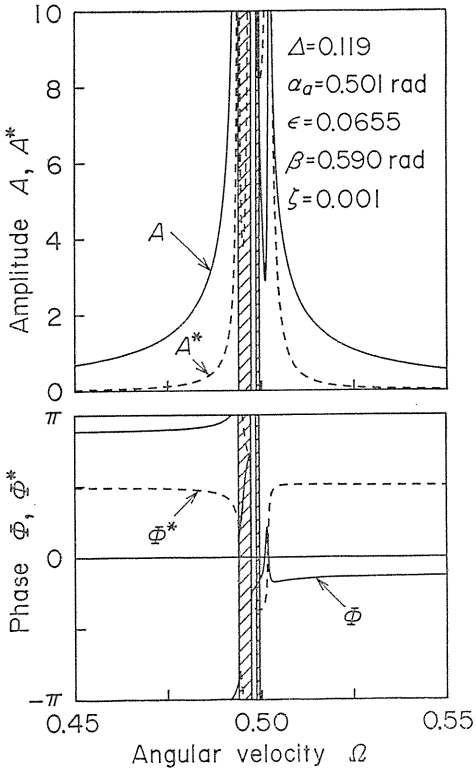

Fig. 6. 2. Amplitude and phase of $[\pm 2\omega]$ vibrations.

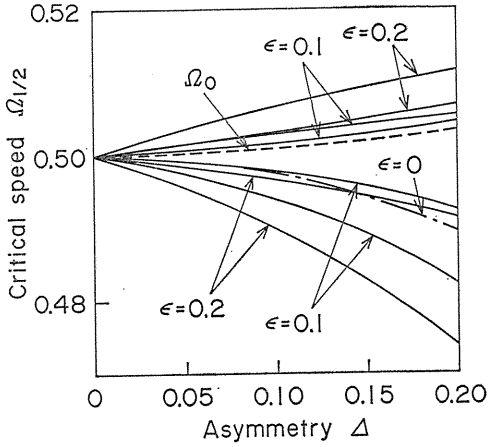

Fig. 6. 3. Critical speed $\Omega_{1/2}$ near $\Omega=1/2$.

As seen from the results of Chapter 4, the solution $\Omega=\Omega_{1/2}$ of Eq. (6. 9) coincides with the borders of the unstable region in which the S-type unstable vibration occurs.

Numerical results for the critical speeds $\Omega_{1/2}$ are shown in Fig. 6. 3. Four critical speeds (solid lines) exist for $\varepsilon \neq 0$, but one critical speed (chain line) does for $\varepsilon=0$. Three critical speeds seem to exist in Fig. 6. 2 because of damping. The amplitude of $[+2\omega]$ vibration becomes zero at a certain value Ω_0 of Ω, which is the solution of $d_4{}^*=0$. This value Ω_0 is shown by the broken line in Fig. 6. 3. In Fig. 6. 2, there is a rotating speed at which the $[+2\omega]$ vibration is sharply reduced, and the $[+2\omega]$ vibration vanishes for $\zeta=0$ at that rotating speed.

6. 3. 2. $\Omega \fallingdotseq 1/4$

$$Z = Ae^{i(4\Omega\tau+\Phi)} + A^*e^{i(-4\Omega\tau+\Phi^*)} + \frac{\Delta A}{12\Omega^2}e^{i(-2\Omega\tau-\Phi+2\beta)} - \frac{\Delta A^*}{20\Omega^2}e^{i(6\Omega\tau-\Phi^*+2\beta)} + \frac{i\Delta U_g}{12\Omega^2}e^{i(2\Omega\tau+2\beta)} \tag{6.10}$$

$$\left.\dot{A} = -\zeta A + \frac{\varepsilon\Delta}{8\Omega}A^*\sin(\Phi+\Phi^*-2\beta) + \frac{\varepsilon\Delta U_g}{8\Omega}\cos(\Phi-2\beta)\right)$$

$$\left.\begin{aligned}
\dot{\Phi} &= d_4 + \frac{\varepsilon \Delta A^*}{8\Omega A}\cos(\Phi+\Phi^*-2\beta) - \frac{\varepsilon \Delta U_g}{8\Omega A}\sin(\Phi-2\beta) \\
\dot{A}^* &= -\zeta A^* - \frac{\varepsilon \Delta}{8\Omega} A \sin(\Phi+\Phi^*-2\beta) \\
\dot{\Phi}^* &= -d_4^* - \frac{\varepsilon \Delta A}{8\Omega A^*}\cos(\Phi+\Phi^*-2\beta)
\end{aligned}\right\} \qquad (6.11)$$

where,

$$\left.\begin{aligned}
d_4 &= \frac{1}{8\Omega}\left(d-\zeta^2-\frac{d^2+16\Delta^2/3}{64\Omega^2}\right) \\
d_4^* &= \frac{1}{8\Omega}\left(d-\zeta^2-\frac{d^2-16\Delta^2/5}{64\Omega^2}\right) \\
d &= 1-16\Omega^2
\end{aligned}\right\} \qquad (6.12)$$

A steady state solution is obtained by substituting Eq. (6. 7) into Eq. (6. 11). Figure 6. 4 shows the numerical results for the amplitudes A and A^*, and the phases Φ and Φ^* of $[+4\omega]$ and $[-4\omega]$ vibrations, respectively. According to Eqs. (6. 10) and (6. 11), the $[+4\omega]$ and $[-4\omega]$ vibrations for $\varepsilon=0$ vanish with time, and the shaft generates only $[+2\omega]$ vibration with the amplitude $4\Delta/3$. For $\varepsilon\neq 0$, the shaft generates $[-2\omega]$ vibration with the amplitude $4\Delta A/3$, and $[+6\omega]$ vibration with the amplitude $4\Delta A^*/5$ in addition to $[+4\omega]$ and $[-4\omega]$ vibrations. The amplitudes A and A^* become larger with an

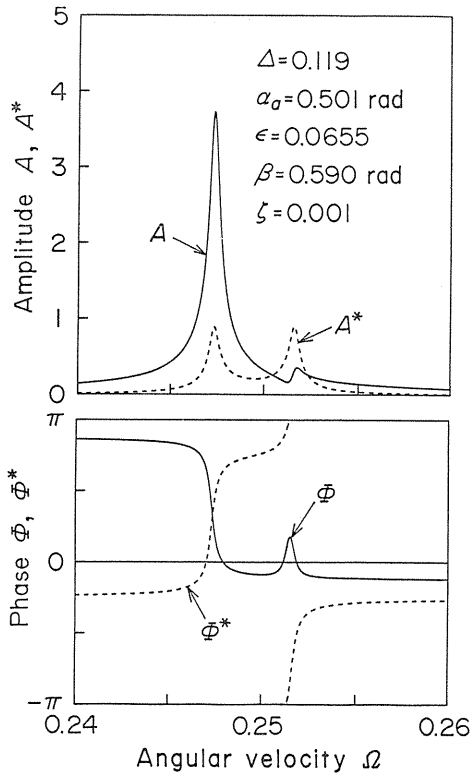

Fig. 6. 4. Amplitude and phase of $[\pm 4\omega]$ vibrations.

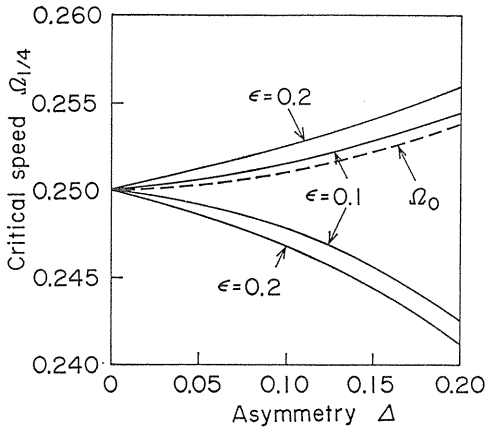

Fig. 6. 5. Critical speed $\Omega_{1/4}$ near $\Omega=1/4$.

increase of ε, and they have two peaks. Of the rotating speeds at which two peaks appear, a lower rotating speed gives $A>A^*$, and a higher one gives $A<A^*$. The two peaks of A^* are nearly equal each other in height.

The critical speeds $\Omega_{1/4}$ are given as the solutions to the following equation.

$$64\Omega^2 d_4 d_4^* - \varepsilon^2 \Delta^2 = 0 \tag{6.13}$$

Numerical results of the critical speeds $\Omega_{1/4}$ are shown in Fig. 6. 5. Two critical speeds emerging near $\Omega=1/4$ separate with an increase in shaft asymmetry or in angular velocity fluctuation. Near this rotating speed, the amplitude A also becomes zero at a certain rotating speed Ω_0, which is a solution of $d_4^*=0$. This value Ω_0 is also indicated by a broken line in Fig. 6. 5. The value of Ω_0 is equal to the rotating speed at which the amplitude A becomes small between the two peaks in Fig. 6. 4, and it becomes zero for $\zeta=0$.

6. 4. Experiments

6. 4. 1. Experimental apparatus and its method

Figure 6. 6 shows a schematic diagram of the experimental apparatus as viewed downward from top. The dimensions of the experimental apparatus are the same as Fig. 2. 5 except for a driven shaft S_h and a rotor D. Each of the driven shaft S_h and the rotor D, as shown in Fig. 6. 7, is separated into two parts at the middle. The driven shaft is assembled with the rotor by a screw. Then the combined asymmetry Δ of driven shaft can be varied arbitrarily by changing the coupling angle of the two asymmetrical shafts.

The rotor D is 90 mm in diameter, 150 mm in length, $m=6.890$ kg in mass, 6.976×10^{-3} kg·m^2 in polar moment of inertia, and 1.658×10^{-2} kg·m^2 in diametral moment of inertia about the gravity center. The driven shaft S_h is 723 mm in length, 2.078 kg in mass, 207.4 GPa in Young's modulus, and 81.54 GPa in shear modulus.

Horizontal and vertical components x and y of rotor displacement are detected by pickups P_3 and P_4, and pulse per one rotation of the drive shaft is detected by pickup P_2. These measured values are recorded in a data recorder.

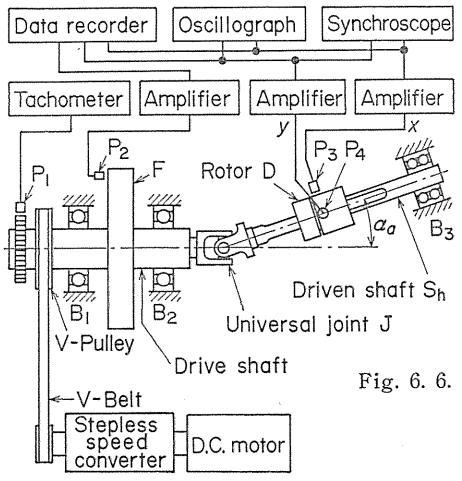

Fig. 6. 6. Plan of experimental apparatus.

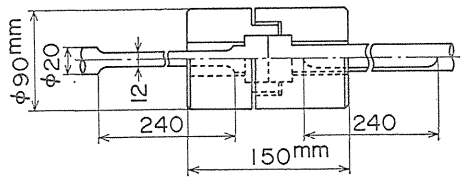

Fig. 6. 7. Assembled driven shaft S_h and rotor D.

6. 4. 2. Experimental results and some discussions

Figures 6. 8 to 6. 13 show resonance curves obtained by frequency analysis of the experimental data.

Figures 6. 8 to 6. 10 show amplitudes and phases of $[+2\omega]$ and $[-2\omega]$ vibrations. In Fig. 6. 8 the shaft asymmetry is very small ($\Delta=0.004$); The results of section 6. 3 tell that the vibrations can hardly occur. But the forced vibration by the secondary moment can occur, because the rotor used in the experiments is not a concentrated mass (refer to appendix). Increase of asymmetry Δ magnifies $[+2\omega]$ vibration, whereas it hardly influences the $[-2\omega]$ vibration. Each of the $[+2\omega]$ and $[-2\omega]$ vibrations consists of the following two forced vibrations. One is a vibration generated by the triple effect of gravity, asymmetry, and angular velocity fluctuation. The other is one caused by the secondary moment. The former $[+2\omega]$ vibration is nearly in phase with the latter $[+2\omega]$ vibration, and the former $[-2\omega]$ vibration is different by $\pi/4$ in phase from the latter $[-2\omega]$ vibration. By this the above-mentioned phenomenon can be explained (see also Figs. 6. 9 and 6. 10).

The amplitudes and phases of $[+4\omega]$ and $[-4\omega]$ vibrations at $\Omega\fallingdotseq 1/4$ are shown in Figs. 6. 11 to 6. 13. In Fig. 6. 11 the asymmetry is very small ($\Delta=0.004$), and the $[+4\omega]$ and $[-4\omega]$ vibrations generated here are the forced ones caused by the secondary moment. When the asymmetry Δ increases as shown in Figs. 6. 12 and 6.

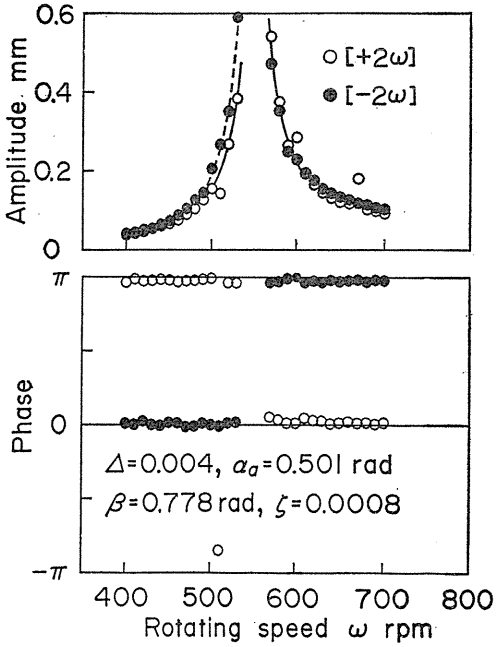

Fig. 6. 8. Amplitude and phase of $[\pm 2\omega]$ vibrations.

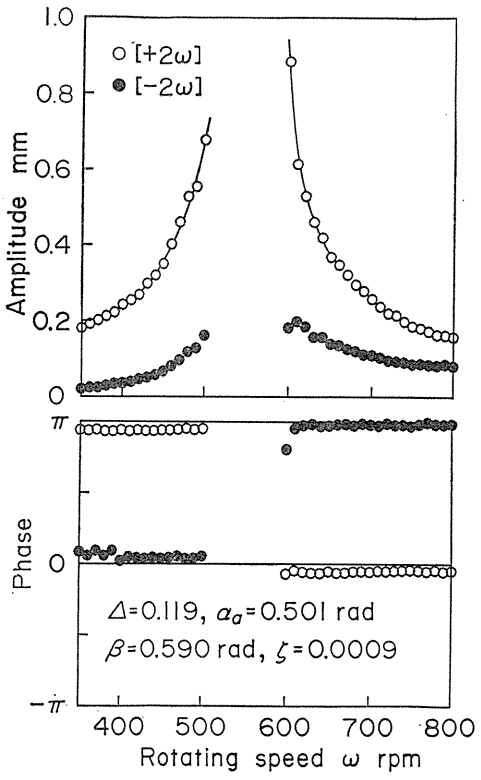

Fig. 6. 9. Amplitude and phase of $[\pm 2\omega]$ vibrations.

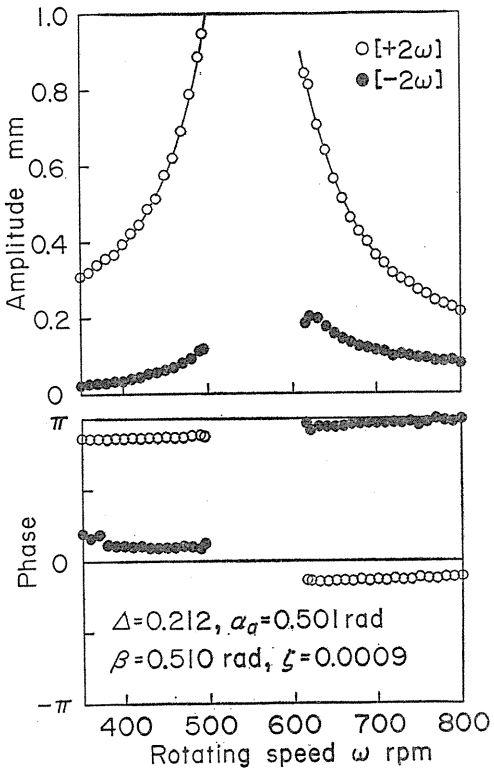

Fig. 6. 10. Amplitude and phase of [±2ω] vibrations.

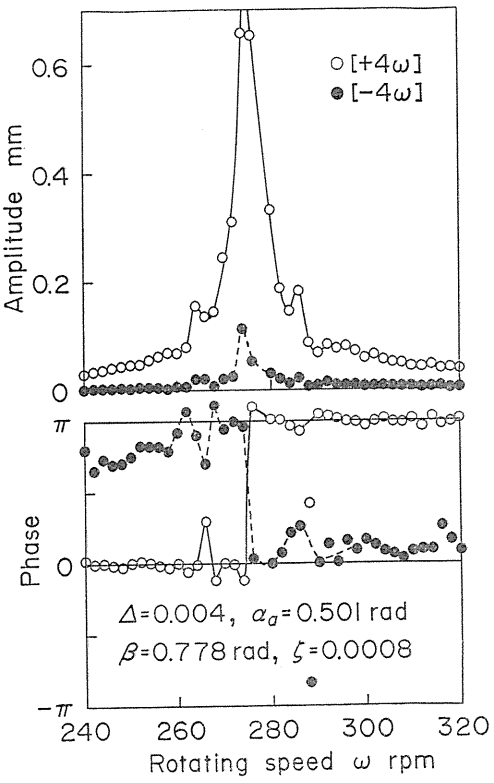

Fig. 6. 11. Amplitude and phase of [±4ω] vibrations.

13, the rotating shaft generates a vibration under the triple effect of gravity, asymmetry, and angular velocity fluctuation in addition to the vibration by the secondary moment. In Fig. 6. 13 two peaks of amplitude appear at $\omega=273$ rpm and 286 rpm. When $\omega=286$ rpm, $[-4\omega]$ vibration is larger in amplitude than $[+4\omega]$ vibration. This coincides well with the analytical results of Fig. 6. 4.

The above-mentioned experimental results coincide well with the analytical results in section 6. 3 except the influence of the forced vibration caused by the secondary moment. Thus the analytical results are confirmed to be valid.

6. 5. Conclusions

The results obtained in this chapter may be summarized as follows:

At nearly half the major critical speed:

(1) In addition to $[+2\omega]$ vibration whirling forward, the rotating shaft generates $[-2\omega]$ and $[+4\omega]$ vibrations whirling backward with double and forward with quadruple as large as ω, the angular velocity of the drive shaft. The $[+4\omega]$ vibration has about $A/3$ times as large as the amplitude of $[-2\omega]$ vibration.

(2) The resonance curves of $[+2\omega]$ and $[-2\omega]$ vibrations have four peaks at most, namely, four critical speeds exist. These critical speeds coincide with boundaries of the region in which S-type unstable vibration occurs. The peaks are reduced to three by small damping.

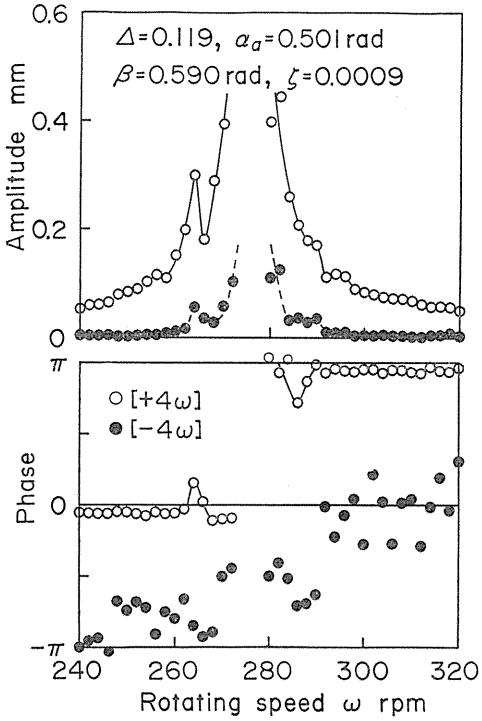

Fig. 6. 12. Amplitude and phase of $[\pm 4\omega]$ vibrations.

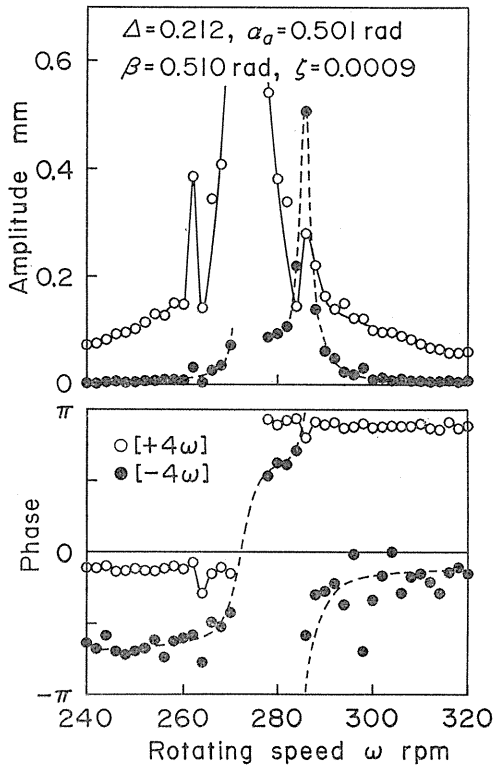

Fig. 6. 13. Amplitude and phase of $[\pm 4\omega]$ vibrations.

(3) $[+2\omega]$ vibration is sharply reduced at a certain rotating speed among the four critical speeds, and the amplitude becomes zero at that rotating speed when there is no damping.

At nearly a quarter of the major critical speed:

(4) The rotating shaft generates $[+2\omega]$, $[-2\omega]$, and $[+6\omega]$ vibrations in addition to $[+4\omega]$ and $[-4\omega]$ vibrations. The $[-2\omega]$ vibration has about $4\Delta/3$ times as large as the amplitude of the $[+4\omega]$ vibration, and the $[+6\omega]$ vibration has about $4\Delta/5$ times as large as the amplitude of the $[-4\omega]$ vibration. The amplitude of $[+2\omega]$ vibration is nearly equal to $4\Delta/3$.

(5) The amplitudes of $[+4\omega]$ and $[-4\omega]$ vibrations have two peaks.

(6) The $[+4\omega]$ vibration becomes very small at a certain rotating speed between these peaks, and the amplitude becomes zero at the rotating speed when there is no damping.

(7) Near a peak at the lower speed, the $[+4\omega]$ vibration is larger than the $[-4\omega]$ vibration, and vice versa near a peak at the higher speed. Two peaks of $[-4\omega]$ vibration are nearly equal in height.

Appendix

The amplitude and phase of the vibration caused by the secondary moment of a universal joint are obtained by using the analytical results in Chapters 1 and 2. Figure 6. 14 shows the result for $[+2\omega]$ and $[-2\omega]$ vibrations. In this numerical calculation, the same parameters as those in Fig. 6. 8 are used. Torsional rigidity δ_t of driven shaft is determined under an assumption that the shaft has a uniform rectangular section 18mm×12mm. Notation I_p indicates a polar moment of inertia of rotor, and l is the shaft length.

An amplitude [mm] is obtained by multiplying the non-dimensional amplitude shown in Fig. 6. 14 by $\delta_{st}=0.75$ mm in Eq. (4. 6). An angular velocity ω [rpm] is obtained by multiplying the non-dimensional angular velocity Ω by $p=1095$ rpm in Eq. (4. 2). Thus, it is known that the amplitude and phase characteristics in Fig. 6. 14 coincide well with those in Fig. 6. 8.

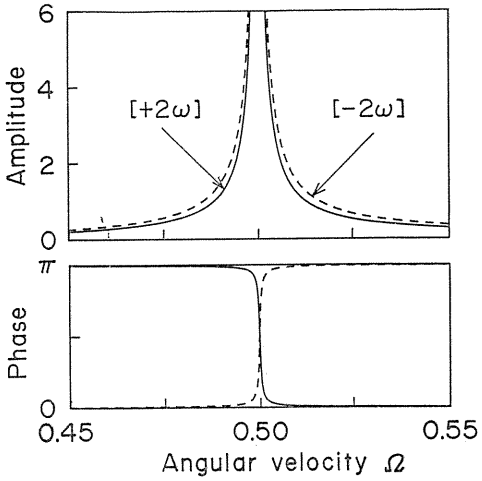

Fig. 6. 14. Amplitude and phase of $[\pm 2\omega]$ vibrations due to the secondary moment.

References

1) R. Burkhalter and P. J. Mazziotti, *The Low Silhouette Drive Line*, SAE Trans., Vol. **64** (Jan., 1956), pp. 379-393.
2) R. Grammel, *Kritische Drehzahl und Kreiselwirkung*, Z. Ver. dtsch. Ing., Vol. **64**, No. 44 (Oct., 1920), pp. 911-914.
3) A. Stodola, *Steam and Gas Turbines*, McGraw-Hill Book Co. Inc., (1927), pp. 424-430.
4) J. P. Den Hartog, *Mechanical Vibrations*, McGraw-Hill Book Co. Inc., (1956), pp. 225-229.
5) W. J. Mc. Q. Rankine, *Centrifugal Whirling of Shafts*, Engineer, Vol. **26** (Apr., 1869).
6) A. L. Kimball and E. H. Hull, *Vibration Phenomena of a Loaded Unbalanced Shaft While Passing Through Its Critical Speed*, Trans. ASME, Vol. **47** (1925), pp. 673-698.
7) Y. Shimoyama and T. Yamamoto, *Vibrations Generated on a Rotating Shaft by Passing through its Critical Speed with Some Angular Acceleration*, Trans. Japan Soc. Mech. Eng. (in Japanese), Vol. **15**, No. 50 (Oct., 1949). pp. I-113-I-121.
8) F. M. Dimentberg, *Flexural Vibrations of Rotating Shafts*, Butterworths, (1961), pp. 42-60.
9) S. Yanabe and A. Tamura, *Vibration on a Shaft Passing through a Critical Speed* (1st Report, *Experiments and Numerical Solutions*), Bull. JSME, Vol. **14**, No. 76 (Oct., 1971), pp. 1050-1058.
10) Reference (3), pp. 1122-1130.
11) Reference (8), pp. 155-186.
12) H. D. Taylor, *Critical-Speed Behavior of Unsymmetrical Shafts*, J. Appl. Mech., Vol. **7**, No. 2 (Jun., 1940), pp. A-71-A-79.
13) P. J. Brosens and S. H. Crandall, *Whirling of Unsymmetrical Rotors*, J. Appl. Mech.,

Vol. 28, No. 3 (Sep., 1961), pp. 355-362.
14) T. Yamamoto and H. Ota, *On the Vibrations of the Shaft Carrying an Unsymmetrical Rotating Body*, Bull. JSME, Vol. 6, No. 21 (Feb., 1963), pp. 29-36.
15) T. Yamamoto and H. Ota, *On the Unstable Vibrations of a Shaft Carrying an Unsymmetrical Rotor*, J. Appl. Mech., Trans. ASME, Vol. 31, Ser. E, No. 3 (Sep., 1964), pp. 515-522.
16) T. Yamamoto, *On Sub-Harmonic and "Summed and Differential Harmonic" Oscillations of Rotating Shaft*, Bull. JSME, Vol. 4, No. 13 (Feb., 1961), pp. 51-58.
17) T. Yamamoto, Y. Ishida, and T. Ikeda, *Summed-and-Differential Harmonic Oscillations of an Unsymmetrical Shaft*, Bull. JSME, Vol. 24, No. 187 (Jan., 1981), pp. 183-191.
18) A. Tondl, *Some Problems of Rotor Dynamics*, Publishing House of the Czechoslovak Academy of Sciences, (1965), pp. 281-297.
19) H. Ota, K. Mizutani, and M. Miwa, *Influence of Unequal Pedestal Stiffness on the Instability Regions of a Rotating Asymmetric Shaft* (2nd Report, *Inclinational Vibrations with Effects of Gyroscopic Action*), Bull. JSME, Vol. 23, No. 183 (Sep., 1980), pp. 1514-1521.
20) H. Ota and K. Mizutani, *Influence of Unequal Pedestal Stiffness on the Instability Regions of an Asymmetrical Rotor*, Bull. JSME, Vol. 24, No. 198 (Dec., 1981), pp. 2133-2140.
21) A. Stodola, *Kritische Drehzahlen rasch umlaufender Wellen*, Z. Ver. dtsch. Ing., Vol. 63, No. 36 (Sep., 1919), pp. 867-869.
22) T. Yamamoto and K. Kono, *On Vibrations of a Rotor with Variable Rotating Speed*, Bull. JSME, Vol. 13, No. 60 (Jun., 1970), pp. 757-765.
23) S. Fujii, *Whirling of an Automotive Propeller Shaft at Lower Speeds* (1st Report), Trans. Japan Soc. Mech. Eng. (in Japanese), Part 1, Vol. 22, No. 119 (Mar., 1956), pp. 178-181.
24) H. Ota, *Mechanism* (in Japanese), (1978), pp. 84-89, Kyoritsu Shuppan Company.
25) B. Porter, *A Theoretical Analysis of the Torsional Oscillation of a System Incorporating a Hooke's Joint*, J. Mech. Eng. Sci., Vol. 3, No. 4 (Apr., 1961), pp. 324-329.
26) V. Zeman, *Stability of Motion of Mechanical Systems with Joints*, Acta Technica, ČSAV, ROČNIK 22, No. 1 (1977), pp. 52-62.
27) S. H. Crandall and P. J. Brosens, *On the Stability of Rotation of a Rotor with Rotationally Unsymmetric Inertia and Stiffness Properties*, J. Appl. Mech, Vol. 28, No. 4 (Dec., 1961), pp. 567-570.
28) O. Föppl, *Kritische Drehzahlen rasch umlaufender Wellen*, Z. Ver. dtsch. Ing., Vol. 63, No. 36 (Sep., 1919), pp. 866-867.
29) R. M. Rosenberg, *On the Dynamical Behavior of Rotating Shafts Driven by Universal (Hooke) Coupling*, J. Appl. Mech., Vol. 25, No. 1 (Mar., 1958), pp. 47-51.
30) S. Fujii, H. Shibata, and T. Shigeta, *Whirling of an Automobile Propeller Shaft at Lower Speeds* (2nd Report), Trans. Japan Soc. Mech. Eng. (in Japanese), Part 1, Vol. 22, No. 119 (Jul., 1956), pp. 489-491.
31) J. A. Kayser, *Drivelines for Heavy Equipment*, SAE Trans., Vol. 70 (1962), pp. 38-42.
32) S. Kato, *Analysis of Exciting Force on the Hooke's Joint Propeller Shaft*, Toyota Engineering (in Japanese), Vol. 21, No. 3 (Jan., 1970), pp. 201-209.
33) J. S. Burdess and L. Maunder, *Speed Variations in a Hooke's Joint* (Discussion), Proc. Inst. Mech. Eng., Vol. 184, Part 31 (1969-1970), p. 658.
34) L. Maunder and J. S. Burdess, *Speed Characteristics of Hooke's Joint Transmissions*, J. Mech. Eng. Sci., Vol. 14, No. 4 (Apr., 1972), pp. 238-244.
35) J. S. Burdess, *The Dynamics of Transmission Shafts Driven by Universal Couplings*, A Thesis Submitted for the Degree of Doctor of Philosophy in the Faculty of Applied Science, University of Newcastle upon Tyne, (Dec., 1973).
36) J. S. Burdess and C. H. J. Fox, *A Theoretical and Experimental Evaluation of the Multigimbal Hooke's Joint Gyroscope*, J. Mech. Eng. Sci., Vol. 23, No. 4 (Apr., 1981), pp. 193-200.
37) N. N. Bogoliubov and Y. A. Mitropolsky, *Asymptotische Methoden in der Theorie der*

Nichtlinearen Schwingungen, Akademie-Verlag, (1965), pp. 164-266.
38) H. Ota and M. Kato, *Lateral Vibrations of a Rotating Shaft Driven by a Universal Joint* (1st Report, *Generation of Even Multiple Vibrations by Secondary Moment*), Bull. JSME, Vol. **27**, No. 231 (Sep., 1984), pp. 2002-2007.
39) H. Ota and M. Kato, *Even Multiple Vibrations of a Rotating Shaft due to Secondary Moment of a Universal Joint*, Proc. 3rd Int. Conf. on Vibrations in Rotating Machinery, York, (Sep., 1984), pp. 199-204.
40) H. Ota, M. Kato, and H. Sugita, *Lateral Vibrations of a Rotating Shaft Driven by a Universal Joint* (2nd Report, *Analyses and Experiments on Even Multiple Vibrations by Secondary Moment*), Bull. JSME, Vol. **28**, No. 242 (Aug., 1985), pp. 1749-1755.
41) Ch. Wehrli, *Dynamisches Verhalten einer einfach besetzten rotierenden Welle mit Kardangelenken*, Z. Angew. Math. Phys., Vol. **15** (1964), pp. 154-166.
42) J. S. Burdess, *The Vibration and Stability of Laterally Flexible Shafts Driven and Supported by Hooke's Joints*, Proc. IUTAM, Springer-Verlag, (1975), pp. 103-127.
43) S. Yanabe, *Vibration of a Shaft Passing Through a Critical Speed* (4th Report, *Effect of Gyroscopic Moment*), Bull. JSME, Vol. **23**, No. 180 (Jul., 1980), pp. 945-952.
44) K. Nonami and M. Miyashita, *Problem of Rotor Passing through Critical Speed with Gyroscopic Effect* (3rd Report, *Case of Rotating Shaft on Flexible Support*), Bull. JSME, Vol. **23**, No. 186 (Dec., 1980), pp. 2104-2110.
45) H. Ota and M. Kato, *Lateral Vibrations of a Rotating Shaft Driven by a Universal Joint* (3rd Report, *Vibrations Caused by Frictions between a Cross-Pin and Yokes*), Trans. Japan Soc. Mech. Eng. (in Japanese), Vol. **52**, No. 479 (Jul., 1986), pp. 1908-1914.
46) Reference (4), pp. 353-363.
47) H. Ota, M. Kato, and M. Mizuno, *Lateral Vibrations of an Asymmetrical Shaft Driven by a Universal Joint* (1st Report, *Generation of Unstable Vibration and Expansion of Unstable Region by Angular Velocity Fluctuation*), Bull. JSME, Vol. **29**, No. 249 (Mar., 1986), pp. 916-923.
48) H. Ota and M. Kato, *Unstable and Forced Vibrations of an Asymmetrical Shaft Driven by a Universal Joint*, Proc. Int. Conf. on Rotordynamics, Tokyo, (Sep., 1986), pp. 493-498.
49) T. Yamamoto and H. Ota, *Dynamics of Machinery* (in Japanese), (1986), pp. 234-240, Asakura Syoten Company.
50) Reference (18), pp. 70-113.
51) R. Gasch and H. Pfützner, *Rotordynamik*, Springer Verlag, (1975), pp. 115-126.
52) H. Ota and K. Mizutani, *Influence of Unequal Pedestal Stiffness on the Instability Regions of a Rotating Asymmetric Shaft* (3rd Report, *Mechanism for Occurrence of Two Types of Unstable Vibrations*), Bull. JSME, Vol. **24**, No. 190 (Apr., 1981), pp. 700-707.
53) H. Ota and M. Kato, *Lateral Vibrations of an Asymmetrical Shaft Driven by a Universal Joint* (2nd Report, *Generation Mechanism of Unstable Vibrations*), Bull. JSME, Vol. **29**, No. 254 (Aug., 1986), pp. 2633-2639.
54) H. Ota and M. Kato, *Lateral Vibrations of an Asymmetrical Shaft Driven by a Universal Joint* (3rd Report, *Analyses and Experiments on Forced Vibrations of Horizontal Shaft Caused by Gravity*), Bull. JSME, Vol. **29**, No. 254 (Aug., 1986), pp. 2640-2646.
55) C. R. Soderberg, *On the Subcritical Speeds of the Rotating Shaft*, Trans. ASME, Vol. **54** (1932), pp. 45-52.
56) D. M. Smith, *The Motion of a Rotor Carried by a Flexible Shaft in Flexible Bearings*, Proc. Roy. Soc. London, Ser. A, Vol. **142**, No. A846 (Oct., 1933), pp. 92-118.
57) D. Robertson, *Whirling of a Shaft with Skew Stiffness*, The Engineer, Vol. **156** (Aug., 1933), pp. 152-153, pp. 179-181, and pp. 213-214.
58) C. M. Laffoon and B. A. Rose, *Special Problems of Two Pole Turbo Generators*, Trans. AIEE, Vol. **59** (Jan., 1940), pp. 30-33.
59) E. H. Hull, *Shaft Whirling as Influenced by Stiffness Asymmetry*, Trans. ASME, Ser. B, Vol. **83**, No. 2 (May, 1961), pp. 219-226.